SUBSEA CRYOGENIC GAS RELEASES

by

ANNE CUMMING CONNELL

Being a thesis submitted in support of an application for the degree of Doctor of Philosophy of the University of Glasgow

November 1986

ProQuest LLC.
789 East Eisenhower Parkway
P.O. Box 1346
Ann Arbor, MI 48106 – 1346

To

my mother

C O N T E N T S

ACKNOWLEDGMENTS

It gives me great pleasure to thank Dr. B. Straughan for his supervision of this work which was carried out in the Department of Mathematics, University of Glasgow. For all his encouragement and the many informative discussions, I am deeply grateful.

My sincere thanks also go to Britoil for the award of a CASE studentship under which this work was carried out. For the initiation of the project and the subject matter I am indebted to Mr. I Walker and Dr. D. Montgomery, formerly of the Department of Research and Development, Britoil. For his continuing supervision, and many helpful suggestions my thanks go to Mr. T. Baxter. Further thanks go to Mr. F. Crawley for his interest and advice.

In addition to the initial studentship further financial support from Britoil allowed me to visit the Atomic Energy Research Establishment at Harwell where I spent a number of very informative weeks. Firstly I should like to express my gratitude to Britoil for this opportunity, and secondly I should like to thank Dr. G.F. Hewitt, Dr. B. Azzopardi and Dr. N. Wilkes of the A.E.R.E. who gave most generously of their time and provided an abundance of helpful advice.

To Professor I.N. Sneddon of the Department of Mathematics I should like to extend thanks for his helpful comments and the encouragement he has given since my undergraduate days.

I also wish to thank Dr. P. Smith for all his administrative work in instigating my period of study.

My warmest thanks go to Mrs. J. Pickering for the excellent job she has made of typing this thesis.

I am also indebted to the Science and Engineering Research Council of Great Britain, without whose award this work would not have been possible.

Finally, my heartfelt thanks are extended to my mother whose continuing understanding, encouragement and help have carried me through my many years of study and research.

SUMMARY

The objective of this research is to develop a mathematical model to describe the dynamic and thermodynamic history of a Subsea Cryogenic Gas Release, and thus allow prediction of buoyancy, area, velocity and temperature on arrival at the sea surface.

The thesis begins with a review of previous work and notes the shortfalls in the models produced. This work concentrates on the main part of the rise, although in reality both initial and final stages would have an effect.

It is assumed that the gas forms a buoyant plume within an axisymmetric geometry. From the conservation laws a system of equations is derived which are then combined with a number of thermodynamic relations in a computer program. The semi-empirical formulae used in describing the thermodynamics relate to methane, this being the major constituent of the natural gas under consideration.

Release rate, depth and pipeline conditions are input variables. Velocity and void-fraction profiles are assumed to be 'equivalent' top-hat, with correspondence between these values and those of gaussian being noted. Assumptions are made to the bubble size and the heat transfer to the gas with sensitivity studies being performed to identify the influence of these parameters.

Initially mass transfer is disregarded, but a second model allows for the dissolution of the gas in the seawater and the effect of this on the surface conditions is assessed.

LIST OF SYMBOLS

A	Cross-sectional area of plume, channel	(m^2)
A_g	Cross-sectional area of plume occupied by gas	(m^2)
A_l	Cross-sectional area of plume occupied by liquid	(m^2)
$A_i (i=1,3)$	Constants in equation for Bunsen coeff. (7.4.16)	(-)
b	plume radius	(m)
$B_i (i=1,3)$	Constants in equation for Bunsen Coeff. (7.4.16)	(-)
c	sonic velocity	(m/s)
c_i	concentration of dissolved methane at the interface	(kg/m^3)
c_∞	concentration of dissolved methane in bulk fluid	(kg/m^3)
c_p	heat capacity per unit mass at constant pressure	$(J/kg°K)$
c_v	heat capacity per unit mass at constant volume	$(J/kg°K)$
C	constant defined by equation (3.4.10)	(-)
Const	constant defined by equation (3.2.14)	(-)
C'	constant defined by equation (3.2.21)	(-)
C''	constant defined by equation (3.2.27)	(-)
d	equivalent plume diameter defined by equation (2.2.34)	(m)

d_e	equivalent bubble diameter	(m)
d_{eff}	equivalent effective bubble diameter defined by equation (2.2.6)	(m)
d_{inj}	width of gas injection device	(m)
d_p	local plume diameter used in equation (2.2.3)	(m)
D	Diffusivity	(m^2/s)
$\hat{D}$	Non-dimensional equivalent plume diameter ($=d/L$)	(-)
$\hat{D}_{eff}$	non-dimensional effective equivalent plume diameter ($=d_{eff}/L$)	(-)
g	acceleration due to gravity	(m/s^2)
$\hat{g}$	gibbs function defined by equation (3.2.3)	(J/kg)
G	volumetric gas flow rate	(m^3/s)
G_o	volumetric release rate	(m^3/s)
h	height above release point ($=z_o-z$)	(m)
$\hat{h}$	enthalpy per unit mass	(J/kg)
h_T	heat transfer coefficient	($W/m^2°K$)
H	Henry's Law constant	(N/m^2)
k	thermal conductivity	($W/m°K$)
k_m	mass transfer coefficient	(m/s)
K	parameter defined by equation (2.2.3)	(-)
K_1	entrainment coefficient defined by equation (2.2.4)	(-)

K_2	parameter defined by equation (2.2.6)	(-)
K_3	bubble spreading parameter defined by equation (2.2.37)	(-)
K_4	constant defined by equation (2.2.63)	(-)
l	solubility expression defined by equation (7.4.6)	(-)
L	length scale	(m)
m	mass	(kg)
$\hat{m}$	molar mass of gas	(mol)
$\dot{m}$	mass flux	(kg/s)
$\dot{m}_{g_o}$	mass release rate	(kg/s)
$\hat{M}$	molecular weight	(kg/mol)
M'	Mach number (=u/c)	(-)
M	Momentum	(kgm/s)
$\dot{M}$	Momentum flux	(N)
$\bar{\dot{M}}$	mean momentum flux	(N)
$\approx{\dot{M}}$	fluctuating component of momentum flux	(N)
$\bar{n}$	number of moles	(-)
n	general index for polytropic gas law defined in (3.3.16)	(-)
N	number of bubbles	(-)
Nu	Nusselt number	(-)
p	pressure	(N/m^2)
$\bar{p}$	pressure inside bubble (Appendix A)	(N/m^2)
Pr	Prandtl number	(-)

δq	energy transferred per unit mass	(J/kg)
ΔQ	energy transferred	(J)
r_a	radial coordinate (r_a=0 at plume centre)	(m)
r	gas constant	(J/kg°K)
R	universal gas constant (=$r\hat{M}$)	(J/mol.°K)
R_a	radius of curvature	(m)
Re	Reynolds number	(-)
s	entropy per unit mass	(J/kg°K)
s_B	surface area of bubble	(m^2)
S	entropy per mole	(cal/mol.°K)
S'	entropy defined by (3.2.18)	(cal/mol.°K)
S_{sat}	entropy of saturated gas	(cal/mol.°K)
S_l	Salinity	($^0/_{00}$)
Sc	Schmidt number	(-)
Sh	Sherwood number	(-)
t	time	(s)
t_c	contact time at interface defined by equation (3.4.12)	(s)
T	temperature	(°K)
T_{sea}	sea temperature	(°K)
u_g	local gas velocity	(m/s)
$\bar{u}_g$	average of u_g over time gas present	(m/s)
u_l	local plume velocity defined by equation (2.2.3)	(m/s)
$\bar{u}_l$	average of u_l over time liquid present	(m/s)
$\tilde{u}_l$	fluctuating component of u_l	(m/s)
u_r	local slip velocity	(m/s)
$\hat{U}$	bubble speed (Appendix A)	(m/s)
U	velocity scale	(m/s)

v	equivalent plume velocity defined by equation (2.2.35)	(m/s)
ν	specific volume	(m^3/kg)
v_B	mean bubble velocity (Appendix C)	(m/s)
v_g	mean gas velocity defined by equation (2.2.37)	(m/s)
v_l	radial liquid velocity defined by equation (2.3.2)	(m/s)
v_r	slip velocity	(m/s)
$\hat{V}$	non-dimensional equivalent plume velocity ($=v_{/U}$)	(-)
V	volume	(m^3)
V_B	volume of bubble	(m^3)
V_c	critical volume	(m^3)
$\hat{V}_r$	non-dimensional slip velocity ($=v_{r/U}$)	(-)
w	vertical velocity	(m/s)
w_r	local slip velocity	(m/s)
We	Weber number	(-)
x	molal concentration	(-)
z	vertical component (= pressure head) (measured downwards from 10m above surface)	(m)
$\hat{Z}$	non-dimensional vertical component ($=z_{/L}$)	(-)
Z	compressibility factor defined by equation (3.2.25)	(-)
α	* void fraction defined by equation (2.2.79)	(-)
β	entrainment coefficient defined by equation (2.3.7)	(-)

* α void fraction defined by equation (2.2.18) (-)

β_N	bunsen absorption coefficient defined by equation (7.4.7)	(-)
γ	ratio of heat capacities ($=c_p/c_v$)	(-)
δ	increment	(-)
Δ	interval; increment	(-)
ε	surface area parameter (Appendix F)	(-)
ξ	vapour fraction	(-)
Θ_m	half-angle for spherical cap bubble (Appendix A)	(rad/deg)
λ	parameter relating width of velocity profile to that of void fraction	(-)
μ	viscosity (dynamic)	(kg/m.s)
ρ	density	(kg/m^3)
$\bar{\rho}$	density inside bubble (Appendix A)	(kg/m^3)
ϕ (T)	arbitrary function defined by equation (3.2.8)	(J/kg)
Φ	mass transfer rate per unit depth defined by equation (7.2.23)	(kg/m.s)

Subscripts

atm	atmospheric
B	bubble; back
c	centre-line values; critical; characteristic
eff	effective
g	gas
g_g	vapour phase of gas
g_l	liquid phase of gas
G	Gaussian

i	component
in	into control volume
inj	injection
l	liquid; local
o	source values; referring to ideal gas; stagnation point
out	out of control volume
p	plume; constant pressure
r	relative; radial
R	reduced conditions
s	solute; surface
sat	saturated
T	tophat

Superscripts

'	values within mixture (Appendix B); max (see eqn 3.2.18)
*	conditions at nozzle throat (Appendix C)

CHAPTER 1

Introduction

With the ever increasing attention being paid to achieving maximum recovery of energy from the oil and gas reserves of the world's oceans, many gas gathering pipeline networks are being constructed to transport the associated gas extracted with the oil to suitable landfalls. This gas was historically disposed of by fuelling offshore facilities and reinjection into the reservoir with the balance wastefully flared.

In addition to the associated gas gathering pipeline systems, present indications suggest that the exploitation of gas and gas condensate fields may be commercially attractive; thus an increase in subsea gas trunklines could reasonably be expected.

The hydrocarbon gas mixtures transported through the gas pipelines are generally maintained above super-critical pressure to prevent liquid dropout; should, however, any significant loss of mechanical integrity of the pipe occur, the escaping gases would instantaneously drop in temperature relative to the new pressure environment (dependent on water depth). For the majority of hydrocarbon mixtures this release temperature would be expected to be in the low cryogenic region of 120 to 180°K, dependent on vapour composition and water depth. From this point the mechanics, hydrodynamics and thermodynamic history of the subsequent vapour rise through the water column is not presently totally understood. Investigation of the evolution of this

gas, and in particular, determination of its characteristics upon reaching the surface is, therefore, desirable. It is important to be able to answer the question of when and where the gas will pass through its lower flammable limit, and hence define the potential hazard interaction length to adjacent platforms, shipping, helicopters etc. It is also necessary to calculate the density deficiency caused at the point of exit, and the area over which this extends.

The petrochemical industry, therefore, has an obvious need for a clearer understanding of this subject, to which this research is aimed. The objective is to develop a computer based mathematical model which can accurately describe the thermodynamic history of a subsea cryogenic gas release as it passes through the water column and describe the buoyancy, velocity, area and temperature of the gas plume on arrival at the sea surface.

The initial inspiration came from the work of Smith (1982), which involved a large release (of the order of 500kg/s) of pure methane from a high pressure pipeline (160 atmospheres) at a depth of 90m, these values being typical of those to be considered in this work. His work, although realising that immediately above the fractured pipe a turbulent gas jet would develop, concentrated on the rise of a single gas bubble.

Several papers have been written on the characteristics of rising gas bubbles, e.g. Davies & Taylor (1950), Moore (1959), Collins (1966), Parlange (1969), Wegener, Sundell and Parlange (1971), Wegener (1973), and Miksis, Vanden-Broeck & Keller (1982), to name but a few. The most

pertinent results to be taken from these papers are, in our case, the shape and velocity of the bubbles. Rosenberg (1950) observed that bubbles of less than 1.24mm in diameter were spherical, while from an equivalent diameter, d_e, of 1.24mm to 7mm they were deformed into an oblate spheroidal shape. For d_e between 7 and 17.6mm and a Reynolds number, Re, between 1600 and 5000 there was a transition stage from oblate spheroid to spherical cap, with almost rectilinear motion. For d_e > 17.6mm (Re > 5000) the bubbles formed were spherical caps and the motion rectilinear. From observations of bubble sizes, which will be commented on at a later stage, it may be assumed that the bubbles formed would be of a spherical cap shape, and the various authors propose a number of expressions for the rise velocity, each being dependent on the bubble size. In the light of our uncertainty towards the exact bubble size encountered, there seems little point in going into detail in deriving the rise velocity and so the formula quoted by Smith (1982), which is that adopted by Davies & Taylor (1950), and whose derivation is given, for completeness, in Appendix A, will be used.

The actual shape of the spherical cap bubble, denoted by the half-angle, Θ_m, and shown in Appendix A has been proposed by Davies & Taylor (1950), Collins (1966) and Wegener et al (1971) and all agree on a value of approximately 50°.

The work of Vanden-Broeck & Keller (1980) and Miksis, Vanden-Broeck & Keller (1981, 1982) was devoted to a

theoretical discussion of the deformation of gas bubbles, and their shape was calculated numerically. Results agreed favourably with experiments. Smith adopts two methods of determining the size of the bubbles produced, both of which predict basal diameters of the order of metres, in conflict with the more widely reported values of 1-2 cm.

The thermodynamic relationships used by Smith are adopted in the thesis, and it is the results of his sensitivity analyses, concluding that the surface release conditions would be determined largely by the bubble size and the heat transfer coefficient, which provoke the sensitivity analyses carried out in Chapter 6.

Clearly, with the large flow rates of gas we wish to consider (of the order of thousands of kilograms per second), giving rise to a multitude of closely packed bubbles, considering the evolution of a single bubble is not likely to model the situation adequately. (Use will still be made, however, of the rise velocity of a single bubble).

A natural progression is to assume that the escaping gas forms a buoyant plume. An extensive literature search was conducted, but material entirely relevant to the problem proved to be very scarce.

Morton, Taylor & Turner (1956), developed an integral theory for single-phase plumes by deriving conservation relations for volume, momentum and density deficiency. They then used experimental observations to fit the velocity and buoyancy profiles to Gaussian distributions. Morton (1959) allowed for the fact that there was a greater

lateral spread of heat than of vertical momentum, and hence, chose two separate Gaussian profiles to fit the velocity and temperature excess measurements. He also extended the work from a uniform environment to a stably-stratified one.

Cederwall & Ditmars (1970) then developed, along similar lines, an integral theory for two-phase bubble plumes, neglecting the contribution to the momentum flux from the turbulence. They also introduced the slip (or relative) velocity associated with the bubbles and the ratio, λ, of gas radius to velocity radius. λ is also referred to in the literature as the Schmidt number (see eg. Milgram (1983)). Kotsovinos & List (1977) attempted to improve the entrainment law suggested by Morton, Taylor and Turner (1956) by assuming a non-constant entrainment parameter. They also observed that it may not be possible to ignore the turbulent flux of buoyancy in a turbulent buoyant plume, which could account for as much as 40% of the transport in the plume.

The work of Brevik (1977) is closely linked to that of Kotsovinos & List (1977), but instead of an entrainment law, he used an energy conservation equation. Both he and Wilkinson (1979) devote their attention to two-dimensional bubble plumes arising from a line source, whereas we are really more interested in a single source, giving rise to an axisymmetric plume.

Unlike most other investigations, which are partly theoretical and partly experimental, Tsang (1984) gives a

purely theoretical set of criteria for modelling bubble plumes.

Haaland (1979), like Kotsovinos & List (1977) looked at the possibility of having a non-constant entrainment parameter. Over the past few years there has been an increase in interest in blowouts of oil/gas beneath the sea, and, as a result a number of papers began to appear on the subject e.g. Topham (1975), Fazal & Milgram (1980), Fanneløp & Sjøen (1980), Mundheim et al. (1981), Milgram & Van Houten (1982), Sjøen (1983) and Milgram (1983).

All the aforementioned papers consider the gas present to be some hydrocarbon mixture, but their experimental work is restricted to air escapes.

Although these papers deal with depths of the order of 10^2m, which is relevant to our model, because the gas involved is released along with an oil escape, the gas flow rate is one or two orders of magnitude less than that encountered in the pure gas escape which we are considering.

The majority of papers make reference to Gaussian distribution when describing characteristic profiles. Hussain & Siegel (1976), however, make use of Tophat profiles and Fazal & Milgram (1980) comment that experimental evidence suggests that short-time-averaged gas fraction distributions may be squarer than Gaussian. Goossens (1979) and Chesters, Van Doom & Goossens (1980) make no assumptions as to the shape of the profile: instead they talk of "equivalent" values of velocity and diameter, which the parameters would have were their profiles top-hat.

The dynamics of the present model, which are detailed in Chapter 2 will follow a similar argument.

Returning to our initial objective, to model the complete history would involve consideration of a number of distinct stages.

1. Initial Stages.
   - Pressure fall in pipeline
   - Expansion of gas at point of discharge
   - Contact area and heat transfer to the turbulent jet initially formed
   - Size and behaviour of bubbles formed at break-up of unstable jet

2. Behaviour throughout main part of rise.
   - Dynamics and thermodynamics of bubble plume rising through significant pressure range with evaporation of liquid phase of the gas
   - Contribution of direct contact heat transfer from the sea to the bubbles
   - Influence of large volume of water entrained by the rising gas

3. Final stages of the rise where surface effects become important and the entrained liquid flows off horizontally

4. The Final dilution of the gas above the sea surface - affected both by the state of the gas upon its arrival at the surface, and the prevailing conditions at that moment.

It is the second of these stages, known in the literature as the Zone of Established Flow, to which this work is directed. A few comments, however, will be made here on the other three stages.

Stage 1:

This is known as the Zone of Flow Establishment and will be important in determining the initial conditions for stage 2. To circumvent this problem a number of assumptions are made. Some of these are mentioned here while others will be introduced later.

(a) Due to the large pressure difference between the pipeline and the ambient pressure outside at the point of release, the escape will be at sonic velocity and the flow will continue at a uniform rate until the pressure in the pipe falls below a critical value (for methane this value is approximately 1.83 times the ambient hydrostatic pressure outside the pipe). After this the rate will be reduced, and the velocity will be subsonic.

(for details see Appendix B)

The most serious conditions are those which arise

immediately following the fracture, and so we are justified in making the assumption of a constant release rate of gas.

(b) The gas is assumed to undergo an adiabatic/isentropic expansion as it leaves the pipe. This represents the worst possible condition, with the greatest drop in temperature. In reality it will probably be somewhere between isentropic and isenthalpic, which would result in a smaller temperature drop.

For small flow rates this region does not extend very high. Fazal & Milgram (1980), quote a height of 5 - 10 times the exit diameter before the 2nd stage is reached. For an exit hole of about 0.4m (typical pipe size) this gives a height of 2 - 4m which is negligible over a total height of 100m. Even the presence of higher release rates should not increase this greatly and so in the model, this height will be ignored and the second stage will be assumed to commence at a depth equal to that of the gas escape.

Milgram (1983) also found that the exact height of stage 1 was unnecessary since the plume equations, which are valid throughout stage 2, are stable to perturbations in the initial conditions.

Stage 3:

This is known as the Zone of Surface Flow and has been considered in some detail by Goossens (1979), Fanneløp & Sjoen (1980)

Milgram & Van Houten (1982) and Milgram & Burgess (1984). The region extends from the upper surface to a depth about equal to the plume diameter. Most of the gas is to be found in the central region, spread over an area about equal to the plume cross-section with some of the bubbles (together with oil drops in the case of an oil/gas escape) surfacing further out.

The slight spreading of the gas by the horizontal movement of the liquid can only improve conditions existing if this stage is ignored: the density deficiency will be reduced and the increased area of contact between the bubbles and the warm surface water will increase the heat transfer and thus increase the gas temperature.

Stage 4:

We shall just mention a few of the factors, suggested by Smith (1982), which would aid the gas dispersion, should it not be positively buoyant.

(a) Heat transfer to the bubbles from the significantly warmer air.

(b) High gas velocity at the surface will tend to project the gas into the atmosphere so that dilution occurs at heights of perhaps 10's of metres.

(c) Heat transfer from the sea-surface to the cloud is enhanced by sea-surface movement.

(d) Accidents (due to e.g. anchor dragging) are more likely in severe weather which will increase speed and amount of atmospheric mixing of the gas cloud.

A very detailed piece of work pertaining to stage 4, sponsored by the U.S. Coast Guard, has just appeared, see Havens & Spicer (1985 a,b,c): this work could easily be used in conjunction with the present to find conditions after the surface escape of gas.

Concentrating on stage 2, Chapter 2 is concerned with deriving a set of dynamic equations from a set of conservation laws.

The initial conditions will be those that arise from stage 1, and it will be assumed that the equations of Chapter 2 are valid all the way to the surface.

Chapter 3 is devoted to the thermodynamics of the model. This does not seem to have been covered in the literature. All references quoted assume an isothermal rise, except for Fanneløp & Sjøen (1980), Fazal & Milgram (1980) and Milgram & Van Houten (1982) who do mention a non-isothermal rise but do not go into any details on the mechanisms involved. In view of the fact that most of the other papers refer to air, an isothermal rise is probably the correct assumption since there will be no dramatic pressure drop, with associated temperature drop, as the air leaves the pipe.

Chapter 4 combines the dynamics and thermodynamics into a computer based mathematical model.

Chapter 5 is concerned with reviewing the experimental work carried out, and assessing how well the observations agree with the numerical predictions.

As mentioned previously, Chapter 6 looks at the sensitivity analyses of bubble size and heat transfer coefficient.

Wegener, Sundell & Parlange (1971) observed spherical cap bubbles of volume 7.5-151 cm^3 in an experiment with air bubbles in a 1.5m tank. Relating this to the "equivalent" diameter which a bubble would have were it spherical we have diameters of 2.43 - 6.61cm. Milgram (1983) observed bubbles of volume 0.01 to 33cm^3 for air bubble plumes in water, with the majority having volumes in the range 0.02 to 0.5cm^3, while Clift, Grace & Weber (1978) quote bubble sizes of 1-2cm, a similar range to Fanneløp & Sjøen (1980) and Topham (1975). It would seem, therefore, that the bubbles formed are most likely to have an equivalent diameter of the order of a few centimetres. The occurrence of larger bubbles, however, could have a dangerous effect on the surface conditions, since for these both in terms of contact area and contact time the contribution of direct warming from the sea water will be reduced. It is important, therefore, to investigate the scale of this effect.

There have been widely varying suggestions as to the value of the heat transfer coefficient, from 8$W/m^2°K$ by Smith (1984) to 100-200 $W/m^2°K$ by L'Ecuyer in his paper "Heat Transfer to a gas bubbling through liquid". The

purpose of the sensitivity analysis is to try to allow predictions to be made for a heat transfer coefficient lying between certain limits, thus removing the requirement of an exact value.

Chapter 7 is an extension to the model to allow for mass transfer through dissolution of the gas in the water. This is done by adding a term to the mass balance equation of the gas and introducing another mass balance equation for the solute. The mass transfer coefficient is discussed, and the necessary adjustments to the program are noted.

A further extension would be to allow for loss of mass through hydrate formation. This has been considered by Topham (1978, 1984a, 1984b) for both the single bubble and the bubble plume. His method is to obtain a rate equation which is then included as an extra term in the equation of mass balance.

His main findings were that the hydrate formation is closely linked to the small scale bubble characteristics such as bubble size and shape. Thus, the behaviour is sensitive to the actual choice of plume model and Topham points out that present models impose severe restrictions in this respect.

Hydrates can exist for natural gas at depths below 200m, while for total hydrate formation Topham concludes that depths of 500m are necessary for single bubbles and at least 800m in the case of a bubble plume, due to the enhanced velocity within the plume.

At present, the depths of interest are approximately

100m, so hydrate formation is not considered. As drilling extends into deeper waters, however, clearly hydrate formation could have a pronounced effect on the state of the gas.

CHAPTER 2

DYNAMICS OF GAS ESCAPE

2.1 Basis for Plume Model

To obtain some starting point for the model, the following assumptions were made.

1. Gas release is from a single source; i.e. it is assumed that the shorter limb of the pipeline would not maintain a continuing release.

2. The gas forms an unconfined buoyant plume.

3. Axisymmetric and non-rotating geometry.

4. Gas concerned is Methane, rather than a multi-component mixture - this simplifies greatly the thermodynamics, and should still give a good indication of the true situation as methane will be the major constituent of the escaping gas. (Typical values, quoted by Britoil, for North Sea gas are 76.10%, 75.35%, 62.28%, 59.58%.)

Using the model defined in Chesters et al. (1980) and Goossens thesis (1979) as a basis, we note the following:

1. No assumption is made as to the radial profiles of the liquid velocity or gas fraction. Instead the local mass and momentum fluxes are used to define an equivalent

diameter d and velocity v which the plume would have were its velocity profile square.

2. No assumption is made as to the contribution to the total momentum flux from the mean flow and the fluctuating velocity component.

Two basic modifications have been incorporated, and the model reformulated.

1. Due to the dramatic decrease in temperature of the gas as it exits the pipe, it will enter the two-phase region and so exist as a mixture of liquid and vapour. Instead of requiring the gas density, ρ_g, and gas velocity, v_g, as in the basic two-phase model mean values for the two-phase bubbles, ρ_B and v_B must be substituted. Using some simple ideas from the continuum methods for mixtures (Appendix C) ρ_B can be expressed in terms of the densities of the two phases, and it will also be assumed that $v_B = v_g$.

2. The expansion is no longer assumed to be isothermal. This introduces the need for thermodynamics, which will be considered in Chapter 3.

2.2 Derivation of the Plume Equations

The plume may be thought of as existing in three distinct stages.

1. Close to the gas-injection plane, the liquid has no vertical motion except in the immediate vicinity of individual bubbles.

2. This wake liquid shares its momentum with adjacent liquid and at some critical height all the liquid between the bubbles is in upward motion. This is the beginning of the second stage when the flow can be truly thought of as a "plume".

3. The plume reaches the surface and the entrained liquid flows off horizontally.

Stage (1) may be thought of as being short in duration but establishing the initial conditions for stage (2). Stage (3) is mentioned in the introduction, but is ignored in the development of the model.

The evolution of the plume is determined by:

1. An increase of momentum flux which leads to an initial contraction in the plume width.

2. An increase in mass flux which then dominates to create an expansion in the plume width.

CONSERVATION EQUATIONS

These are derived by consideration of a control volume element of the plume.*

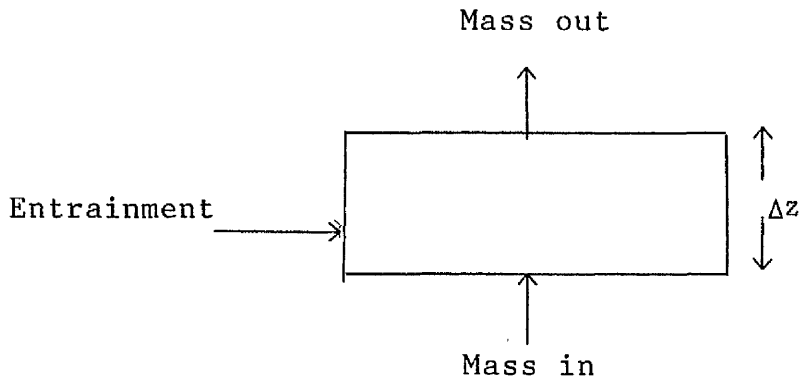

CONSERVATION OF MASS

GAS

Under the assumption of NO MASS TRANSFER, the mass flux of gas, $\dot{m}_g$, will be constant. This may be written as

$$\dot{m}_{g_{out}} = \dot{m}_{g_{in}}$$

where a dot above a symbol will denote a rate, or flux. Thus,

$$\frac{d\dot{m}_g}{dz} = 0 \qquad (2.2.1)$$

which implies

$$\dot{m}_g = \dot{m}_{g_o} \qquad (2.2.2)$$

where $\dot{m}_{g_o}$ is the initial mass flux.

* where the vertical parts of the control surface lie outside the plume.

LIQUID

Letting $\dot{m}_l$ be the mass flux of liquid we can write

$\dot{m}_{l_{out}}$ = $\dot{m}_{l_{in}}$ + rate of liquid mass entrainment into control volume

Taking the limit as $\Delta z \to 0$

$$\frac{d\dot{m}_l}{dz} = - \text{Rate of entrainment}$$

ENTRAINMENT LAW

Assuming that the radial flow of liquid into the plume will be proportional to the vertical plume velocity, the turbulent entrainment law for single-phase axisymmetric plumes suggested by Turner (1969) is

$$\frac{d\dot{m}_l}{dz} = - K \rho_l u_l d_p \qquad (2.2.3)$$

where u_l = local plume velocity

d_p = local plume diameter

and K is a constant, assumed to be the same to within experimental error as that for single-phase free jets.

From experiment work Ricou and Spalding (1961) found that, in terms of the equivalent velocity, v, and the equivalent diameter, d, the entrainment law may be written as

$$\frac{d\dot{m}_l}{dz} = - K_1 \rho_l v d \qquad (2.2.4)$$

where

$$K_1 = 0.25$$

A similar expression was derived by Morton, Taylor and Turner (1956), but with $K_1 = 0.26$

In our case, the presence of the gas bubbles will increase the diameter, and hence the circumference of the plume, thus increasing the area of entraining surface. This may be accounted for by restating (2.2.4) as

$$\frac{\dot{dm}_l}{dz} = -k_1 \rho_l v d_{eff} \qquad (2.2.5)$$

where d_{eff} is defined in terms of the equivalent diameter in the absence of gas, d, and the cross-sectional area of the gas, A_g, by

$$\frac{\pi d_{eff}^2}{4} = \frac{\pi d^2}{4} + K_2 A_g, \; K_2 = 0(1) \text{ constant} \qquad (2.2.6)$$

K_1 may also be altered, but at this stage we assumed that $K_1 = 0(0.25)$. (2.2.7)

CONSERVATION OF MOMENTUM

Consideration of the forces acting on the control volume yields

$$\text{Downward force} = \text{weight of control volume}$$
$$= g[\rho_l A_l + \rho_B A_g] \; (-\Delta z) \qquad (2.2.8)$$

where, as noted at beginning of chapter, ρ_B refers to the mean density of the two-phase bubbles.

where A_l, A_g refer to the cross sectional areas of liquid and gas respectively and g denotes the acceleration due to gravity.

Similarly,

$$\text{Upward force} = \text{Buoyancy} = \text{weight of displaced liquid} = g[\rho_l (A_l + A_g)] (-\Delta z) \qquad (2.2.9)$$

Using the relation

$$\text{Force} = \text{Rate of change of momentum} \qquad (2.2.10)$$

and calculating the net force from (2.2.8) and (2.2.9) we obtain

$$\dot{\Delta M} = g(\rho_l - \rho_B) A_g (-\Delta z) \qquad (2.2.11)$$

where $\dot{M}$ denotes the momentum flux.

Taking the limit as $\Delta z \to 0$

$$\frac{d\dot{M}}{dz} = -g(\rho_l - \rho_B) A_g \qquad (2.2.12)$$

In this derivation the following assumptions have been made.

1. The viscous and Reynolds stresses on the vertical parts of the control surface may be neglected as this part of the surface lies outside the zone of large velocity gradients.

2. The extra forces exerted on the horizontal portions of

the control surface due to departures from the hydrostatic pressure, $\rho_1 g z$, together with the surface tension force on bubbles cut by the surface may also be neglected.

It is now necessary to write down expressions for the mean mass and momentum fluxes. Before writing these in terms of the equivalent values, v and d we shall consider the more generalised situation.

TIME AVERAGING

(Details of averaging techniques may be found in Ishii (1975)) This has the effect of

1. Smoothing out the turbulent fluctuations associated with the two-phase flow.

2. Transforming the two phases which alternately occupy a given point into two weighted continua which exist simultaneously at this point.

As is customary for single-phase flow and is also possible for two-phase flow, density fluctuations are neglected

i.e.

$$\rho_1 = \bar{\rho}_1 \qquad (2.2.13)$$

and so we only consider the velocity. We can express the liquid velocity, u_1, in terms of its mean and fluctuating component as follows

$$u_1 = \bar{u}_1 + \tilde{u}_1 \qquad (2.2.14)$$

where the overbar indicates the average over the time the liquid is present,

i.e.
$$\bar{u}_1 = \frac{1}{\Delta t_1} \int_{\Delta t_1} u_1 \, dt \qquad (2.2.15)$$

We use the above idea to write down expressions for the mean mass and momentum fluxes.

MASS FLUX

For the liquid, at a given point

$$\text{mass flux/area} = \begin{cases} \rho_1 u_1 & \text{if liquid is present} \\ 0 & \text{if no liquid is present} \end{cases} \qquad (2.2.16)$$

Thus, over a time increment, Δt

$$\text{mean mass flux} = \frac{1}{\Delta t} \int_{\Delta t_1} \rho_1 u_1 dt + \frac{1}{\Delta t} \int_{\Delta t_g} 0 \, dt$$

$$= \frac{\Delta t_1}{\Delta t} \rho_1 \underbrace{\frac{1}{\Delta t_1} \int_{\Delta t_1} u_1 \, dt}_{\bar{u}_1} \qquad (2.2.17)$$

where Δt_1, Δt_g refer respectively to the time the liquid and the gas is present but,

$$\text{if } \hat{\alpha} = \text{fraction of time gas present} = \frac{\Delta t_g}{\Delta t} \qquad (2.2.18)$$

then

$$\text{mean mass flux at a point} = \rho_l(1-\hat{\alpha})\,\bar{\bar{u}}_l \qquad (2.2.19)$$

Integrating across the plume gives the mass flux at a given depth

$$\dot{m}_l = \rho_l \int_0^\infty (1-\hat{\alpha})\,\bar{\bar{u}}_l\, 2\pi r_a\, dr_a \qquad (2.2.20)$$

Similarly for the gas

$$\dot{m}_g = \rho_g \int_0^\infty \hat{\alpha}\,\bar{\bar{u}}_g\, 2\pi r_a\, dr_a \qquad (2.2.21)$$

where the double overbar denotes an average taken over the time the gas is present.

MOMENTUM FLUX

In this case, for liquid at a certain point

$$\text{Momentum flux / area} = \begin{cases} \rho_l u_l^2 & \text{if liquid present} \\ 0 & \text{otherwise} \end{cases} \qquad (2.2.22)$$

giving

$$\text{mean value of Momentum flux at a point} = \frac{1}{\Delta t}\int_{\Delta t_l} \rho_l u_l^2\, dt + \frac{1}{\Delta t}\int_{\Delta t_g} 0\, dt$$

$$= \frac{\Delta t_1}{\Delta t} \rho_1 \frac{1}{\Delta t_1} \underbrace{\int_{\Delta t_1} u_1^2 \, dt}_{\overline{u_1^2}}$$

$$= \rho_1 (1-\hat{\alpha}) \overline{u_1^2} \qquad (2.2.23)$$

and integrating across plume we have that the mean Momentum flux at a given height is given by,

$$\dot{M}_1 = \rho_1 \int_0^\infty (1-\hat{\alpha}) \overline{u_1^2} \, 2\pi r_\alpha \, dr_\alpha \qquad (2.2.24)$$

$$= \bar{\dot{M}}_1 + \tilde{\dot{M}}_1 \qquad (2.2.25)$$

where

$$\bar{\dot{M}}_1 = \rho_1 \int_0^\infty (1-\hat{\alpha}) \overline{u}_1^2 \, 2\pi r_\alpha \, dr_\alpha \qquad (2.2.26)$$

$$\tilde{\dot{M}} = \rho_1 \int_0^\infty (1-\hat{\alpha}) \overline{\tilde{u}_1^2} \, 2\pi r_\alpha \, dr_\alpha \qquad (2.2.27)$$

the equality arising from the fact that

$$\overline{u_1^2} = \overline{u}_1^2 + \overline{\tilde{u}_1^2} \qquad (2.2.28)$$

(Appendix D)

As for the mass flux, we can express the mean Momentum flux for the gas

$$\dot{M}_g = \rho_g \int_0^\infty \hat{\alpha}\, \overline{u_g^2}\; 2\pi r_a\, dr_a \qquad (2.2.29)$$

which again may be split into two parts, one arising from the mean flow and the other due to the fluctuating component of the velocity.

For single-phase free turbulent jets, it has been shown that $\tilde{\dot{M}}_l \simeq 0.1\, \bar{\dot{M}}_l$ so that concentrating on the mean velocity should give reasonable results. In the case of two-phase buoyant plumes the two terms may, at least initially, be of the same order and so neglect of $\tilde{\dot{M}}_l$ would lead to an apparent loss of momentum.

Experimental results of Chesters et al (1980) show that $\bar{\dot{M}}_l$ may be as little as 40% of the total momentum flux, $\dot{M}_l$, near the base of the plume although the ratio $\bar{\dot{M}}_l/\dot{M}_l$ tends to rise to around 0.8 further up the plume.

Chesters et al (1980) neglected the momentum of the gas which was negligible in comparison to that of the liquid. In refining the equations, however, to take account of the gas itself existing in two phases, it is not necessarily obvious that the momentum of the gas bubbles may be ignored and so this term will be retained.

Combining equations (2.2.24) and (2.2.29) yields

$$\dot{M} = 2\pi\rho_l \int_0^\infty (1-\hat{\alpha})\, \overline{u_l^2}\; r_a dr_a + 2\pi\rho_g \int_0^\infty \hat{\alpha}\, \overline{u_g^2}\; r_a\, dr_a \qquad (2.2.30)$$

Neglecting the contributions from the fluctuating

components (2.2.30) reduces to

$$\dot{M} = 2\pi \rho_l \int_0^\infty (1-\hat{\alpha})\, \bar{u}_l^{\,2}\, r_\infty dr_\infty + 2\pi \rho_g \int_0^\infty \hat{\alpha}\, \bar{\bar{u}}_g^{\,2}\, r_\infty\, dr_\infty \quad . \quad (2.2.31)$$

We do not, however, use equations (2.2.20), (2.2.21) and (2.2.31) directly.

In terms of the equivalent velocity, v, and diameter, d, assuming negligible gas fraction, $\hat{\alpha}$, we can write down the following expressions for the mean mass and momentum fluxes.

$$\dot{m}_l = \rho_l \frac{\pi d^2}{4} v \quad (2.2.32)$$

$$\dot{M}_l = \rho_l \frac{\pi d^2}{4} v^2 = \dot{m}_l v \quad (2.2.33)$$

which give v, d in terms of these fluxes as

$$d \equiv \frac{2\dot{m}_l}{\sqrt{\pi \rho_l \dot{M}_l}} \quad (2.2.34)$$

$$v = \frac{\dot{M}_l}{\dot{m}_l} \quad (2.2.35)$$

SLIP VELOCITY

We re-express the gas velocity, u_g, as

$$u_g = u_l + u_r \quad (2.2.36)$$

where u_r = slip velocity

= relative velocity of the bubbles with respect to the surrounding liquid

Similarly, in terms of v, we may express the mean gas velocity at a given cross-section, v_g, as

$$v_g = K_3 v + v_r \qquad K_3 = O(1) \qquad (2.2.37)$$

where $K_3 v$ = mean velocity of liquid in which the bubbles are situated

v_r = mean relative velocity of the bubbles with respect to the surrounding liquid at a given cross-section

and v_r = u_r if we assume u_r is constant across the plume.

Assumptions

1. Except initially where the gas fraction may be high, v_r may be approximated by the free rise velocity of a single bubble.

2. v_r is related to the size of the bubbles by

$$v_r = \sqrt{5 d_e} \qquad (2.2.38)$$

where d_e is the equivalent bubble diameter (see Appendix A).

Observations on bubble size have already been mentioned in Chapter 1. Using (2.34) they predict velocities of 20-30 cm/s. Haberman & Morton (1954) suggest a slip velocity of 0.28m/s for natural gas. Brevik (1977) infers that v_r should be 0.4m/s, which is somewhat larger than the normal free rise velocity of a single bubble but he feels that due to the strong turbulence in the air-bubble plume the two situations are not directly comparable. He does, however, conclude that the results are not sensitive to small chances in v_r, a point also raised by Milgram (1983). He used a value of v_r = 0.35m/s, based on his observations of bubble size together with the correlation of Haberman & Morton (1954). He found that the effect of varying the value of v_r by 0.05m/s was to produce a change in the vertical plume velocity of about 3%. Neglecting the slip velocity altogether, however, gave a variation of 20%.

It seems safe to say, therefore, that the exact value of v_r is not essential, but it cannot be discounted altogether.

The present model will in general use a bubble size to give $v_r \simeq 0.3$m/s.

In terms of the average gas velocity, v_g, we may write the following expression for the mean mass flux of gas.

$$\dot{m}_g = \rho_B \, v_g \, A_g \qquad (2.2.39)$$

and similarly, for the momentum flux

$$\dot{M}_g = \rho_B \, v_g^2 A_g = \dot{m}_g \, v_g \qquad (2.2.40)$$

Using equations (2.2.5) and (2.2.32), and assuming ρ_l is constant

$$\frac{\pi}{4}\rho_l\left[2dv\frac{d(d)}{dz}+d^2\frac{dv}{dz}\right]=-K_1\rho_l v d_{eff} \qquad (2.3.41)$$

while equations (2.2.2), (2.2.12) and (2.2.33) yield

$$\frac{\pi}{4}\rho_l\left[2dv^2\frac{d(d)}{dz}+2d^2v\frac{dv}{dz}\right]+\dot{m}_{g_o}\frac{dv}{dz}g=-g(\rho_l-\rho_B)A_g \qquad (2.2.42)$$

using eqn (2.2.6) to substitute for d_{eff},

$$d_{eff}=\left[d^2+\frac{4K_2}{\pi}A_g\right]^{\frac{1}{2}} \qquad (2.2.43)$$

and eqn (2.2.37) to substitute for v_g

$$\frac{dv_g}{dz}=K_3\frac{dv}{dz}+\frac{dv_r}{dz} \qquad (2.2.44)$$

we can then rewrite (2.2.41) and (2.2.42) as

$$\frac{\pi}{4}\rho_l\left[2dv\frac{d(d)}{dz}+d^2\frac{dv}{dz}\right]=-K_1\rho_l vd\left[1+\frac{4K_2A_g}{\pi d^2}\right]^{\frac{1}{2}} \qquad (2.2.45)$$

$$\frac{\pi}{4}\rho_l 2dv^2\frac{d(d)}{dz}+\left[\frac{\pi}{4}\rho_l 2d^2v+K_3\dot{m}_{g_o}\right]\frac{dv}{dz}+\dot{m}_{g_o}\frac{dv_r}{dz}$$

$$=-g(\rho_l-\rho_B)A_g \qquad (2.2.46)$$

Subtracting v x (2.2.45) from (2.2.46) gives

$$\left[\frac{\pi}{4}\rho_1 d^2 v + K_3 \dot{m}_{g_o}\right] \frac{dv}{dz} = -g(\rho_1 - \rho_B)A_g - \dot{m}_{g_o} \frac{dv_r}{dz}$$

$$+ K_1 \rho_1 v^2 d \left[1 + \frac{4K_2 A_g}{\pi d^2}\right]^{\frac{1}{2}} \qquad (2.2.47)$$

subtracting $(2v + \frac{K_3 \dot{m}_{g_o}}{\frac{\pi}{4}\rho_1 d^2})$ x (2.2.45) from (2.2.46) gives

$$-2 \frac{\pi}{4} \rho_1 v^2 d \frac{d(d)}{dz} - \frac{\pi}{4}\rho_1 v \frac{2dK_3 \dot{m}_{g_o}}{\rho_1 \frac{\pi}{4} d^2} \frac{d(d)}{dz} + \dot{m}_{g_o} \frac{dv_r}{dz}$$

$$= - g (\rho_1 - \rho_B)A_g + K_1 \rho_1 v(2v + \frac{K_3 \dot{m}_{g_o}}{\rho_1 \pi d^2/4}).$$

$$d\left[1 + \frac{4K_2 A_g}{\pi d^2}\right]^{\frac{1}{2}} \qquad (2.2.48)$$

i.e.

$$\frac{d(d)}{dz} = \frac{g(\rho_1 - \rho_B) A_g + \dot{m}_{g_o} \frac{dv_r}{dz} - K_1 \rho_1 dv (2v + \frac{K_3 \dot{m}_{g_o}}{(\pi \rho_1 d^2/4)}) \left[1 + \frac{4K_2 A_g}{\pi d^2}\right]^{\frac{1}{2}}}{(2\rho_1 \pi \frac{dv^2}{4} + \frac{2v}{d} K_3 \dot{m}_{g_o})} \qquad (2.2.49)$$

and

$$\frac{dv}{dz} = \frac{-g(\rho_1 - \rho_B) A_g - \dot{m}_{g_o} \frac{dv_r}{dz} + K_1 \rho_1 v^2 d \left[1 + \frac{4K_2 A_g}{\pi d^2}\right]^{\frac{1}{2}}}{\left(\rho_1 \pi \frac{d^2 v}{4} + K_3 \dot{m}_{g_o}\right)} \qquad (2.2.50)$$

Using the relations

$$A_g = \frac{\dot{m}_{g_o}}{\rho_B v_g} \qquad (2.2.51)$$

and $$v_g = K_3 v + v_r \qquad (2.2.52)$$

we finally arive at

$$\frac{d(d)}{dz} = \frac{g \dot{m}_{g_o} \frac{(\rho_1 - \rho_B)}{\rho_B (K_3 v + v_r)} + \dot{m}_{g_o} \frac{dv_r}{dz} - K_1 \rho_1 dv^2 \left[2 + \frac{K_3 \dot{m}_{g_o}}{\rho_1 \pi d^2 v/4}\right] \left[\frac{1 + 4K_2 \dot{m}_{g_o}}{\rho_B \pi d^2 (K_3 v + v_r)}\right]^{\frac{1}{2}}}{2\rho_1 \pi \frac{dv^2}{4} \left[1 + \frac{K_3 \dot{m}_{g_o}}{\rho_1 \pi d^2 v/4}\right]} \qquad (2.2.53)$$

and

$$\frac{dv}{dz} = \frac{-g \frac{\dot{m}_{g_o} (\rho_1 - \rho_B)}{\rho_B (K_3 v + v_r)} - \dot{m}_{g_o} \frac{dv_r}{dz} + K_1 \rho_1 dv^2 \left[1 + \frac{4K_2 \dot{m}_{g_o}}{\pi \rho_B d^2 (K_3 v + v_r)}\right]^{\frac{1}{2}}}{\rho_1 \pi \frac{d^2 v}{4} \left[1 + \frac{K_3 \dot{m}_{g_o}}{\rho_1 \pi d^2 v/4}\right]} \qquad (2.2.54)$$

Equations (2.2.53) and (2.2.54) form a system of ordinary differential equations, which may be solved numerically.

CONSIDERATION OF TERM $\frac{dv_r}{dz}$

With v_r given by equation (2.2.38) we have

$$\frac{dv_r}{dz} = \sqrt{\frac{5}{4d_e}} \frac{d(d_e)}{dz} \qquad (2.2.55)$$

The value of this term is, therefore, dependent on the growth pattern of the bubbles in the plume. This has not been fully analysed yet, and so to make the equations as simple as possible it has been assumed that the bubble size does not grow, but rather that as the volume increases the bubbles break up into a larger number of similarly sized bubbles.

Hence

$$\frac{dv_r}{dz} = 0 \qquad (2.2.56)$$

and this term may be omitted from eqns (2.2.53) and (2.2.54).

Perhaps a more realistic assumption would be that the bubbles increased to some critical volume, V_c, say, where they then split to form two bubbles, each of volume $\frac{1}{2}V_c$, which would then follow the same pattern of expanding and splitting. Fanneløp & Sjøen (1980) note that individual bubbles will grow to a critical size, break up, and grow

again.

Sevik & Park (1973) and Lewis & Davidson (1982) are concerned with the splitting up of bubbles, and both papers propose a critical Weber number, We, at which this will occur. The Weber number can be thought of as a ratio of pressure forces to surface tension force. This, however, has not been investigated further and so the assumption (2.2.56) will stand.

Making our simplification, however, reduces the equations to

$$\frac{d(d)}{dz} = \frac{g\dot{m}_{g_o}(\rho_1 - \rho_B) - k_1\rho_1 dv^2\left[2 + \frac{K_3\dot{m}_{g_o}}{\rho_1\pi d^2 v/4}\right]\left[1 + \frac{4K_2\dot{m}_{g_o}}{\rho_B\pi d^2(K_3v+v_r)}\right]^{\frac{1}{2}}}{2\rho_1\frac{\pi dv^2}{4}\left[1 + \frac{K_3\dot{m}_{g_o}}{\rho_1\pi d^2 v/4}\right]} \qquad (2.2.57)$$

$$\frac{dv}{dz} = \frac{-g\dot{m}_{g_o}(\rho_1-\rho_B) + K_1\rho_1 dv^2\left[1 + \frac{4K_2\dot{m}_{g_o}}{\rho_B\pi d^2(K_3v+v_r)}\right]^{\frac{1}{2}}}{\rho_1\frac{\pi d^2 v}{4}\left[1 + \frac{K_3\dot{m}_{g_o}}{\rho_1\pi d^2 v/4}\right]} \qquad (2.2.58)$$

If we let

$$h = z_o - z = \text{height above injector} \qquad (2.2.59)$$

$$\frac{d}{dh} = \frac{-d}{dz} \qquad (2.2.60)$$

and so, equations (2.2.57) and (2.2.58) become

$$\frac{d(d)}{dh} = \frac{-\dot{m}_{g_o}(\rho_1 - \rho_B) + K_1\rho_1 dv^2\left[2 + \frac{K_3\dot{m}_{g_o}}{\rho_B(K_3v+v_r)}\right]\left[1+\frac{4K_2\dot{m}_{g_o}}{\rho_1\pi d^2v/4}\right]^{\frac{1}{2}}}{2\rho_1\frac{\pi dv^2}{4}\left[1 + \frac{K_3\dot{m}_{g_o}}{\rho_B\pi d^2(K_3v+v_r)}\right]} \qquad (2.2.61)$$

$$\frac{dv}{dh} = \frac{\dot{m}_{g_o}(\rho_1-\rho_B) - K_1\rho_1 dv^2\left[1 + \frac{4K_2\dot{m}_{g_o}}{\rho_B\pi d^2(K_3v+v_r)}\right]^{\frac{1}{2}}}{\rho_1\frac{\pi d^2v}{4}\left[1 + \frac{K_3\dot{m}_{g_o}}{\rho_1\pi d^2v/4}\right]} \qquad (2.2.62)$$

INITIAL CONDITIONS

As previously indicated, these are determined by the transition from stage 1 to stage 2, whereby all the liquid between the bubbles first attains an upward velocity. Thus, the liquid immediately surrounding the bubbles moves with velocity of the order of v_r, while the velocity of the liquid exactly between the bubbles is almost zero. We, therefore, make the assumption

$$v_o = K_4 v_r \qquad K_4 = O(0.5) \qquad (2.2.63)$$

for the initial equivalent plume velocity, v_o.

The other initial condition we require to solve the system of ordinary differential equations is d_o.

Again following Chesters et.al (1980), Goossens (1979), if we assume the bubbles rise rectilinearly in stage 1, we shall have

$$(d_{eff})_o = d_{inj} \text{ (the width of the gas injection device)} \qquad (2.2.64)$$

and so

$$\pi \frac{d_{inj}^2}{4} = \pi \frac{d_o^2}{4} + K_2 A_g \qquad (2.2.65)$$

Now

$$A_{g_o} = \frac{\dot{m}_g}{\rho_{g_o}(K_3 v_o + v_r)} \qquad (2.2.66)$$

and so

$$\begin{aligned} d_o^2 &= d_{inj}^2 - \frac{4K_2}{\pi} A_{g_o} \\ &= d_{inj}^2 - \frac{4K_2 \dot{m}_g}{\rho_{g_o} \pi v_r (1+K_3K_4)} \qquad (2.2.67) \\ &= d_{inj}^2 - \frac{4K_2 G_o}{\pi v_r (1+K_3K_4)} \qquad (2.2.67) \end{aligned}$$

where G_o denotes the initial volumetric flow rate. Using this value of d_o, however, would lead to problems for the case we are interested in where the flow rates, G_o, are high.

As may be seen from eqn (2.2.67), there are two limits

1. When second term on RHS ->0, we have

$$d_o = d_{inj} \qquad (2.2.68)$$

This is the case for very small gas flow rates

2. When second term on RHS -> d_{inj}^2, we have

$$d_o = 0 \qquad (2.2.69)$$

This is the case when the injector area is all covered with gas while no liquid is entrained inside the gas jet, and occurs for high gas flow rates.

Thus, it is this second limit which causes problems in our case.

It can be seen that if the diameter of gas injection or initial relative velocity of the bubbles (which is related to the bubble size) is too small or the rate of gas flow is too great then the second term will be larger than the first term on the RHS of (2.2.67) and so the equation cannot be used to determine the initial value d_o.

Since d_o ->0 as the gas flow rate increases, it seems reasonable to assume for our cases of high flow rates that $d_o = 0$.

It should be noted that the gas jet formed will break up into a bubble plume and start to entrain liquid at some hight above the injector which will be much greater than in the case of bubbles forming immediately at the lower gas flow rates.

There is evidence (Kobus, 1973), that the overall plume behaviour is not altered, and in the light of our depths of

interest being large (i.e. $0(10^2)$m), we shall still ignore the height of stage 1.

Upon returning to the system of equations (2.2.61), (2.2.62), it can be seen that due to the way the diameter appears, putting $d_o = 0$ would cause problems.

If, however, we modify the system by expressing d in terms of the cross sectional area of the liquid, A_1, defined by

$$A_1 = \frac{\pi d^2}{4} \tag{2.2.70}$$

then

$$\frac{dA_1}{dz} = \frac{\pi}{2} d \frac{d(d)}{dz} \tag{2.2.71}$$

and,

$$\frac{d(d)}{dz} = \frac{\dot{m}_{g_o}(\rho_1 - \rho_B)}{\rho_B(K_3 v + v_r)} - \frac{K_1 \rho_1 dv^2 [1+4K_2\dot{m}_{g_o}/\pi d^2 \rho_B(K_3 v+v_r)]^{\frac{1}{2}} [2+K_3\dot{m}_{g_o}/\rho_1 \pi d^2 v/4]}{2\rho_1 \pi dv^2/4 [1 + K_3\dot{m}_{g_o}/\rho_1 \pi d^2 v/4]}$$

$$= \frac{(\rho_1-\rho_B)\dot{m}_{g_o}}{\rho_B(K_3 v+v_r)} - \frac{K_1\rho_1 dv^2 [1 + K_2\dot{m}_{g_o}/A_1\rho_B(K_3 v+v_r)]^{\frac{1}{2}} [2 + K_3\dot{m}_{g_o}/\rho_1 A_1 v]}{D}$$

where $D = 2\rho_1 v^2 \frac{A_1}{d}\left[1 + \frac{K_3 \dot{m} g_o}{\rho_1 A_1 v}\right]$

$$= \frac{\frac{(\rho_1 - \rho_B) g \dot{m} g_o}{\rho_B (K_3 v + v_r)} d - K_1 \rho_1 d^2 v^2 \left[1 + \frac{K_2 \dot{m} g_o}{A_1 \rho_B (K_3 v + v_r)}\right]^{\frac{1}{2}} \left[2 + \frac{K_3 \dot{m} g_o}{\rho_1 A_1 v}\right]}{2\rho_1 v^2 A_1 \left[1 + \frac{K_3 \dot{m} g_o}{\rho_1 A_1 v}\right]}$$

Hence,

$$\frac{\pi}{2} d \frac{d(d)}{dz} = \frac{\pi d^2}{2} \frac{(\rho_1 - \rho_B) g \dot{m} g_o}{\rho_B (K_3 v + v_r)} - K_1 \rho_1 d^2 v^2 \frac{\frac{\pi d}{2}\left[1 + \frac{K_2 \dot{m} g_o}{A_1 \rho_B (K_3 v + v_r)}\right]^{\frac{1}{2}} \left[2 + \frac{K_3 \dot{m} g_o}{\rho_1 A_1 v}\right]}{2\rho_1 v^2 A_1 \left[1 + \frac{K_3 \dot{m} g_o}{\rho_1 A_1 v}\right]}$$

$$\Rightarrow \frac{dA_1}{dz} = \frac{2A_1 (\rho_1 - \rho_B) g \dot{m} g_o}{\rho_B (K_3 v + v_r)} - \frac{2K_1 \rho_1 v^2 A_1 \left(\frac{4A_1}{\pi}\right)^{\frac{1}{2}} \left[1 + \frac{K_2 \dot{m} g_o}{A_1 \rho_B (K_3 v + v_r)}\right]^{\frac{1}{2}} \left[2 + \frac{K_3 \dot{m} g_o}{\rho_1 A_1 v}\right]}{2\rho_1 v^2 A_1 \left[1 + \frac{K_3 \dot{m} g_o}{\rho_1 A_1 v}\right]}$$

$$= \frac{\frac{A_1(\rho_1-\rho_B)g\dot{m}_{g_o}}{\rho_B(K_3v+v_r)} - \frac{2K_1\rho_1v^2}{\sqrt{\pi}}\left[A_1 + \frac{K_2\dot{m}_{g_o}}{\rho_B(K_3v+v_r)}\right]^{\frac{1}{2}}\left[2A_1+\frac{K_3\dot{m}_{g_o}}{\rho_1v}\right]}{\rho_1v^2\left[A_1+\frac{K_3\dot{m}_{g_o}}{\rho_1v}\right]}$$

$$= \frac{\frac{A_1(\rho_1-\rho_B)g\dot{m}_{g_o}}{\rho_B(K_3v+v_r)} - \frac{2K_1}{\sqrt{\pi}}v[2A_1\rho_1v + K_3\dot{m}_{g_o}]\left[A_1+\frac{K_2\dot{m}_{g_o}}{\rho_B(K_3v+v_r)}\right]^{\frac{1}{2}}}{v[\rho_1vA_1+K_3\dot{m}_{g_o}]}$$

$$= \frac{\frac{(\rho_1-\rho_B)g\dot{m}_{g_o}A_1}{\rho_Bv(K_3v+v_r)} - \frac{2K_1(2A_1\rho_1v+K_3\dot{m}_{g_o})}{\sqrt{\pi}}\left[A_1+\frac{K_2\dot{m}_{g_o}}{\rho_B(K_3v+v_r)}\right]^{\frac{1}{2}}}{(\rho_1vA_1+K_3\dot{m}_{g_o})} \qquad (2.2.72)$$

and

$$\frac{dv}{dz} = \frac{-g\dot{m}_{g_o}(\rho_1-\rho_B) + K_1\rho_1dv^2\left[1+4K_2\dot{m}_{g_o}\right]^{\frac{1}{2}}}{\rho_B(K_3v+v_r)} \qquad \pi d^2\rho_B(K_3v+v_r)$$

$$\rho_1\pi\frac{d^2v}{4}\left[1+\frac{K_3\dot{m}_{g_o}}{\rho_1\pi d^2v/4}\right]$$

$$= \frac{\frac{-g\dot{m}_{g_o}(\rho_1-\rho_B)}{\rho_B(K_3v+v_r)} + K_1\rho_1v^2\left(\frac{4A_1}{\pi}\right)^{\frac{1}{2}}\left[1+\frac{K_2\dot{m}_{g_o}}{\rho_BA_1(K_3v+v_r)}\right]^{\frac{1}{2}}}{\rho_1vA_1\left[1+\frac{K_3\dot{m}_{g_o}}{\rho_1vA_1}\right]}$$

$$= \frac{-g\dot{m}_{g_o}(\rho_l - \rho_B) + \frac{2K_1}{\sqrt{\pi}} \rho_l v^2 \left[A_1 + \frac{K_2 \dot{m}_{g_o}}{\rho_B(K_3 v + v_r)}\right]^{\frac{1}{2}}}{(\rho_l v A_l + K_3 \dot{m}_{g_o})} \qquad (2.2.73)$$

or, letting $h = z_o - z$, $\frac{d}{dh} = -\frac{d}{dz}$

$$\frac{dA_1}{dh} = \frac{\frac{2K_1}{\sqrt{\pi}} (2A_1\rho_l v + K_3\dot{m}_{g_o})\left[A_1 + \frac{K_2\dot{m}_{g_o}}{\rho_B(K_3 v + v_r)}\right]^{\frac{1}{2}} - \frac{g\dot{m}_{g_o}(\rho_l - \rho_B)A_1}{\rho_B v(K_3 v + v_r)}}{(\rho_l v A_1 + K_3 \dot{m}_{g_o})} \qquad (2.2.74)$$

$$\frac{dv}{dh} = \frac{\frac{g\dot{m}_{g_o}(\rho_l - \rho_B)}{\rho_B(K_3 v + v_r)} - \frac{2K_1}{\sqrt{\pi}} \rho_l v^2 \left[A_1 + \frac{K_2\dot{m}_{g_o}}{\rho_B(K_3 v + v_r)}\right]^{\frac{1}{2}}}{(\rho_l v A_1 + K_3 \dot{m}_{g_o})} \qquad (2.2.75)$$

and then (2.2.74), (2.2.75) may be solved numerically to give A_1, v.

VOID FRACTION

The void fraction, α, is an important parameter in the development of the model. It will be required in calculating the density deficiency of the sea water.

The void fraction may be defined as

$$\alpha \equiv \frac{\text{cross-sectional area of plume occupied by gas}}{\text{cross-sectional area of plume}} \qquad (2.2.76)$$

Using (2.2.6) this may be written as

$$\alpha = \frac{K_2 A_g}{\frac{\pi d^2}{4} + K_2 A_g} \qquad (2.2.77)$$

Use of (2.2.51), (2.2.52) and (2.2.70) reduces this to

$$\alpha = \frac{K_2 \dot{m}_{g_o} / \rho_B (K_3 v + v_r)}{A_1 + K_2 \dot{m}_{g_o} / \rho_B (K_3 v + v_r)} \qquad (2.2.78)$$

A little manipulation results in

$$\alpha = \frac{K_2 \dot{m}_{g_o}}{K_2 \dot{m}_{g_o} + A_1 \rho_B (K_3 v + v_r)} \qquad (2.2.79)$$

which may then be evaluated at each step, once A_1, v have been determined.

2.3 Note on Derivation - work of Sjøen (1983)

The arguments of Chesters et.al.(1980), involving a control volume do not seem entirely rigorous. Sjøen (1983) gives a very detailed derivation of the plume equations. The Sjøen model, however, seemed to show many similarities to the Chesters model and so, in order to be able to use Sjøen's results for comparison purposes, a check was made as to how closely the models matched, where the differences,

if any, existed; and how such differences altered the solutions obtained.

Sjøen begins with the general conservation equations of mass and momentum for both the gas and liquid phases, plus extra jump conditions for interfacial mass and momentum balance. From here he employs a number of simplifying procedures.

1. He takes weighted time averages to smooth out turbulent fluctuations and transform the two phases which alternately occupy a point into two weighted continua which exist simultaneously at that point.

2. He assumes stationary flow, axisymmetric and non-rotating geometry, no interfacial mass transfer, incompressible liquid phase and neglects viscous stresses, pressure differences between phases, surface tension, body forces other than gravity and density fluctuations.

3. Each variable is expressed as the sum of a weighted time average plus a fluctuating component.

4. The two momentum equations are combined to produce a "Mixture-Momentum" model which allows interfacial stresses to be replaced by relative velocities between the phases at each interface - these being easier to measure.

The closure problem is discussed, and to reduce the number of variables an order of magnitude estimate removes

the gas phase terms from the mixture momentum equation (this simplification being one of those made by Chesters, but without detailed verification).

Finally, by integrating across the plume, the system of partial differential equations is reduced to a set of integral equations which can then be further reduced to a set of ordinary differential equations by the application of appropriate velocity and void fraction profiles, together with suitable boundary conditions. As with Chesters' paper, Sjøen mentions the contribution made to the momentum flux by the fluctuating component of the velocity, but concludes that the contribution will be of lesser importance in the full scale than in the corresponding model and so may justifiably be ignored.

This leaves the set of integral equations as, Sjøen (1983), p.59,

$$2\pi \int_0^\infty \alpha\rho_g \, (w_1 + w_{r_a}) \, r_a \, dr_a = \dot{m}_{g_o} \qquad (2.3.1)$$

$$\frac{d}{dz} \int_0^\infty (1-\alpha) \, w_1 \, r_a \, dr_a = - \left[r_a \, v_1 \right]_{r_a \to \infty} \qquad (2.3.2)$$

$$\frac{d}{dz} \int_0^\infty (1-\alpha) \, w_1^2 \, r_a \, dr_a = g \int_0^\infty \alpha \, r_a \, dr_a \qquad (2.3.3)$$

where velocities, w, refer to time-averaged values.

These may be directly related to the equations derived from the control volume considerations of Chesters

et al. (1980), as we now show.

Since ρ_g is assumed constant across the plume, and using the mean value theorem for integrals, (2.3.1) may be written as

$$\rho_g \, v_g \, 2\pi \int_0^\infty \alpha r_\alpha \, dr_\alpha = \dot{m}_{g_o} \tag{2.3.4}$$

where v_g is the mean gas velocity over the area where bubbles are present

but $$2\pi \int_0^\infty \alpha \, r_\alpha \, dr_\alpha = A_g \tag{2.3.5}$$

so that eqn (2.3.1) reduces to

$$\rho_g \, v_g \, A_g = \dot{m}_{g_o} \tag{2.3.6}$$

which corresponds exactly with eqns (2.2.2), (2.2.39)

In the case of eqn (2.3.2), the R.H.S. refers to the inflow of entrained liquid, and by applying a similar hypothesis to the one proposed by Taylor (1945), he replaces $-[r_\alpha v_l]_{r_\alpha \to \infty}$ by

$$\beta \, b w_c \tag{2.3.7}$$

where

β = entrainment parameter

b = characteristic plume radius

w_c = centre-line vertical velocity

since ρ_1 is constant we now rewrite eqn (2.3.2) as

$$\frac{d}{dz}\rho_1 \int_0^\infty (1-\alpha)\, w_1\, 2\pi\, r_a\, dr_a = 2\pi\, \beta\, b\, w_c \rho_1 \quad . \quad (2.3.8)$$

Comparing this with eqns (2.2.5) and (2.2.20) it may be seen that there is exact correspondence if

$$K_1 \rho_1 v\, d_{eff} = 2\pi\, \beta\, b\, w_c \rho_1 \quad (2.3.9)$$

(the negative sign accounting for the fact that Chesters and Sjøen measure z in opposite directions)

ie if

$$K_1 v\, d_{eff} = 2\pi\, \beta\, b\, w_c \quad (2.3.10)$$

then β must be interpreted as

$$\beta = \frac{K_1}{\pi} \frac{v}{w_c} \frac{d_{eff}}{2b} \quad (2.3.11)$$

From experimental observations, values for β have been proposed e.g. for a Gaussian profile Fanneløp & Sjøen give $\beta_G = 0.07 - 0.08$ for small flow rates rising with increasing flow rates or increasing source depth to a value approaching $\beta_G = 0.1$.

Haaland (1979) questions the possibility of a constant value for the entrainment parameter in a buoyant plume when his observations suggest that β is approximately 0.057. initially, in the jet region, but becomes around 0.085 in the plume region. He goes on to derive a variable expression for the entrainment parameter. Milgram (1983) also allows for the entrainment to be dependent upon local plume

properties.

In the present model, however, we shall keep things as simple as possible by maintaining a constant entrainment parameter. The relationship between an equivalent entrainment parameter, corresponding to an equivalent diameter and velocity, and the constant K_1 can be seen by comparing the expressions for the liquid entrainment, (2.2.5) and (E.11), and noting that $v = w_T$, $d_{eff} = 2b_T$. The result is that

$$K_1 = \pi \beta \tag{2.3.12}$$

Finally, rewriting eqn (2.3.3) as

$$\frac{d}{dz} \rho_1 \int_o^\infty (1-\alpha)\, w_1^2\, 2\pi\, r_\alpha\, dr_\alpha = g\rho_1 \int_o^\infty \alpha 2\pi\, r_\alpha\, dr_\alpha \tag{2.3.13}$$

and comparing it with eqns (2.2.12) and (2.2.26) it may be seen that there is correspondence, using eqn (2.3.5), and allowing for the fact that Sjøen has ignored the contribution to the momentum from the fluctuating component of the velocity .

Again the negative sign accounts for the difference in the direction of z.

The only difference is that in the actual model considered in this work the density of the bubbles is not ignored, although it was in Chesters' model, giving rise to the term $(\rho_1 - \rho_B)$ rather than simply ρ_1.

Sjøen's work then concentrates on assigning Gaussian

profiles to the velocity and void fraction.

$$w_l = w_{c_l} e^{-(r_a/b)^2}$$
$$\alpha = \alpha_{c_l} e^{-(r_a/\lambda b)^2} \qquad (2.3.14)$$

so that

b = the effective half-width of the plume

λb = the effective half-width of the part occupied by bubbles *

and

w_c, α_c are centre-line values

whereas Chesters' "equivalent" velocity and diameter refer to Top Hat profiles.

$$w_l = \begin{cases} w_c & |r_a| \leqslant b_T \\ 0 & |r_a| > b_T \end{cases} \qquad (2.3.15)$$

$$\alpha = \begin{cases} \alpha_c & |r_a| \leqslant \lambda_T b_T \\ 0 & |r_a| > \lambda_T b_T \end{cases}$$

with $v \equiv w_c$, $d_{eff} \equiv 2b_T$ and $\lambda_T = 1$

Since the basic set of differential equations is the same, comparisons may be made of the solutions so long as the relationships between Top Hat and Gaussian values are known.

The relationships used are summarised below, and shown in detail in Appendix E.

* λ is the ratio of void fraction profile to velocity profile defined in the list of symbols.

$$w_G = 2\, w_T \tag{2.3.16}$$

$$b_G = \frac{b_T}{\sqrt{2}} \tag{2.3.17}$$

$$\alpha_G = \frac{2}{\lambda_G^2} \tag{2.3.18}$$

$$\beta_G = \frac{\beta_T}{\sqrt{2}} \tag{2.3.19}$$

$$K_3 = \begin{cases} 1 & \text{Top Hat} \\ \dfrac{1}{1+\lambda_G^2} & \text{Gaussian} \end{cases} \tag{2.3.20}$$

Sjøen discusses in detail a number of asymptotic solutions,* the simplest of which corresponds exactly to the one mentioned by Chesters et al. Sjøen goes on to use the asymptotic equations to obtain initial values for z, b and w. Due to the fact that he ignores the gas momentum, he has an upper limit of $\alpha_c = 0.5$ and this gives a minimum value of z, from which the plume equations may be used. Corresponding to this minimum z, values of b and w are found from the asymptotic expansions. Due to the fact that the present work does not ignore the gas momentum, and that the depths involved would be large, it was thought to be accurate enough to assume the equations were valid from the point of release, although it was realised that there would exist a region, presumed to be small in height in comparison to the total depth, where this would not in fact be true.

* e.g. $v_r \to 0$ and the Boussinesq approximation.

CHAPTER 3

THERMODYNAMICS

3.1 Temperature-Entropy diagram

The escaping gas is assumed to undergo an isentropic expansion as it leaves the pipe, followed by an expansion as the gas rises due to the falling hydrostatic pressure plus some contribution due to heat transfer. The paths the gas may follow are summarised on the temperature-entropy diagram (fig. 3.1.1).

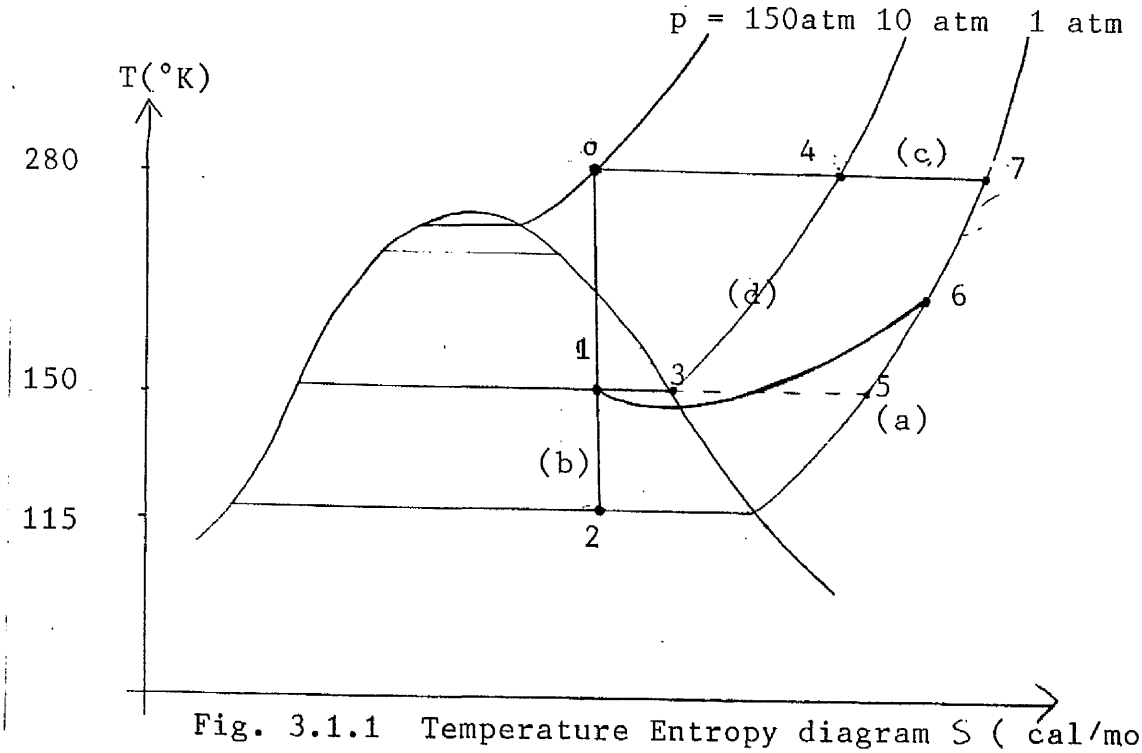

Fig. 3.1.1 Temperature Entropy diagram

Forbidden zones

(a) $p < p_{atm}$

(b) cannot decrease entropy

(c) cannot have gas becoming hotter than the sea

(d) cannot increase pressure as gas rises

The point 0 corresponds to the release point, and the line 0-1 to the isentropic/adiabatic expansion as the gas leaves the pipe.

There are then four possible routes to describe the rise of the gas to the surface.

1. 1-2: This is one extreme - there is no heat transfer and the rise is completely adiabatic/isentropic.

2. 1-3-4-7: This is the other extreme case - there is an instantaneous rise in temperature to that of the surrounding sea and subsequent heat transfer will maintain this temperature.
   The entropy will increase as the bubble expands isothermally to atmospheric pressure.

3. 1-6: This curve shows the most probable situation, lying somewhere between the two extremes. Its actual shape will depend on the amount of heat transfer (see below).

4. 1-3-5: This is a special case of possibility (3) which is possible, but highly unlikely - the amount of heat transfer is precisely that required to

maintain the gas at the temperature with which it left the pipe.

Effect of heat transfer on shape of curve in case (3)

Details of the First Law of Thermodynamics can be found in Van Wylen & Sonntag (1978). It is possible to write the first law in the form

$$c_v dT + p d\nu = \delta q = c_p dT - \nu dp \qquad (3.1.1)$$

where c_v, c_p are the specific heats at constant volume and pressure, respectively, T is the temperature, p the pressure, ν the specific volume and δq the energy transfer per unit mass.

Thus,

$$c_p dT = \delta q + \nu dp \qquad (3.1.2)$$

where the term νdp is negative for the rising gas.

The variation of T with p, therefore, and thus the shape of the curve 1-6, depends on δq. If $|\nu dp| > \delta q$ initially there will be a drop in temperature.

Also, note that case (4) corresponds to

$$|\delta q| = |\nu dp| \quad (\text{ie } dT = 0) \qquad (3.1.3)$$

3.2 Derivation of Entropy Equation

Consideration of the thermodynamics of the problem necessitates the modelling of the temperature throughout the rise.

The first step is to derive an equation for the temperature, T, in terms of the pressure, p, and the specific entropy, s, defined by

$$ds = \frac{\delta q}{T} \qquad (3.2.1)$$

where δq is, as before, the energy transferred per unit mass.

Consider the important thermodynamic relations (to be found in Van Wylen & Sonntag (1978))

$$Tds = d\hat{h} - \nu dp \qquad (3.2.2)$$

$$\hat{g} = \hat{h} - Ts \qquad (3.2.3)$$

where $\hat{h}$ is the specific enthalpy, ν is the specific volume and $\hat{g}$ is the Gibbs function.

Equation (3.2.2) may be applied to irreversible, as well as reversible, processes between two given states but the integration must be performed along a reversible path between the same two states.

The latter equation yields

$$d\hat{g} = d\hat{h} - Tds - sdT \qquad (3.2.4)$$

and substituting from (3.2.2) leads to

$$d\hat{g} = \nu dp - sdT \qquad (3.2.5)$$

from which we can write

$$\left(\frac{\partial \hat{g}}{\partial p}\right)_T = \nu \qquad \left(\frac{\partial \hat{g}}{\partial T}\right)_p = s \qquad (3.2.6a,b)$$

Using the Ideal Gas Equation of state

$$\nu = \frac{rT}{p} \qquad (3.2.7)$$

where r is the gas constant, (3.2.6(a)) may be solved to give

$$\hat{g} = rT\ln p + \phi(T) \qquad (3.2.8)$$

and using (3.2.6(b))

$$-s = r\ln p + \phi'(T) \qquad (3.2.9)$$

Making use of the definition of specific heat capacity at constant pressure.

$$c_p \equiv T\left(\frac{\partial s}{\partial T}\right)_p = \left(\frac{\partial \hat{h}}{\partial T}\right)_p \qquad (3.2.10)$$

(3.2.9) yields

$$-T\left(\frac{\partial s}{\partial T}\right)_p = T\phi''(T) = -c_p \qquad (3.2.11)$$

Thus

$$\phi''(T) = \frac{-c_p}{T}$$

and hence

$$\phi'(T) = -\int \frac{c_p}{T}\, dT \qquad (3.2.12)$$

so that from (3.2.9)

$$s = \int \frac{c_p}{T}\, dT - r\ln p \qquad (3.2.13)$$

If c_p is assumed constant, and the gas is ideal

$$s = c_{p_o} \ln T - r\ln p + \text{Const} \qquad (3.2.14)$$

where the subscript on c_p refers to the gas being ideal.

If it is not reasonable to assume a constant specific heat, then an empirical specifc heat may be used.

Rearranging

$$T = \exp\left\{ \frac{s}{c_{p_o}} + \frac{r \ln p}{c_{p_o}} - \frac{\text{Const}}{c_{p_o}} \right\} \qquad (3.2.15)$$

The actual equation used in the model has a few modifications from this theoretical one.

(a) It is assumed that $p = 10^4 z$ (3.2.16)

(b) A curve-fit to data from the T-s diagram for methane is performed

(c) Allowance is made for the possibility that the gas may enter the 2-phase region

This leads to the equation (Smith, 1982)

$$T = \exp\left\{ \frac{S'}{8} + \frac{\ln z}{3.65} - 0.457 \right\} \qquad (3.2.17)$$

where

$$S' = \max\{ S, S_{sat} \} \qquad (3.2.18)$$

and S_{sat} can be approximated by the curve fit

$$S_{sat} = \frac{158 - 5 \ln z}{4} \qquad (3.2.19)$$

Note that S is measured in cal/mol.°K, rather than SI units, which s is measured in.

To compare eqns. (3.2.15) and (3.2.17), substituting (3.2.16) into (3.2.15) gives

$$T = \exp\left\{ \frac{s}{c_{p_o}} + \frac{\ln z}{(c_{p_{o/r}})} - C' \right\} \qquad (3.2.20)$$

where

$$C' = \frac{\text{Const}}{c_{p_o}} - \frac{\ln(10^4)}{(c_{p_{o/r}})} \qquad (3.2.21)$$

For methane (at 300K) (Van Wylen & Sonntag (1978))

$$c_{p_o} = 2.2537 \quad kJ/kg°K = 8.6341 \text{ cal/mol°K}$$

$$r = 0.51835 \quad kJ/kg°K \qquad (3.2.22)$$

$$\Rightarrow \quad c_{p_{o/r}} = 4.3478 \qquad (3.2.23)$$

giving

$$T = \exp\left\{ \frac{S}{8.6341} + \frac{\ln z}{4.3478} - C' \right\} \qquad (3.2.24)$$

Comparing this to eqn (3.2.17) shows some variation.

One way to try to explain this is to consider, instead of the ideal gas law, a modified version.

$$pv = ZrT \qquad (3.2.25)$$

where Z = compressibility factor

If all other assumptions are maintained, the effect is to replace r by rZ in eqns (3.2.15) and (3.2.20), giving

$$T = \exp\left\{ \frac{s}{c_{p_o}} + \frac{\ln Z}{(c_{p_{o/Zr}})} - C'' \right\} \qquad (3.2.26)$$

with

$$c'' = \frac{\text{Const}}{c_{p_o}} - \frac{\ln(10^4)}{(c_{p_{o/r}} Z)} \qquad (3.2.27)$$

The value of Z for methane, however, varies approximately from 0.8 to 1.0 so that c_{p_o}/rZ varies from 4.35 to 5.43 which does not help the discrepancy.

The most likely reason for the variation in the two euqations is that Smith adopted an empirical law like (3.2.20) and then carried out a curve-fit to find the appropriate constants.

A comparison was made of values of S,T as calculated by eqn (3.2.17) and those read off the Temperature -Entropy diagram, for a pressure of 1 atm (ie z = 10m).

The results are shown in Table 3.2.1

From this it may be seen that over the given temperature range, which covers those temperatures likely to be encountered, the agreement is quite good, given the inaccuracy in reading values from the graph, and also the assumption in converting atmospheric pressure into a pressure head of 10m.

It would, therefore, seem perfectly acceptable to use eqn (3.2.17) for the calculation of the temperature.

Attempts to produce another equation based more closely on the theoretical equation using c_{p_o} and $c_{p_{o/r}}$ have not produced any better agreement.

T(°K)	S (cal/mol°K)	T(°K) [Calculated]
133	37.7	132.5
143	38.2	141.0
153	38.9	153.9
163	39.2	159.8
173	39.8	172.3
183	40.3	183.4
193	40.8	195.2
203	41.1	202.7
213	41.4	210.4
223	41.8	221.2
233	42.1	229.6
243	42.4	238.4
253	42.7	247.5
263	43.0	257.0
273	43.4	270.2
283	43.7	280.5
293	44.0	291.2
303	44.3	302.3

Table 3.2.1 Comparison of entropies.

3.3 Form of Expansion

Previous work (Chesters, (1980), Sjøen (1983) and others) has concentrated on an isothermal expansion. The present work no longer insists on this restriction. It must be checked how relaxing this constraint affects the system of equations.

For the case considered by Chesters, the following thermodynamic relation holds

$$pV = \text{const} \qquad (3.3.1)$$

Relating the hydrostatic pressure to the pressure head, z,

$$\rho_l g z \frac{m}{\rho_g} = \text{const}$$

Assuming the mass, m, of gas in the bubbles remains constant we may simplify and rearrange the above equation to obtain

$$\rho_g = \frac{z}{z_o} \rho_{g_o} \qquad (3.3.2)$$

where the o subscript refers to some reference position. The RHS of (3.3.2) is then substituted for ρ_g in the set of equations.

Equally well, (3.3.2) could have been added as another separate equation and this is what was done in the present work. The form of the equation, however, is somewhat changed, since (3.3.1) no longer holds.

From the Ideal Gas Law, expressed in a slightly different form from (3.2.7),

$$pV = \bar{n}RT \qquad (3.3.3)$$

under the assumption that the pressure may be approximated by

$$p = 10^4 z \qquad (3.3.4)$$

the following expression is derived for the gas density

$$\rho_g = \frac{10^4 \hat{M} z}{RT} \qquad (3.3.5)$$

where $\hat{M}$ is the molecular weight and R is the Universal gas constant, equal to $r\hat{M}$. From equation (3.3.5) it may be seen that the density varies with depth and temperature. Since, at a given depth, z is fixed, irrespective of the form of expansion, the only way this can influence the density is through the temperature.

For constant T, (3.3.5) is identical to (3.3.2).

For varying T, the variation in density with depth will depend also on the form of the temperature change which reflects the form of the expansion.

Hence, in the set of ODE's to be solved, the appearance of the gas density ρ_B, which depends on ρ_g, where ρ_g is calculated from (3.3.5), having first calculated T from an expression relating to the form of the expansion, means that the method of expansion is being taken into account.

ANALYSIS OF FORM OF EXPANSION

The initial expansion as the gas leaves the pipeline is assumed to be adiabatic. If this also applied throughout the rise then using the relation for a reversible adiabatic process between two states 1 and 2

$$P_1 V_1^{\gamma} = P_2 V_2^{\gamma} \qquad (3.3.6)$$

where γ = ratio of heat capacities = c_{p/c_v} (3.3.7)

Combining equation (3.3.6) with equation (3.3.3)

$$\frac{p_1}{p_2}\left(\frac{p_2}{p_1}\right)^{1/\gamma} = \frac{T_1}{T_2}$$

which implies

$$\frac{T_1}{T_2} = \left(\frac{p_1}{p_2}\right)^{1-1/\gamma}$$

or using (3.3.4)

$$\frac{T_1}{T_2} = \left(\frac{z_1}{z_2}\right)^{1-1/\gamma} \tag{3.3.8}$$

If we let $T_1 = T$, $z_1 = z$ be conditions at depth z, and let $T_2 = T_o$, $z_2 = z_o$ be initial conditions, then (3.3.8) may be rewritten as

$$\frac{T}{T_o} = \left(\frac{z}{z_o}\right)^{1-1/\gamma}$$

leading to

$$\frac{z}{T} = \frac{z_o}{T_o}\left(\frac{z}{z_o}\right)^{1/\gamma} \tag{3.3.9}$$

From the derivation of the entropy equation we have the expression

$$\frac{T}{T_o} = \left(\frac{z}{z_o}\right)^{r/c_p} \exp\left\{\frac{s-s_o}{c_p}\right\} \tag{3.3.10}$$

This may be rewritten as

$$\frac{z}{T} = \frac{z_o}{T_o}\left(\frac{z}{z_o}\right)^{1-r/c_p} \exp\left\{-\frac{(s-s_o)}{c_p}\right\} \qquad (3.3.11)$$

But $$r = c_p - c_v \qquad (3.3.12)$$

and so $$1 - r/c_p = \frac{c_v}{c_p} = 1/\gamma \qquad (3.3.13)$$

Hence,

$$\frac{z}{T} = \frac{z_o}{T_o}\left(\frac{z}{z_o}\right)^{1/\gamma} \exp\left\{-\frac{(s-s_o)}{c_p}\right\} \qquad (3.3.14)$$

From this, it can be seen that there is equality between (3.3.9) and (3.3.14)

$$\Leftrightarrow \quad \exp\left\{-\left(\frac{s-s_o}{c_p}\right)\right\} = 1$$

i.e.

$$\Leftrightarrow \quad s = s_o \qquad (3.3.15)$$

which is consistent with the fact that a reversible, adiabatic expansion is isentropic.

For a non-isentropic process, (3.3.15) does not hold and, therefore, neither does (3.3.9).

When a gas undergoes a reversible process in which there is a heat transfer, however, the process often takes place in such a manner that a general polytropic gas law holds, namely

$$pv^n = \text{constant} \qquad (3.3.16)$$

with $n = 0$ corresponding to isobaric process

$n = 1$ corresponding to isothermal

$n = \gamma$ corresponding to adiabatic

(See, for example, Van Wylen & Sonntag (1978)

For such a process, (3.3.9) is generalised to

$$\frac{z}{T} = \frac{z_o}{T_o}\left(\frac{z}{z_o}\right)^{1/n} \quad (n \neq 0) \tag{3.3.17}$$

Equating this to (3.3.14) gives

$$\frac{z_o}{T_o}\left(\frac{z}{z_o}\right)^{1/n} = \frac{z_o}{z_o}\left(\frac{z}{z_o}\right)^{1/\gamma} \exp\left\{-\frac{(s-s_o)}{c_p}\right\}$$

from which follows

$$\left(\frac{z}{z_o}\right)^{1/n - 1/\gamma} = \exp\left\{-\frac{(s-s_o)}{c_p}\right\} \tag{3.3.18}$$

solving this for n

$$\left(\frac{1}{n} - \frac{1}{\gamma}\right) \ln\left(\frac{z}{z_o}\right) = -\frac{(s-s_o)}{c_p}$$

and so

$$\frac{1}{n} = \frac{1}{\gamma} - \frac{(s-s_o)}{c_p \ln(z/z_o)}$$

or, since $z < z_o$ for rising bubbles,

$$\frac{1}{n} = \frac{1}{\gamma} + \frac{(s-s_o)}{c_p \ln(z_o/z)} \tag{3.3.19}$$

Also,

$$s > s_o$$

and so

$$\frac{1}{n} > \frac{1}{\gamma}$$

or

$$n < \gamma \qquad (n, \gamma > 0) \qquad (3.3.20)$$

Returning to (3.3.19); suppose z_1, z_2 represent two depths with corresponding entropies s_1, s_2

Then,

$$\frac{1}{n_1} = \frac{1}{\gamma} + \frac{s_1 - s_o}{c_p \ln(z_o/z_1)} \qquad (3.3.21a,b)$$

$$\frac{1}{n_2} = \frac{1}{\gamma} + \frac{s_2 - s_o}{c_p \ln(z_o/z_2)}$$

If we assume γ, c_p do not vary with depth

$$\frac{1}{n_1} - \frac{1}{n_2} = \frac{1}{c_p}\left[\frac{(s_1 - s_o)}{\ln(z_o/z_1)} - \frac{(s_2 - s_o)}{\ln(z_o/z_2)}\right] \qquad (3.3.22)$$

A polytropic process requires that n be constant, i.e.

$n_1 = n_2 = n$, and hence

$$\frac{s_1 - s_o}{\ln(z_o/z_1)} = \frac{s_2 - s_o}{\ln(z_o/z_2)}$$

It follows that

$$s_2 = s_o + \frac{(s_1 - s_o)\ln(z_o/z_2)}{\ln(z_o/z_1)}$$

and

$$s_2 - s_1 = \frac{(s_o - s_1)\ln(\frac{z_o}{z_1}) + (s_1 - s_o)\ln(\frac{z_o}{z_2})}{\ln\frac{z_o}{z_1}}$$

$$= \frac{(s_1 - s_o)\ln(z_1/z_2)}{\ln(\frac{z_o}{z_1})}$$

substituting from (3.3.21(a)) and remembering $n_1 = n$ (constant) we arrive at

$$s_2 - s_1 = c_p\left(\frac{1}{n} - \frac{1}{\gamma}\right)\ln\left(\frac{z_1}{z_2}\right) \qquad (3.3.23)$$

which shows the variation in entropy with depth which would produce a polytropic process.

Note that for n = 1, (3.2.23) becomes

$$s_2 - s_1 = c_p(1 - 1/\gamma)\ln\left(\frac{z_1}{z_2}\right)$$

which is identical to (3.3.14) with

$$s = s_1,\ z = z_1;\ s_o = s_2,\ z_o = z_2 \text{ and } T = T_o$$

This verifies that n = 1 corresponds to the isothermal process.

Starting with equation (3.3.10)

$$\frac{T}{T_o} = \left(\frac{z}{z_o}\right)^{1-1/\gamma} \cdot \exp\left\{\frac{s - s_o}{c_p}\right\} \qquad (3.3.24)$$

If the gas cools as it rises

$$T < T_o$$

$$z < z_o \qquad (3.3.25)$$

Thus

$$\frac{T}{T_o} < 1$$

and so from (3.3.24)

$$\left(\frac{z}{z_o}\right)^{1-1/\gamma} \exp\left\{\frac{s-s_o}{c_p}\right\} < 1$$

which means

$$(1-1/\gamma) \ln\left(\frac{z}{z_o}\right) + \frac{s-s_o}{c_p} < 0$$

or

$$\frac{s-s_o}{c_p} < (1-1/\gamma) \ln\left(\frac{z_o}{z}\right)$$

Using equation (3.3.19)

$$\left(\frac{1}{n} - \frac{1}{\gamma}\right) \ln\left(\frac{z_o}{z}\right) < \left(1-\frac{1}{\gamma}\right) \ln\left(\frac{z_o}{z}\right)$$

but $\ln\left(\frac{z_o}{z}\right) > 0$

and, therefore

$$\frac{1}{n} - \frac{1}{\gamma} < 1 - 1/\gamma$$

hence, necessarily

$$n > 1 \qquad (3.3.26)$$

Similarly, if the gas heats up as it rises

$$T > T_o$$

$$z < z_o \qquad (3.3.27)$$

then

$$n < 1 \qquad (3.3.28)$$

Finally, returning to equation (3.3.17)

for a polytropic gas law

$$\frac{T}{T_o} = \left(\frac{z}{z_o}\right)^{1-1/n} \qquad (3.3.29)$$

so using either (3.3.24) or (3.3.29)

the density may be expressed as

$$\rho_g = \frac{10^4 \hat{M} z}{RT_o \left[\left(\frac{z}{z_o}\right)^{1-1/\gamma} \exp\left\{\frac{s-s_o}{c_p}\right\}\right]}$$

$$= \frac{10^4 \hat{M}z}{RT_o} \left[\left(\frac{z_o}{z} \right)^{1-1/\gamma} \exp\left\{ - \frac{(s-s_o)}{c_p} \right\} \right]$$

$$= \frac{10^4 \hat{M}z_o}{RT_o} \left[\left(\frac{z}{z_o} \right)^{1/\gamma} \exp\left\{ - \frac{(s-s_o)}{c_p} \right\} \right]$$

OR)

$$\rho_g = \frac{10^4 \hat{M}z}{RT_o \left(\frac{z}{z_o} \right)^{1-1/n}}$$

$$= \frac{10^4 \hat{M}z_o \left(\frac{z}{z_o} \right)^{1/n}}{RT_o}$$

where $1/n$ is given by (3.3.19)

In terms of the actual temperature equation used (3.2.17)

$$\rho_g = \begin{cases} \dfrac{10^4 \hat{M}z_o}{RT_o} \left[\left(\dfrac{z}{z_o} \right)^{1-1/3.65} \exp\left\{ - \dfrac{(S-S_o)}{8} \right\} \right] \\ \qquad\qquad S \text{ in cal/mol } {}^\circ K \\ \dfrac{10^4 \hat{M}z_o}{RT_o} \left(\dfrac{z}{z_o} \right)^{1/n} \quad ; \quad \dfrac{1}{n} = \left(1 - \dfrac{1}{3.65}\right) + \dfrac{(S-S_o)}{8 \ln\left(\dfrac{z_o}{z}\right)} \end{cases}$$

(3.3.30)

Hence, the form of the thermal expansion is expressed through the variation in the expression for the density.

DENSITY OF BUBBLES

It must be remembered that the present work allows for the fact that the gas may enter the two-phase region and hence the actual density of the gas, in terms of the

liquid and vapour phases, is given in Appendix C as

$$\rho_B = \frac{\rho_{g_g} \rho_{g_l}}{\xi \rho_{g_l} + (1-\xi)\rho_{g_g}} \qquad (3.3.31)$$

where ξ = fraction in vapour phase

and, again from curve-fitting the Temperature-Entropy diagram for methane (Smith, 1982), in this two phase region we may write

$$\xi = \frac{(2S - 3.5\ \ln z - 29)}{(50 - 6\ln z)} \qquad (3.3.32)$$

Outwith the two-phase region, i.e. for s greater that the saturated entropy for a given pressure,

ξ = 1 and (3.3.31) reduces to

$$\rho_B = \rho_{g_g} \qquad (3.3.33)$$

3.4 Heat Transfer

An important factor in determining the final state of the gas is the heat transfer from the sea to the bubbles - it is this process which will lessen the severity of the situation. (i.e. increase the gas buoyancy and velocity)

The basic principles of Heat Transfer may be found in

many books e.g. Cornwell (1977) and Butterworth & Hewitt (1977).

The method adopted in calculating the heat transfer to the plume was as follows.

1. At a given height the approximate heat transfer to a single bubble was calculated by use of an overall Heat Transfer Coefficient, h_T.

2. This value was then multiplied by the number of bubbles existing in the plume cross-section at that height.

Thus, in a time interval Δt, the amount of energy transferred , ΔQ is given by

$$\Delta Q = N \Delta t \, s_B \, h_T \, \Delta T \qquad (3.4.1)$$

where N = number of bubbles present

s_B = surface area of bubble

h_T = heat transfer coefficient

ΔT = difference in temperature between the sea water, T_{sea}, and the gas, T

This may then be transformed into an expression for the change in entropy, S, (where S is measured in cal/mol.°K), as shown.

$$\Delta S = \frac{\Delta Q}{(4.1868)\hat{m}T} \qquad (3.4.2)$$

where $\hat{m}$ = molar mass of gas to which ΔQ is transferred

and the factor 4.1868 converts joules into calories

Expressing the surface area S_B as ϵd_e^2

where

$$\epsilon = \frac{\pi(3+\cos\Theta)}{4[(1-\cos\Theta)(2+\cos\Theta)^2]^{\frac{1}{3}}} \qquad (3.4.3)$$

as shown in Appendix F

and noting that

$\hat{m} = \frac{N\rho_B V_B}{\hat{M}}$, where V_B is the volume of one bubble

equations (3.4.1) and (3.4.2) may be combined to give

$$\Delta S = \frac{6\epsilon}{\pi\rho_B d_e} \Delta t \left(\frac{0.016}{4.1868}\right) h_T \left(\frac{T_{sea}}{T} - 1\right) \qquad (3.4.4)$$

since $\hat{M} = 0.016$ for CH_4

Taking the limit as $\Delta t \to 0$

$$\frac{dS}{dt} = \frac{6\epsilon}{\pi\rho_B d_e} \left(\frac{0.016}{4.1868}\right) h_T \left(\frac{T_{sea}}{T} - 1\right) \qquad (3.4.5)$$

and

$$\frac{dS}{dh} = \frac{dS}{dt} \cdot \frac{dt}{dz} \cdot \frac{dz}{dh} = \frac{6\epsilon}{\pi\rho_B d_e v_g} \left(\frac{0.016}{4.1868}\right) h_T \left(\frac{T_{sea}}{T} - 1\right) \qquad (3.4.6)$$

HEAT TRANSFER COEFFICIENT

Due to the large differences in heat capacities between the gas and the liquid, it is reasonable to assume that the

heat transfer resistance is entirely on the gas side, and thus calculate only one heat transfer coefficient.

An appropriate expression with which to begin our derivation is (Leclair & Hamielec (1971)).

$$Nu = C\, Re^{\frac{1}{2}}\, Pr^{\frac{1}{2}} \qquad (3.4.7)$$

where the Nusselt number, Nu, the Reynolds number, Re, and the Prandtl number, Pr, are defined by

$$Nu = \frac{h_T d_e}{k} \qquad (3.4.8a,b,c)$$

$$Re = \frac{\rho_B v_r d_e}{\mu} \qquad Pr = \frac{c_p \mu}{k}$$

k is the thermal conductivity, while μ is the viscosity.

Upon substitution (3.4.7) reduces to

$$h_T = C \left[\frac{\rho_B v_r k c_p}{d_e} \right]^{\frac{1}{2}} \qquad (3.4.9)$$

and Leclair & Hamielec (1971) propose that

$$C = \frac{1.13}{\sqrt{1-\alpha}} \qquad (3.4.10)$$

where α is the gas fraction

Smith (1982) adopts the penetration theory prediction for the unsteady state convective heat transfer into a flat stationary surface which yields, for a single bubble

$$h_T = 2 \left[\frac{k c_p \rho_B}{\pi t_c} \right]^{\frac{1}{2}} \qquad (t_c \not\to 0) \qquad (3.4.11)$$

t_c represents the contact time at the interface, which may be interpreted as the time the bubble takes to pass a certain point. Assuming the speed of the single bubble to be $\sqrt{5 d_e}$, and the vertical height of the spherical cap to be 0.41 d_e, t_c may be written as

$$t_c = \frac{0.41\ d_e}{\sqrt{5\ d_e}} \simeq 0.2\sqrt{d_e} \qquad (3.4.12)$$

and (3.4.11) reduces to

$$h_T = 1.76 \left[\frac{k c_p \rho_B v_r}{d_e} \right]^{\frac{1}{2}} \qquad (3.4.13)$$

where v_r in this case is the individual bubble velocity. For a spherical bubble of vertical height d_e, with a similar velocity to spherical cap,

$$h_T = 1.13 \left[\frac{k\ c_p \rho_B v_r}{d_e} \right]^{\frac{1}{2}} \qquad (3.4.14)$$

VALUES USED FOR h_T

1. Initial suggestion of Smith (1982) was a value of 80 $W/m^2{}^\circ K$, based on equation (3.4.13) for a 1-2m bubble, a slight increase over the calculated value being proposed to take into account
   (a) the curvature of the surface
   (b) the probability of turbulent mixing

   Although this value was thought to be rather high for a

convective gas film coefficient, it was thought to be acceptable due to the circulation and mixing occurring in the bubbles leading to a rapid rate of surface renewal.

2. On the basis of experimental evidence Smith (1984) suggested that his initial estimate was a factor of 10 too large, and that a value of 8 $W/m^2°K$ was more realistic.

3. Equation (3.4.9), with C given by (3.4.10), combined with a constant value for h_T when $\alpha > 0.9$ to deal with the singularity in (3.4.9), at $\alpha = 1$, was then assumed. The value of the thermal conductivity, k, is temperature dependent, and is expressed in terms of a cubic function by performing a curve-fit to data points obtained from Perry & Green (1984). The resulting function is

$$k = [-0.213\,(T/100)^3 + 1.778\,(T/100)^2 - 3.593\,(T/100) + 3.948\,] \times 10^{-2} \qquad (3.4.15)$$

The constant value, u_{CONS}, used for $\alpha > 0.9$ was found by doing a number of runs with different fixed values and choosing the one which allowed a smooth change over to eqn (3.4.9) once α was reduced to 0.9.

This value turned out to be 300 $W/m^2°K$. At first glance, this seems to be rather high, but at the initial "blow-out" instant turbulent mixing will strongly enhance

heat transfer, and so such a large value is likely to be acceptable to the oil industry. From its initial value h_T decreased according to (3.4.9), (3.4.10) until at the surface it was of the order of $50 W/m^2 °K$.

Thus, the form of the heat transfer coefficient is

$$h_T = \begin{cases} 300 & \alpha > 0.9 \\ \frac{1.13}{\sqrt{1-\alpha}} \left[\frac{\rho_B v_r k c_p}{d_e} \right]^{\frac{1}{2}} & \alpha \leq 0.9 \end{cases} \qquad (3.4.16)$$

Since methods 1, 2 and 3 give rather conflicting proposals as to the numerical values of h_T, a sensitivity analysis was performed to evaluate the importance of this parameter on the evolution of the plume. The results of this can be found in Chapter 6.

3.5 Note on Isothermal Case

This corresponds to the 2nd route mentioned in section 3.1 and assumes that the gas and the sea-water share the same temperature throughout the rise.

It can be seen from Fig. 3.1.1 that the entropy of the gas increases as the pressure falls. Equation (3.4.6), however, cannot be used to calculate the changing entropy because it assigns a value of zero to $\frac{ds}{dz}$ for $T = T_{sea}$.

Since T is fixed, (3.2.17) can be re-expressed in the form

$$S' = 8 \{ \ln T - \frac{1}{3.65} \ln z + 0.457 \} \qquad (3.5.1)$$

where S' is given by (3.2.18).

and thus S' may be calculated as a function of z.

Comparison of S' with S_{sat}, (3.2.19) will then give rise to two possibilities

1. $S' > S_{sat}$, when S' will denote the actual entropy, S, of the gas (3.5.2a,b)

2. $S' = S_{sat}$, when it can only be said that $S \leq S'$, and the actual entropy is not known.

If possibility (3.5.2(b)) occurs, then it may be that S is some unknown value such that $S < S_{sat}$. In such a case, the vapour fraction is less than 1, but as the value of S is unknown it is not possible to calculate this vapour fraction, and hence the mean density of the bubbles. The whole calculation process then breaks down.

For possibility (3.5.2.(a)) to occur, the following equation holds

$$8 \{ \ln T - \frac{\ln z}{3.65} + 0.457 \} > \frac{158 - 51 \ln z}{4}$$

which restricts z as

$$z < \exp \{ \frac{\ln T - 4.4805}{0.1177} \} \qquad (3.5.3)$$

Thus, for the case of T = 280K, possibility (1) occurs for all values of z such that

$$z < 18161 \qquad (3.5.4)$$

Reducing T will, of course reduce z and, for example, at T = 150K, it is necessary that

$$z < 90$$

for (3.5.2(a)) to hold.

It is only necessary to ensure (3.5.3) holds for z_o, as it will then hold for all values of $z < z_o$, and the calculations can continue to the surface.

Since $S > S_{sat}$, it can also be said that the vapour fraction will be unity throughout the rise.

In this case, differentiation of (3.5.1) leaves us with

$$\frac{dS}{dz} = -\frac{8}{3.65z} \qquad (3.5.5)$$

in place of (3.4.6), or in terms of h,

$$\frac{dS}{dh} = \frac{8}{3.65\,(z_o-h)} \qquad (3.5.6)$$

CHAPTER 4

THE MODEL

4.1 General

In order to formulate the mathematical model, it is necessary to combine the Dynamics and the Thermodynamics.

Equations (2.2.74) and (2.2.75) are two coupled non-linear ordinary differential equations in the three dependent variables A_1, v and ρ_B. ρ_B is determined from a set of equations arising from the thermodynamics, namely (2.2.79), (3.2.17) - (3.2.19), (3.3.5), (3.3.31) - (3.3.33), (3.4.6), (3.4.15) and (3.4.16).

The method employed to solve the equations involves a numerical fourth-order Runge-Kutta scheme incorporated in a NAG subroutine, whereby the system is integrated stepwise from a set of initial values.

The actual system to be integrated consists of (2.2.74), (2.2.75) and (3.4.6) or (3.5.6), which are rewritten below.

$$\frac{dA_1}{dh} = \frac{\dfrac{2K_1}{\sqrt{\pi}}(2A_1\rho_1 v + K_3\dot{m}_{g_o})\left[A_1 + \dfrac{K_2\dot{m}_{g_o}}{\rho_B(K_3v+v_r)}\right]^{\frac{1}{2}} - \dot{m}_{g_o}(\rho_1-\rho_B)A_1}{\rho_B v(K_3v+v_r)}}{(\rho_1 v A_1 + K_3\dot{m}_{g_o})} \qquad (4.1.1)$$

$$\frac{dv}{dh} = \frac{\dot{m}_{g_o}(\rho_1-\rho_B) - \dfrac{2K_1}{\sqrt{\pi}}\rho_1 v^2\left[A_1 + \dfrac{K_2\dot{m}_{g_o}}{\rho_B(K_3v+v_r)}\right]^{\frac{1}{2}}}{(\rho_1 v A_1 + K_3\dot{m}_{g_o})} \qquad (4.1.2)$$

$$\frac{dS}{dh} = \begin{cases} \dfrac{6\varepsilon}{\pi\rho_B d_e (K_3 v + v_r)} \left(\dfrac{0.016}{4.186}\right) h_T \left(\dfrac{T_{sea}}{T} - 1\right) & \text{(non-isothermal case)} \\ \dfrac{8}{3.65(z_o - h)} & \text{(isothermal case)} \end{cases} \tag{4.1.3}$$

while those necessary for closure are rewritten as follows:

$$\rho_B = \frac{\rho_{g_g}\,\rho_{g_l}}{\xi\rho_{g_l} + (1-\xi)\rho_{g_g}} \tag{4.1.4}$$

$$\rho_{g_g} = \frac{10^4 \hat{M} z}{RT} \tag{4.1.5}$$

$$z = z_o - h \tag{4.1.6}$$

$$\xi = \begin{cases} \dfrac{2S - 3.5 \ln z - 29}{50 - 6 \ln z} & S < S_{sat} \\ 1 & \text{otherwise} \end{cases} \tag{4.1.7}$$

$$T = \exp\left\{ \frac{S'}{8} + \frac{\ln z}{3.65} - 0.457 \right\} \tag{4.1.8}$$

$$S' = \max\,(S,\, S_{sat}) \tag{4.1.9}$$

$$S_{sat} = \frac{158 - 5 \ln z}{4} \tag{4.1.10}$$

$$\varepsilon = \frac{\pi(3+\cos\theta)}{[4(1-\cos\theta)(2+\cos\theta)^2]^{\frac{1}{3}}} \tag{4.1.11}$$

$$h_T = \begin{cases} \frac{1.13}{\sqrt{1-\alpha}} \left[\frac{\rho_B v_r \; k \; c_p}{d_e}\right]^{\frac{1}{2}} & \alpha \leqslant 0.9 \\ \text{UCONS} & \alpha > 0.9 \end{cases} \qquad (4.1.12)$$

$$\alpha = \frac{K_2 \dot{m}_{g_o}}{K_2 \dot{m}_{g_o} + A_1 \rho_B (K_3 v + v_r)} \qquad (4.1.13)$$

$$k = [-0.213(T/_{100})^3 + 1.778(T/_{100})^2 - 3.593(T/_{100}) + 3.948] \times 10^{-2} \qquad (4.1.14)$$

4.2 Initial Values

The numerical integration technique requires a set of initial conditions. These are given by

$$h_o = 0$$
$$v_o = K_4 \; v_r \qquad K_4 = 0(0.5) \qquad (4.2.1)$$
$$A_{l_o} = 0$$
$$S_o = \begin{cases} \text{pipeline entropy (non-isothermal)} \\ 8\left[\ln T_s - \frac{\ln z_o}{3.65} + 0.457\right] \quad \text{(isothermal)} \end{cases}$$

From equations (4.1.1) to (4.1.14) plus (4.2.1), it can be seen that the following set of parameters must also be specified.

$K_1, K_2, K_3, K_4, \dot{m}_{g_o}, d_e, v_r, z_o, \hat{M}, \Theta,$

T_{sea} and UCONS

assuming g, ρ_l, ρ_{g_l}, R and c_p all to be constants.

Those which must be entered on each run of the program are

1. The depth of the pipeline escape ($=z_o-10$)

2. The bubble size (d_e) which also determines the slip velocity (v_r) by eqn (2.2.38)

3. The mass release rate ($\dot{m}_{g_o}$) - either input directly or calculated, via eqn (B.18), Appendix B, from the size of the escape hole.

The other parameters are set to standard values, given in Table 4.2.1, but the program is designed to allow these values to change.

The standard value of S_o comes from a pipeline condition of p = 140 atmospheres and T = 280K. The value of UCONS denotes the initial fixed value of the heat transfer coefficient as described in section 3.4.

The value of K_1, (2.2.5), may be altered by entering a value for the entrainment parameter, β, and using equation (2.3.11) for the case where $w_c = v$, $2b = d_{eff}$, (i.e. a Top Hat profile), this reduces to

$$K_1 = \cdot \pi\beta . \qquad (4.2.2)$$

The value of $K_2=1$ (see eqn (2.2.6), corresponds to the bubbles lying wholly within the plume, and is the only case considered.

The value of K_3, (2.2.37), corresponds to a Top Hat profile and may be altered to model different profiles.

e.g. $2/(1+\lambda_G^2)$ for a Gaussian profile (Appendix E)

Table 4.2.1

PARAMETER	STANDARD VALUE
K_1	0.25
K_2	1
K_3	1
K_4	0.5
$\hat{M}$	0.016
$\dot{\Theta}$	$5\pi/18 (50°)$
T_{sea}	280
UCONS	300
S_o	32.2

4.3 Numerical Procedure

The main components of each step in the numerical integration are as follows:

1. Use of (4.1.6) translates the height risen, h, into a pressure head, z.

2. Comparison of the actual entropy of the gas with that of saturated gas at the same depth (i.e.pressure), (4.1.10), determines the fraction of gas in the vapour phase (4.1.7).

3. Knowledge of the entropy allows calculation of the temperature of the gas, (4.1.8), (4.1.9).

4. Calculation of the density of the vapour phase, ρ_{g_g}, using the ideal gas law (4.1.5) plus (4.1.4) gives the mean density of the bubbles.

5. From the temperature it is then possible to calculate the thermal conductivity, k, from (4.1.14) and hence, via (4.1.12) the heat transfer coefficient can be found. The value of α, (4.1.13), on the first step is obtained from the initial conditions (giving a value of $\alpha = 1$) and thereafter is calculated from the conditions at the previous step (i.e. those of A_1, v and ρ_B).

6. Equations (4.1.1) - (4.1.3) are then integrated and the values of h, A_1, v and S updated.

7. Using (2.2.37), (2.2.43) and (4.1.13) the values of v_g, d_{eff} and α are calculated, while the time elapsed is updated using the equation

$$t_{new} = t_{old} + \frac{\Delta h}{v_g} \qquad (4.3.1)$$

where t_{old} was assigned a value of zero on the first step.

The integration then moves on to the next step and the above components are repeated.

The integration ceases when the surface is reached. At intervals, dictated by another input parameter,

the values of t, depth, v_g, d_{eff}, T, S, ξ, ρ_B and α are printed.

4.4 Variations

(A) To use the program to make comparisons with experimental work, or the numerical work of Sjøen (1983), certain modifications are built into the program.

1. The gas involved can be air, rather than methane.

2. Rather than specifying d_e and $\dot{m}_{g_o}$ it is possible to specify the atmospheric volume rate of release plus the slip velocity.

3. It is assumed that there will be no great drop in pressure as the air is released. Hence there will be no drop in temperature, and so the gas will be at the same temperature as the sea water and the rise will be isothermal.

4. The equations relating to entropy and vapour fraction are not applicable to air. Due to the higher temperature, the air will be completely in the vapour phase, and ξ is assigned a value of 1.0 throughout. We are not interested in the entropy directly, since we know the temperature and can calculate the gas density from this via (4.1.5). It is possible, therefore, to ignore (4.1.3) and reduce the system to two equations.

5. The molecular weight is automatically changed for air calculations to

$$\hat{M} = 0.029 \quad kg/mol. \qquad (4.4.1)$$

B. Referring to 3.1 which gave four possible routes to describe thermodynamically the rise of the gas. Route (3) is the one described in the general program.

Route (4) is highly unlikely and so is not considered.

The other two routes; the opposite extremes are catered for.

1. For no heat transfer, it is simply necessary to set the heat transfer coefficient to zero, i.e. set UCONS to zero, and do not change to the variable from (4.1.12).

2. The other extreme case, where the rise is isothermal, has been discussed at the end of 3.4.

The entropy is calculated from equation (3.5.1) and compared to that of saturated gas (4.1.10). If $S' = S_{sat}$, then the necessary calculations cannot be made and so the program is stopped.

If $S' > S_{sat}$, the entropy calculated from (3.5.1) is the actual entropy of the gas, the vapour fraction is 1.0, and the rest of the calculations are as for main case.

4.5 Validation of Model

The first step was to compare the results with those obtained by Chesters et al (1980), since the equations used were initially motivated by their system. This necessitated using the variation which allowed for air to be used as the gas.

To make a direct comparison, non-dimensionalised values were required. Rather than reformulate the system of equations in non-dimensional form, the results, themselves, were non-dimensionalised, using the same scaling as Chesters, namely,

$$\left.\begin{aligned} \hat{Z} &= z/_{L} \\ \hat{D} &= d/_{L} \end{aligned}\right\} \qquad L = (G_o^2/_g)^{1/5} \qquad (4.5.1)$$

$$\hat{V} = v/_{U} \qquad U = (G_o g^2)^{1/5} \qquad (4.5.2)$$

A little care was required in the correlation of the output.

1. A conversion factor is necessary to convert

   $\hat{D}_{eff}$ to $\hat{D}$

   Now,

$$\frac{\pi d_{eff}^2}{4} = \frac{\pi d^2}{4} + K_2 A_g \qquad \text{by (2.2.6)}$$

$$\Rightarrow \quad 1 = d^2/_{d_{eff}^2} + \frac{K_2 A_g}{\pi d_{eff}^2/4}$$

$$= d^2/d_{eff}^2 + \alpha.$$

Thus,

$$d = \sqrt{1 - \alpha}\, d_{eff} \qquad (4.5.3)$$

and hence,

$$\hat{D} = \sqrt{1 - \alpha}\, \hat{D}_{eff} \qquad (4.5.4)$$

2. In a similar way to 1. it is necessary to convert

$$v_g \text{ to } \hat{V}_g$$

Now (2.2.37) yields

$$v_g = K_3 v + v_r$$

$$\Rightarrow \quad \frac{v_g}{U} = \frac{K_3 v}{U} + \frac{v_r}{U}$$

$$\text{i.e.} \quad \hat{V}_g = K_3 \hat{V} + \hat{V}_r \qquad (4.5.5)$$

3. Values of $\hat{Z}_o - \hat{Z}$ are required, where $\hat{Z}$ refers to the pressure head, but the output from the program refers to true depths.

Letting

z_o^1 = pressure head corresponding to z_o

z^1 = pressure head corresponding to z

then

$$z_o^1 = z_o + 10$$

$$z^1 = z + 10$$

and

$$\hat{Z}_o{}^1 = \frac{z_o{}^1}{L} = \frac{z_o + 10}{L} = \hat{Z}_o + 10/_L$$

$$\hat{Z}^1 = \frac{z^1}{L} = \frac{z + 10}{L} = \hat{Z} + 10/_L$$

Therefore,

$$\hat{Z}_o{}^1 - \hat{Z}^1 = \hat{Z}_o - \hat{Z} \qquad (4.5.6)$$

so that it makes no difference whether we use true depths or pressure heads.

It may be, however, that $\hat{Z}_o{}^1 - \hat{Z}_o$ will not come close to $\hat{Z}_o$.

At the surface $z^1 = 10$, so that at any point of the rise $z^1 \geqslant 10$.

Thus,

$$z_o{}^1 - z^1 \leqslant z_o{}^1 - 10$$

$$\Rightarrow \quad \hat{Z}_o{}^1 - \hat{Z}^1 \leqslant \hat{Z}_o{}^1 - 10/_L \qquad (4.5.7)$$

If the volume release rate is small, then L is small (4.5.1), and $\hat{Z}_o{}^1 - \hat{Z}^1$ is significantly less than $\hat{Z}_o{}^1$.

4. The values of the constants K_1 - K_4 were the same as those used by Chesters.

5. Output from the present model will always yield a value of $\hat{D}_o = 0$, since this comes from the initial

value of A_1 which was zero, on the assumption that initially the area of the plume was entirely gas.

This is not in total agreement with Chesters who assumes a standard value of $\hat{D}_o = 2$. From the sensitivity analysis done on $\hat{D}_o$ by Chesters, it only affects the solutions slightly in the initial stages, where the model does not describe conditions accurately anyway. After this the results are independent of decreasing the value of $\hat{D}_o$.

RESULTS

Table 4.5.1 shows values of $\hat{D}$ at a number of values of $\hat{Z}_o - \hat{Z}$ for a number of cases.

For values of $\hat{Z}_o{}^1$ and $\hat{V}_r$ equal to those standard ones of Chesters, the agreement is very good, except for the first reading which is a little high. This, however, is in the initial region where model is not thought to be accurate.

The sensitivity studies of Chesters predict that variation in $\hat{V}_r$ has little effect on $\hat{D}$, while variation in $\hat{Z}_o{}^1$ does give rise to slight changes; a smaller than standard $\hat{Z}_o{}^1$ leading to an increase in $\hat{D}$, while a larger than standard value shows very little change in $\hat{D}$.

Cases 3-7 have larger values of $\hat{Z}_o{}^1$ but show little variation in $\hat{D}$ (last two values of $\hat{D}$ in each case are rather high, but again program may not accurately predict conditions close to the surface).

Cases 8, 9 have a lower value of $\hat{Z}_o{}^1$ and initially show larger values of $\hat{D}$ though this increase does seem to disappear in last values.

Table 4.5.1 $\hat{D}$ vs $\hat{Z}_o - \hat{Z}$

	$G_o (m^3/s)$	$\hat{Z}_o$	$\hat{Z}_o - \hat{Z}$ / $\hat{V}_r$	25	50	75	100	150	200	250	300	400	450
	Chesters	500	0.25	4.8	10.0	15.0	20.8	30.5	39.2	47.8	55.0	68.0	71.0
1	0.0104	500	0.25	5.5	10.0	14.7	19.5	28.7	38.0	46.5	54.2	68.0	
2	0.000325	500	0.25	5.6	10.2	15.0	19.8		*				
3	0.0104	598	0.25	5.5	10.0	14.5	19.5	29.0	38.0	47.0	55.5	71.5	78.0
4	0.00325	890	0.25	6.0	11.0	15.5	20.0	29.5	39.0	48.0	57.0	75.0	83.5
5	0.0789	541.5	0.25	6.0	10.75	15.2	20.0	29.0	38.0	47.0	55.7	70.0	75.0
6	0.00409	1572	0.27	6.0	10.5	15.0	20.0	29.0	39.0	48.0	58.0	76.0	86.0
7	0.00583	1687	0.25	6.0	10.0	14.0	18.0	28.0	38.0	47.0	56.0	76.0	86.0
8	0.00483	276	0.23	6.0	10.9	15.8	20.6	29.6		*			
9	0.00724	234	0.215	6.0	11.1	16.3	21.2			*			

* Values missing due to scaling

Table 4.5.2 shows an identical set of cases involving the nondimensional velocity $\hat{V}$.

All cases show very good agreement with the results of Chesters, except, perhaps close to the surface where values are a little low. Thus, the variation in $\hat{Z}_o^1$ has little effect on the results as noted by Chesters, while the slight variation in $\hat{V}_r$ in cases 8,9 is linked to a very slight increase in values of V, again backing up the observations of Chesters.

CONCLUSION

These two sets of results show that, at least in the main part of the rise, the present model gives solutions very close to those of Chesters.

Table 4.5.2

$\hat{V}$ is $\hat{Z}_o - \hat{Z}$

	G_o ($m^3/_s$)	$\hat{Z}_o$	$\hat{V}_r$ \ $\hat{Z}_o - \hat{Z}$	25	50	75	100	150	200	250	300	400	450
	Chesters	500	0.25	0.92	0.74	0.65	0.57	0.54	0.51	0.50	0.48	0.56	0.62
1	0.0104	500	0.25	0.90	0.73	0.65	0.59	0.53	0.50	0.49	0.48	0.53	
2	0.000325	500	0.25	0.89	0.72	0.65	0.59			*			
3	0.0104	598	0.25	0.89	0.73	0.64	0.59	0.53	0.49	0.47	0.46	0.46	0.48
4	0.000325	890	0.25	0.88	0.71	0.63	0.58	0.51	0.47	0.44	0.41	0.40	0.40
5	0.0789	541.5	0.25	0.87	0.72	0.64	0.58	0.53	0.50	0.49	0.48	0.49	0.52
6	0.00409	1572	0.27	0.89	0.71	0.62	0.57	0.48	0.44	0.41	0.39	0.36	0.35
7	0.00583	1687	0.25	0.88	0.73	0.65	0.59	0.51	0.45	0.42	0.39	0.36	0.35
8	0.00483	276	0.23	0.88	0.72	0.65	0.62	0.59		*			
9	0.00724	234	0.215	0.86	0.72	0.66	0.62			*			

* Values missing due to scaling

4.6 Sjøen Results vs Present Model

It has already been noted in Chapter 2 how closely the theory behind the present model matched that of Sjøen (1983). Here a comparison is made of the two sets of solutions obtained for the same input conditions of depth, flow rate and slip velocity.

Variations in Standard Program

1. Calculations based on air

2. Volume flow rate and slip velocity input rather than mass flow rate and bubble diameter.

3. To take into account the variation between Gaussian and Top Hat profiles, the constants K_1, K_3 are altered.

   (a) Value of K_1

   From Appendix E, (E.20),

   $$\beta_T = \sqrt{2}\,\beta_G$$

   and hence,

   $$K_1 = \pi\beta_T = \sqrt{2}\pi\beta_G \qquad (4.6.1)$$

   (b) Value of K_3

   From eqn. (2.2.37)

   $$v_g = K_3 v + v_r \qquad (4.6.2)$$

where, as shown in Appendix E,

$$K_3 = \begin{cases} 1 & \text{for Top Hat profiles} \\ \dfrac{2}{1+\lambda_G^2} & \text{for Gaussian profiles} \end{cases} \qquad (4.6.3)$$

The subscripts G, T will denote Gaussian, Top Hat values respectively.

w_G, b_G, α_G, λ_G, may be interpreted as exactly the values of centre-line velocity, effective plume radius, centre-line void fraction and scaling parameter for void fraction profile quoted in Sjoen's results.

w_T and b_T may be interpreted as v and $d_{eff/2}$ from the present model, with α_T equal to the uniform void fraction.

Since the present program outputs values of the average gas velocity, this must be translated into a value for w_T, using (4.6.2) namely

$$w_T = v = \frac{(1+\lambda_G^2)}{2} (v_g - v_r) \qquad (4.6.4)$$

Linear interpolation has been used to evaluate v, d_{eff} and α_T at depths corresponding to those given by Sjøen.

RESULTS

Table 4.6.1 shows the surface values of liquid velocity, plume radius and void fraction in 12 cases, along with the ratios of Sjoen's values to those of the present model (Gaussian to Top Hat).

Case No.	w_G	w_T	w_G/w_T	b_G	b_T	b_G/b_T	α_G	α_T	α_G/α_T	λ_G
1	0.364	0.180	2.02	.118	0.172	0.686	0.0165	0.00379	4.35	0.7
2	0.280	0.139	2.01	0.0973	0.141	0.690	0.0133	0.00236	5.64	0.61
3	0.649	0.322	2.02	0.843	1.205	0.700	0.00712	0.00173	4.12	0.7
4	0.730	0.361	2.02	1.05	1.50	0.700	0.00860	0.00207	4.15	0.7
5	0.826	0.409	2.02	1.08	1.555	0.695	0.0110	0.00265	4.15	0.7
6	0.874	0.431	2.03	1.19	1.725	0.690	0.0128	0.00304	4.21	0.7
7	1.07	0.528	2.03	2.25	3.20	0.703	0.00825	0.00205	4.02	0.7
8	1.22	0.603	2.02	3.96	5.65	0.701	0.0134	0.00324	4.14	0.7
9	0.999	0.495	2.02	7.36	10.4	0.708	0.00496	0.00122	4.07	0.7
10	0.477	0.221	2.02	0.270	0.392	0.689	0.00673	0.00160	4.21	0.7
11	0.535	0.263	2.03	0.329	0.477	0.690	0.00897	0.00237	3.78	0.74
12	0.628	0.309	2.03	0.386	0.560	0.689	0.0108	0.00322	3.35	0.79

Table 4.6.1: Comparison of velocity, plume width and gas fraction: subscripts G, T (Gaussian, Top Hat) refer to Sjoen's results and present model respectively.

Comparing these ratios with the theoretical predictions, based on the assumption of a negligible void fraction and $\lambda_T = 1$, as shown in Appendix E.

$$\frac{w_G}{w_T} = 2$$

$$\frac{b_G}{b_T} = \frac{1}{\sqrt{2}}$$

$$\frac{\alpha_G}{\alpha_T} = \frac{2}{\lambda_G^2} = \begin{cases} 4.08 & \lambda_G = 0.7 \\ 5.37 & \lambda_G = 0.61 \\ 3.65 & \lambda_G = 0.74 \\ 3.20 & \lambda_G = 0.79 \end{cases} \qquad (4.6.7)$$

We can see that there is good agreement in all cases. The fact that in general the velocity and void fraction ratios were found to be slightly larger, and the radius ratio slightly smaller than the theoretical values fits in well with the trends suggested in Appendix E for non-negligible void fraction.

Tables 4.6.2 to 4.4.6 concentrate on cases 1, 2, 7, 8, & 11 and show the corresponding values throughout the rise, rather than just those at the surface.

The term nm^3/s refers to "normal" m^3/s, i.e. at standard temperature and pressure

Table 4.6.2 Case 1 depth = 1.093m, flow rate = 0.000 1416 nm^3/s

z	w_G	w_T	w_G/w_T	b_G	b_T	b_G/b_T	α_G	α_T	α_G/α_T
0.168	0.654	0.323	2.02	0.0192	0.0322	0.596	3.82×10^{-1}	0.677×10^{-1}	5.64
0.279	0.578	0.279	2.07	0.0305	0.0488	0.625	1.67 "	0.329 "	5.08
0.325	0.551	0.267	2.06	0.0354	0.0560	0.632	1.29 "	0.262 "	4.92
0.381	0.523	0.254	2.06	0.0413	0.0640	0.645	9.87×10^{-2}	2.05×10^{-2}	4.81
0.427	0.504	0.245	2.06	0.0462	0.0710	0.651	8.12 "	1.72 "	4.72
0.483	0.483	0.235	2.06	0.0522	0.0795	0.657	6.59 "	1.41 "	4.67
0.52	0.469	0.229	2.05	0.0571	0.0865	0.660	5.64 "	1.22 "	4.62
0.584	0.453	0.221	2.05	0.0630	0.0950	0.663	4.76 "	1.04 "	4.58
0.640	0.439	0.215	2.04	0.0690	0.104	0.663	4.08 "	0.900 "	4.53
0.686	0.428	0.210	2.04	0.0739	0.110	0.672	3.62 "	0.805 "	4.50
0.742	0.417	0.204	2.04	0.0799	0.119	0.671	3.17 "	0.709 "	4.47
0.788	0.408	0.200	2.04	0.0848	0.126	0.673	2.86 "	0.644 "	4.44
0.843	0.399	0.196	2.04	0.0908	0.134	0.678	2.55 "	0.577 "	4.42
0.890	0.391	0.192	2.04	0.0957	0.142	0.674	2.33 "	0.528 "	4.41
0.945	0.383	0.188	2.04	0.102	0.150	0.680	2.10 "	0.480 "	4.38
0.991	0.377	0.186	2.03	0.107	0.156	0.686	1.94 "	0.445 "	4.36
1.05	0.370	0.182	2.03	0.113	0.166	0.681	1.77 "	0.405 "	4.37
1.09	0.364	0.180	2.02	0.118	0.172	0.686	1.65 "	0.379 "	4.35

Table 4.6.3: Case 2. depth = 1.065m, flow rate = 0.0000425nm^3/s

z	w_G	w_T	$w_G/_T$	b_G	b_T	$b_G/_{b_T}$	α_G	α_T	$\alpha_G/_{\alpha_T}$
0.135	0.538	0.265	2.03	0.0130	0.0210	0.619	4.16×10^{-1}	0.589×10^{-1}	7.06
0.190	0.493	0.241	2.05	0.178	0.0283	0.629	2.37 "	0.362 "	6.55
0.246	0.456	0.222	2.05	0.0229	0.0355	0.645	1.55 "	0.245 "	6.33
0.293	0.432	0.211	2.05	0.0271	0.0416	0.651	1.16 "	0.187 "	6.20
0.349	0.408	0.200	2.04	0.0321	0.0486	0.660	8.63×10^{-2}	1.43×10^{-2}	6.03
0.395	0.391	0.191	2.05	0.0363	0.0545	0.666	6.99 "	1.17 "	5.97
0.451	0.374	0.184	2.03	0.0414	0.0620	0.668	5.60 "	0.943 "	5.94
0.491	0.362	0.178	2.03	0.0457	0.0680	0.672	4.74 "	0.809 "	5.86
0.553	0.349	0.172	2.03	0.0507	0.0750	0.676	3.97 "	0.684 "	5.80
0.600	0.340	0.167	2.04	0.0550	0.0810	0.679	3.46 "	0.598 "	5.79
0.656	0.329	0.163	2.02	0.0601	0.0880	0.683	2.98 "	0.517 "	5.76
0.711	0.320	0.158	2.03	0.0652	0.0950	0.686	2.60 "	0.454 "	5.73
0.758	0.314	0.155	2.03	0.0694	0.102	0.680	2.34 "	0.410 "	5.71
0.814	0.306	0.151	2.03	0.0745	0.109	0.683	2.08 "	0.365 "	5.70
0.860	0.300	0.149	2.01	0.0787	0.115	0.684	1.89 "	0.334 "	5.66
0.916	0.294	0.145	2.03	0.0838	0.122	0.687	1.71 "	0.302 "	5.66
0.963	0.289	0.143	2.03	0.0880	0.128	0.688	1.57 "	0.278 "	5.65
1.02	0.284	0.141	2.01	0.0931	0.136	0.685	1.43 "	0.254 "	5.63
1.06	0.280	0.139	2.01	0.0973	0.141	0.690	1.33 "	0.236 "	5.64

Table 4.6.4 Case 7. depth = 32.06 m, flow rate = 0.060nm^3/s

z	w_G	w_T	w_G/w_T	b_G	b_T	b_G/b_T	α_G	α_T	α_G/α_T
1.43	2.04	0.998	2.04	0.119	0.198	0.601	4.42×10^{-1}	0.800×10^{-1}	5.52
3.27	1.65	0.797	2.07	0.258	0.395	0.653	1.18×10^{-1}	0.251 "	4.70
5.11	1.44	0.700	2.06	0.400	0.595	0.672	5.79×10^{-2}	1.28×10^{-2}	4.52
6.64	1.33	0.648	2.05	0.517	0.765	0.676	3.85 "	0.856 "	4.50
8.48	1.24	0.611	2.03	0.657	0.965	0.681	2.66 "	0.600 "	4.43
10.0	1.19	0.580	2.05	0.773	1.12	0.690	2.09 "	0.478 "	4.37
11.8	1.14	0.559	2.04	0.910	1.32	0.689	1.65 "	0.386 "	4.27
13.4	1.11	0.542	2.05	1.02	1.48	0.689	1.41 "	0.328 "	4.30
15.2	1.08	0.528	2.05	1.16	1.66	0.699	1.20 "	0.281 "	4.27
16.7	1.06	0.519	2.04	1.27	1.82	0.698	1.07 "	0.252 "	4.25
18.6	1.04	0.511	2.04	1.40	2.02	0.693	9.62×10^{-3}	2.27×10^{-3}	4.24
20.4	1.03	0.506	2.04	1.53	2.18	0.702	8.83 "	2.09 "	4.22
22.0	1.02	0.503	2.03	1.63	2.34	0.697	8.35 "	1.98 "	4.22
23.8	1.02	0.502	2.03	1.75	2.52	0.694	7.96 "	1.90 "	4.19
25.3	1.02	0.502	2.03	1.85	2.65	0.698	7.77 "	1.86 "	4.18
27.2	1.03	0.506	2.04	1.97	2.82	0.699	7.69 "	1.84 "	4.18
28.7	1.03	0.510	2.02	2.06	2.94	0.701	7.76 "	1.86 "	4.17
30.5	1.05	0.519	2.02	2.16	3.08	0.701	8.02 "	1.94 "	4.13
32.1	1.07	0.528	2.03	2.25	3.20	0.703	8.25 "	2.05 "	4.02

Table 4.6.5 Case 8. depth = 23.74 m, flow rate = 0.33nm^3/s

z	w_G	w_T	$w_{G/wT}$	b_G	b_T	$b_{G/T}$	α_G	α_T	α_G/α_T
1.57	2.13	1.04	2.05	0.305	0.510	0.598	4.49×10^{-1}	0.814×10^{-1}	5.52
2.90	1.86	0.887	2.10	0.537	0.865	0.621	1.71 "	0.335 "	5.10
4.23	1.66	0.805	2.06	0.775	1.19	0.651	9.39×10^{-2}	1.97×10^{-2}	4.77
5.34	1.56	0.752	2.07	0.973	1.47	0.662	6.55 "	1.42 "	4.61
6.67	1.46	0.708	2.06	1.21	1.80	0.672	4.68 "	1.04 "	4.50
7.77	1.40	0.685	2.04	1.41	2.08	0.678	3.74 "	0.844 "	4.43
9.11	1.35	0.656	2.06	1.64	2.41	0.680	2.99 "	0.680 "	4.40
10.2	1.31	0.641	2.04	1.83	2.69	0.680	2.57 "	0.583 "	4.41
11.5	1.28	0.626	2.04	2.06	3.00	0.687	2.20 "	0.506 "	4.35
12.7	1.25	0.611	2.05	2.25	3.29	0.684	1.97 "	0.452 "	4.36
14.0	1.23	0.603	2.04	2.47	3.59	0.688	1.76 "	0.410 "	4.29
15.3	1.22	0.596	2.05	2.69	3.89	0.692	1.61 "	0.377 "	4.27
16.4	1.21	0.592	2.04	2.87	4.14	0.693	1.51 "	0.355 "	4.25
17.8	1.20	0.589	2.04	3.08	4.46	0.691	1.42 "	0.335 "	4.24
18.9	1.20	0.588	2.04	3.26	4.70	0.694	1.37 "	0.325 "	4.22
20.2	1.20	0.589	2.04	3.46	4.97	0.696	1.33 "	0.317 "	4.20
21.3	1.20	0.592	2.03	3.62	5.20	0.696	1.32 "	0.315 "	4.19
22.6	1.21	0.596	2.03	3.81	5.45	0.699	1.32 "	0.317 "	4.16
23.7	1.22	0.603	2.02	3.96	5.65	0.701	1.34 "	0.324 "	4.14

Table 4.6.6 Case 11. depth = 4.11m, flow rate = 0.001171 nm^3/s

z	w_G	w_T	w_G/w_T	b_G	b_T	b_G/b_T	α_G	α_T	α_G/α_T
0.424	1.05	0.526	2.00	0.0368	0.0600	0.613	3.60×10^{-1}	0.736×10^{-1}	4.89
0.645	0.965	0.466	2.10	0.0535	0.0865	0.618	1.83 "	0.391 "	4.68
0.866	0.883	0.426	2.07	0.0710	0.112	0.634	1.12 "	0.252 "	4.44
1.05	0.830	0.402	2.06	0.0857	0.132	0.649	8.07×10^{-2}	1.89×10^{-2}	4.27
1.27	0.779	0.378	2.06	0.103	0.158	0.652	5.85 "	1.39 "	4.21
1.46	0.744	0.362	2.06	0.118	0.179	0.659	4.66 "	1.13 "	4.12
1.68	0.710	0.345	2.06	0.136	0.204	0.667	3.68 "	0.904 "	4.07
1.86	0.685	0.334	2.05	0.151	0.224	0.674	3.10 "	0.772 "	4.02
2.08	0.660	0.323	2.04	0.169	0.250	0.676	2.58 "	0.648 "	3.98
2.27	0.642	0.314	2.04	0.183	0.272	0.673	2.25 "	0.566 "	3.98
2.49	0.623	0.304	2.05	0.201	0.296	0.679	1.93 "	0.492 "	3.92
2.71	0.606	0.297	2.04	0.219	0.320	0.684	1.69 "	0.433 "	3.90
2.89	0.594	0.292	2.03	0.233	0.340	0.685	1.52 "	0.394 "	3.86
3.11	0.580	0.285	2.04	0.251	0.366	0.686	1.36 "	0.352	3.86
3.30	0.570	0.280	2.04	0.266	0.387	0.687	1.25 "	0.323 "	3.87
3.52	0.559	0.275	2.03	0.283	0.412	0.687	1.13 "	0.294 "	3.84
3.70	0.551	0.271	2.03	0.297	0.432	0.688	1.05 "	0.275 "	3.82
3.93	0.542	0.266	2.04	0.315	0.457	0.689	9.64×10^{-3}	2.52×10^{-3}	3.83
4.11	0.535	0.263	2.03	0.327	0.477	0.686	8.97 x "	2.37 "	3.78

Each table shows the same trend in the three ratios:

Velocity - begins at a value higher than the theoretical prediction and gradually decreases to its surface value

Radius - begins at a value lower than theory predicts and increases to its surface value

Void Fraction - varies as the velocity

These three observations are as expected and reflect the fact that in the initial stages, the effect of the non-negligible void fraction is most pronounced.

A final comparison made was that of Mass Flux at the surface, which it would seem reasonable to assume should be the same irrespective of the choice of profile.

From Appendix E(E5, E6), we have the two expressions for Mass flux of liquid

$$\dot{m}_G = \pi\rho_l \, w_G \, b_G^2 \left(1 - \frac{\alpha_G}{1+1/\lambda_G^2}\right) \qquad (4.6.8)$$

$$\dot{m}_T = \pi\rho_l \, w_T \, b_T^2 \, (1 - \alpha_T) \qquad (\lambda_T = 1) \qquad (4.6.9)$$

Table 4.6.7 gives the results of calculation of mass flux at the surface for the 12 cases considered previously, where, as before, subscript G refers to Sjøen value and T to those of present model.

Case Number	m_G	m_T	$m_T - m_G$	$\frac{(m_T - m_G)}{m_G} \times 100\%$
1	15.8	16.7	0.9	5.70
2	8.3	8.66	0.36	4.38
3	1.45×10^3	1.47×10^3	20	1.38
4	2.52×10^3	2.55×10^3	30	1.19
5	3.02×10^3	3.10×10^3	80	2.65
6	3.87×10^3	4.02×10^3	150	3.88
7	1.70×10^4	1.70×10^4	0	0
8	5.98×10^4	6.03×10^4	500	0.84
9	1.70×10^5	1.68×10^5	-2000	-1.18
10	1.02×10^2	1.07×10^2	5	4.90
11	1.81×10^2	1.88×10^2	7	3.87
12	2.93×10^2	3.03×10^2	10	3.41

Table 4.6.7 Comparison of Liquid Mass flux at the surface

RESULTS

It can be seen from the relative differences that there is very good agreement between m_G and m_T in all 12 cases. The moduli of the relative differences, in fact, have a mean of 2.78% and a sample standard deviation of 1.83%, while the true relative differences have a mean of 2.58% and a sample standard deviation of 2.12%.

OVERALL CONCLUSION

The numerical results bear out the claim that the two models are very similar, and that by making use of the relationships in Appendix E, the present model can be used to predict Gaussian values.

CHAPTER 5

SURVEY OF EXPERIMENTAL RESULTS

5.1 General

A brief review is given of known bubble plume experiments. How relevant they are to the present work is debatable. This project was undertaken for the oil industry, which is interested in massive release rates of hydrocarbon gas, whereas the few experimental results available are concerned with relatively small releases of air. Indeed the volumetric flow rates used in the experiments are lower by a factor of thousands. In most cases, also, the depth of release is lower by a factor of 10^2; two exceptions being Topham (1975) and Milgram (1983). Since the surface tension of natural gas against water is similar to that of air against water it is thought that an escape of air bubbles should have the same characteristics as a gas "blowout". This reasoning, however, breaks down at great pressure, i.e. large release depths.

5.2 Review of Bubble Plume Experiments

Kobus (1968) conducted his experiments in an 8 by 280 metre tank with a release depth of 4.5m, and various release rates of between 0.00013 and 0.006 normal m^3/s. The only data obtained was that of the velocity profile at certain heights.

The experiments of Goossens (1979) were on a very small scale with a release depth of 0.28m and airflow rates of the order of 10^{-5} - 10^{-4} m^3/s, similar to those of Tekeli &

Maxwell (1978), although they had a slightly deeper tank giving a release depth of 1m.

Fanneløp & Sjøen (1980) performed experiments in a 10.5 by 260m towing tank with a depth of 10m. They used airflow rates of 0.005 - 0.022 normal m^3/s and measured fluid velocities, as well as influx towards plume (to determine the entrainment parameter).

Fazal & Milgram (1980) used a cylindrical tank of diameter 1.65m and a release depth of 3.9m. They quote only one release rate of 0.00236 normal m^3/s. Their measurements covered air-bubble velocity and momentum flux (from which they derived the liquid velocity) plus the gas fraction distribution within the plume.

Milgram & Van Houten (1982) had a similar laboratory set up to Fazal & Milgram (1982), but considered four release rates varying from 0.000205 to 0.002341 normal m^3/s. They measured bubble and liquid velocity distributions, momentum flux distribution and mean centre-line gas fraction.

Those on a larger scale, which were conducted in open water,include Topham (1975) who used release depths of 23m and 60m and release rates of between 0.06 and 0.36 normal m^3/s.

These release rates are of the same order as that quoted by Topham in a 'standard Beaufort Sea blowout', which refers to an oil blowout with dissolved gas contained in the oil reservoir. Here the escaping gas rate was 0.66 normal m^3/s.

This, however, is still far less than a typical

volumetric release rate encountered in the pure gas escapes being considered in this thesis which is more likely to be 1500 normal m^3/s. Topham only obtained measurements of flow velocity vs radius at various heights. Milgram (1983) considered a release depth of 50m and flow rates of up to 0.59 normal m^3/s, thus considering situations similar to those of Topham (1975). Milgram, too, only managed to make measurements involving velocity profiles.

5.3 Use of Experimental work

A number of parameters used in the theoretical model are assigned standard values, based on experimental observations. These include the slip velocity, v_r, the entrainment parameter, β, and the gas/velocity radius ratio, λ. This last parameter is also referred to as the Schmidt number (see e.g. Milgram & Van Houten (1982)).

Previous mention has been made of typical values of v_r, and β in section 2.2.

Typical values of λ have been suggested, either by visual observation or by comparison of void fraction profile to velocity profile.

Fanneløp & Sjøen (1980) estimate that $\lambda = 0.65 \pm 0.1$, while Milgram & Van Houten (1982) predict a range of values, $\lambda = 0.59 - 0.86$.

Milgram (1983) notes that larger scale plumes, having an increased plume velocity but the same bubble size distribution as smaller ones should reflect an increased value for λ (although still <1.0). His numerical results

for varying λ show that a change of 0.1 in λ leads to a barely detectable change in plume characteristics, a view echoed by Sjøen (1983).

He, therefore, concludes that any value of λ between 0.8 and 0.9 would be appropriate in all but the very small and slow plumes when a value of 0.8 should be used.

5.4 Comparisons of Experiments with Theory

The experimental results of Tekeli & Maxwell (1978) Topham (1975), Fanneløp & Sjøen (1980) and Milgram & Van Houten (1982) are compared by Sjøen (1983) to his theoretical model. In section 4.6 we compared Sjøen's model to the present one, using, in fact, the very set of results he used in his comparison with the experimental values. Having shown the two models to be in fairly good agreement, it is only necessary, therefore, to comment on the results of Sjøen's comparison of theory with experiment.

His conclusion is that over the range of depths and release rates the agreement is very good, the most noticeable discrepancy being in the plume velocity where the theoretical predictions are somewhat higher than the measured mean values.

This may be explained by the fact that the theoretical model ignores the contribution to the momentum flux from the fluctuating component of the velocity. This was noted by Milgram & Van Houten (1982) and Milgram (1983) and a correction made by introducing a momentum-amplification factor. While this factor is significantly greater than 1

in small scale laboratory experiments, it is reduced to a value close to 1 for larger laboratory experiments and is expected to be very close to 1 in the case of subsea pipeline ruptures.

CHAPTER 6

SENSITIVITY STUDIES

6.1 General

As noted in Chapter 1, Smith (1982) concluded that two crucial parameters in determining the surface conditions were the bubble size, d_e, and the heat transfer coefficient, h_T. The reason for this may be seen by examining the expression for the heat transfer (3.4.1).

Clearly, the amount of heat transfer will influence the surface conditions, and this is affected by the bubble size (for equal volumes, the total effective surface area available for heat transfer is reduced as the bubble size is increased), and the heat transfer coefficient.

Change in bubble size will also affect the slip velocity and this too will have a bearing on the plume behaviour.

Available evidence on heat transfer coefficients, e.g. L'Ecuyer, is very limited, while bubble sizes quoted in the literature, e.g. Clift,Grace & Weber (1978) are almost entirely concerned with air released at a rate which is lower by a factor of thousands than the massive release rates experienced in the oil industry and to which this work is aimed.

It should be possible to determine, theoretically, a "critical" bubble size on the basis of some kind of stability argument. Vanden-Broeck & Keller(1980) and Miksis, Vanden Broeck & Keller (1981) considered this approach. They, however, encountered great difficulty while considering only a very idealised problem with axial symmetry. Hence,

in view of the time available, a sensitivity analysis was thought to be the best method of obtaining some sort of answer.

It was hoped that, by performing a sensitivity analysis on each of the two variables, d_e and h_T, it would be possible to investigate their influence on the final state of the gas and to ascertain how precisely each must be described to allow accurate prediction of surface conditions.

6.2 Initial Investigation

The effect of heat transfer was first assessed by considering the two extremes in Fig. 3.1.1 along with a general case allowing for an intermediate amount of heat transfer. Thus, the following cases were looked at

(a) Non-isothermal without heat transfer (route (1))

(b) Non-isothermal with heat transfer (route (3))
   (i) fixed heat transfer coeff; h_T=8
   (ii) variable heat transfer coeff; as given by equation (3.4.16)

(c) Isothermal (route (2))

All other parameters were held constant, and the standard set of values is given in Table 6.2.1.

Parameter	Standard Value
S_o	32.2
K_1	0.25
K_2	1.0
K_3	1.0
K_4	0.5
T_{sea}	280
Depth	80
d_e	0.018
$\dot{m}_{g_o}$	2200

Table 6.2.1: Standard set of parameter values

The surface values of various parameters in each of the four cases are summarised in Table 6.2.2. Linear extrapolation was used to obtain values exactly at the surface, from the last two values output by the program, which lay in the range $10^{-3} < z < 1.5$.

Case / Parameter	a	b(1)	b(2)	c
Time	7.98	7.05	6.35	6.39
v_g	11.0	14.6	14.7	14.7
d_{eff}	19.8	22.6	24.0	24.1
ρ_B	2.21	0.790	0.703	0.686
T	116	244	274	280
S	32.2	42.5	43.5	43.6
α	0.292	0.479	0.463	0.466
ξ	0.756	1.0	1.0	1.0

Table 6.2.2 Surface values for varying amounts of heat transfer.

RESULTS AND CONCLUSIONS

The main points to be taken from Table 6.2.2 are the variation in gas velocity, plume width and gas temperature as the heat transfer increases (since the variable heat transfer coefficient is always greater than the fixed value of b(1), the heat transfer is greater in b(2) than in b(1)).

It can be seen that all three variables increase with increasing heat transfer. The most dramatic changes are from case (a) to b(1) while the changes from b(2) to (c) are very slight.

The values for ρ_B and S are directly related to the temperature and need not be considered separately. It may be noted, however, that the significantly larger value of ρ_B

in case (a), which is not proportional to the drop in temperature, is due to the fact that $\xi < 1$ implying that there is some liquid gas present.

From equation (4.1.13) it can be seen that α varies inversely with ρ_B, v_g and d_{eff}. The very large value of ρ_B in case (a) leads to the small value in α. In the other three cases, however, as v_g and d_{eff} increase, ρ_B decreases and the result is that α is very much the same.

From this, it seems to suggest that the effect of increasing heat transfer is to increase gas velocity, plume width and gas temperature while the void fraction will not change significantly so long as temperature is great enough for all gas to exist in vapour phase.

We shall now go on to examine the influence of the Heat Transfer coefficient in more detail.

6.3. Sensitivity Analysis of Heat Transfer Coefficient

The effect of varying the Heat Transfer Coefficient is now considered in more detail.

The procedure is as follows

1. The standard set of conditions are as given in Table 6.1.1.

2. A non-isothermal expansion is assumed with a constant value for the heat transfer coefficient, h_T.

3. h_T is varied through the values
   0,1,2,3,4,5,6,7,8,9,10,20,30,40,50,60,70,80,90,100

RESULTS AND CONCLUSIONS

Table (6.3.1) shows the surface values of a number of parameters for each value of h_T, linear extrapolation again being used to give the values exactly at the surface.

As noted in 6.2, the three parameters of most interest are the gas velocity, the plume diameter and the gas temperature.

Graphs of final gas velocity, plume diameter and temperature against h_T are shown in Fig. 6.3.1 (a),(b),(c).

It can be seen that all three show a similar trend: an increase with h_T up to approximately $h_T = 10$, followed by a levelling off to an asymptotic limit. By comparison with the final column of Table 6.2.2, this asymptotic limit corresponds to the isothermal case.

This limiting value is achieved earliest by the velocity, then the temperature, and finally by the diameter.

A reasonable conclusion to be drawn would appear to be that for $h_T > 40$, the surface values of all three parameters are independent of h_T and are equal to the values encountered for an isothermal rise.

It was then decided to investigate the manner in which each of these parameters reaches its surface value, and see if this shows any variation with h_T.

The following three graphs

(a) Depth vs velocity for varying h_T [9,10,20,30,...,100]

(b) Depth vs diameter for varying h_T [9,10,20,40,60,80,100]

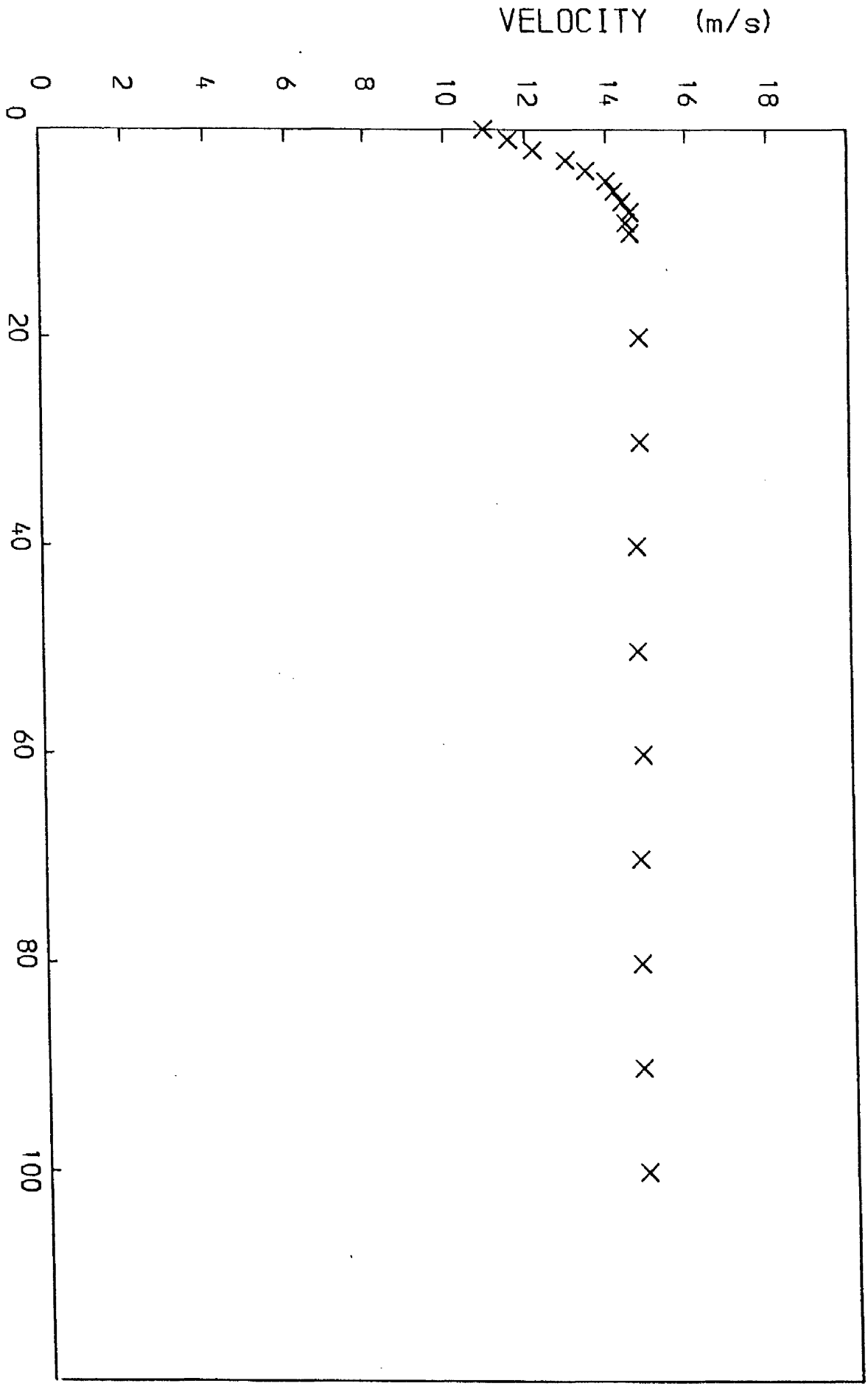
VELOCITY (m/s)
0
2
4
6
8
10
12
14
16
18
0
20
40
60
80
100

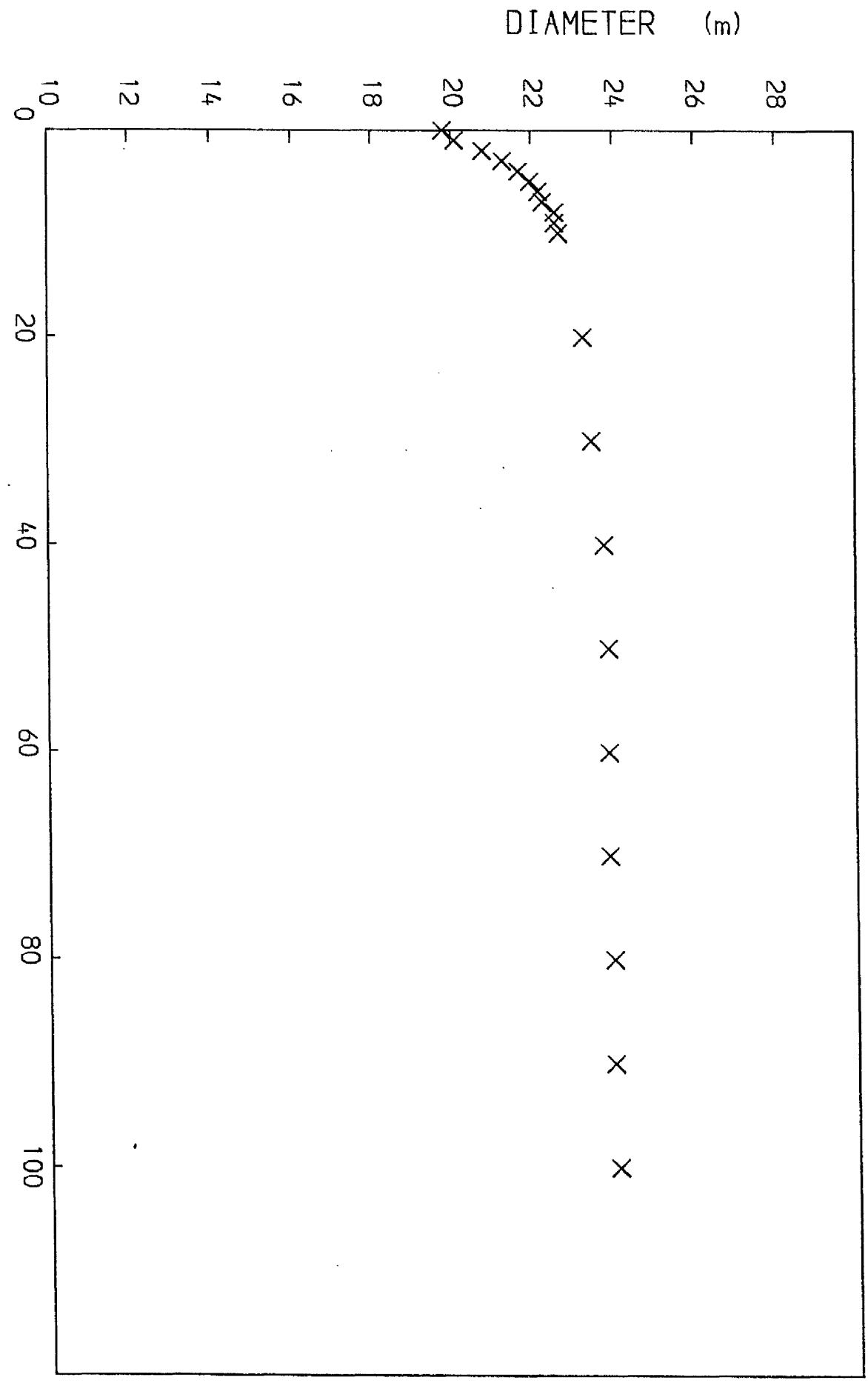

Figure 6.3.1(b): Standard depth and release rate

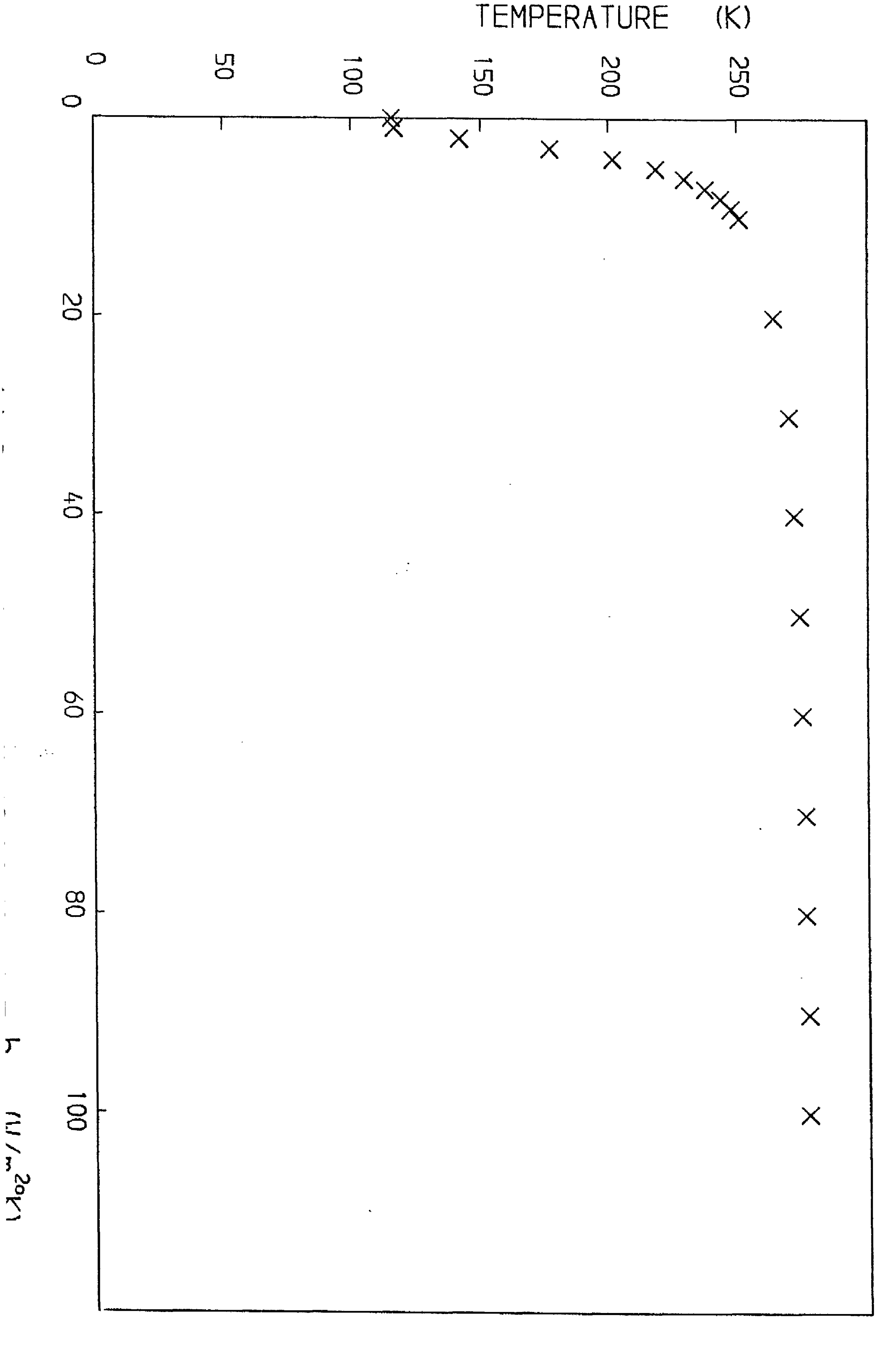
TEMPERATURE (K)
0
50
100
150
200
250
0
20
40
60
80
100

Heat Transfer coeff [W/m^2K]	Time to rise, t (s)	Gas Velocity v_g (m/s)	Plume diam d_{eff} (m)	ξ_B	ρ_B (k_g/m^3)	Void Fraction α	Final Temp T (K)	Final Entropy, S [cal/mol K]
0	7.98	11.0	19.8	0.756	2.21	0.292	116	32.2
1	7.85	11.6	20.1	0.922	1.80	0.330	117	35.1
2	7.71	12.2	20.8	1.0	1.36	0.388	142	38.2
3	7.56	13.0	21.3	1.0	1.10	0.430	177	40.0
4	7.42	13.5	21.7	1.0	0.953	0.455	202	41.1
5	7.30	14.0	22.0	1.0	0.880	0.470	219	41.7
6	7.20	14.2	22.2	1.0	0.836	0.476	230	42.1
7	7.12	14.4	22.3	1.0	0.809	0.479	238	42.4
8	7.05	14.6	22.6	1.0	0.790	0.479	244	42.5
9	7.00	14.5	22.6	1.0	0.777	0.477	248	42.6
10	6.94	14.6	22.7	1.0	0.767	0.481	251	42.8
20	6.68	14.8	23.3	1.0	0.726	0.475	264	43.2
30	6.58	14.8	23.5	1.0	0.713	0.473	270	43.4
40	6.52	14.7	23.8	1.0	0.707	0.474	272	43.5
50	6.50	14.7	23.9	1.0	0.702	0.469	274	43.4
60	6.48	14.8	23.9	1.0	0.700	0.471	275	43.5
70	6.46	14.7	23.9	1.0	0.699	0.470	276	43.6
80	6.45	14.7	24.0	1.0	0.697	0.470	276	43.6
90	6.45	14.7	24.0	1.0	0.696	0.469	277	43.5
100	6.44	14.8	24.1	1.0	0.695	0.469	277	43.6

Table 6.3.1

(c) Depth vs temperature for varying h_T [9,10,20,30,...100] are shown in Fig. 6.3.2 (a),(c),(b).

RESULTS AND CONCLUSIONS

Fig. 6.3.2(a) shows that for $h_T > 20$, where the surface velocities are approximately constant, the velocities are independent of h_T from a depth of 30m to the surface and follow a common path. At depths greater than 30m, the paths begin to diverge one by one, the lower h_T is the sooner the values diverge from the common path until at a depth of 70m there is a distinct variation in velocity with heat transfer coefficient.

Fig. 6.3.2.(c) shows that for $h_T > 40$, the diameter is independent of h_T throughout the rise. From Fig. 6.3.1(b) it can be seen that it is only for $h_T \geqslant 40$ that the surface diameter is independent of h_T. For lower values of h_T, the variation in d_{eff} with h_T is independent of depth.

Fig. 6.3.2(b) shows that the greater h_T is the more quickly the temperature reaches its maximum value. For $h_T = 20$, the gas undergoes an isothermal expansion over approximately the final 30m while for $h_T = 100$, the rise is isothermal after the first 10m.

To conclude, it seems that from a depth of 30m to the surface, the gas velocity, plume diameter and gas temperature are independent of the exact value of h_T as long as it exceeds some critical value, evidently in the range 20-40. Below this, the velocity and temperature do show some variation with h_T although this is only very appreciable in

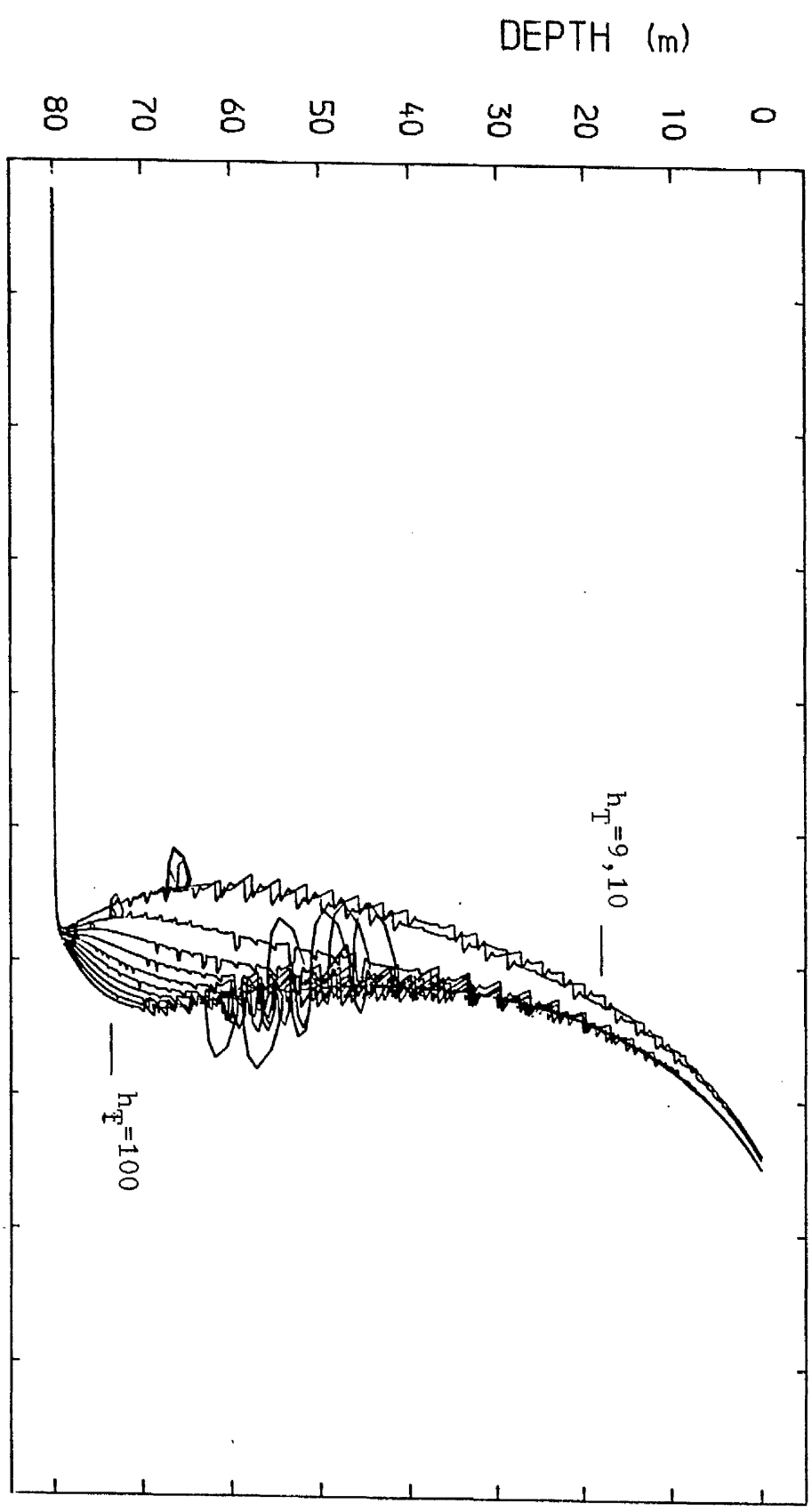

Figure 6.3.2.(a): standard depth and release rate

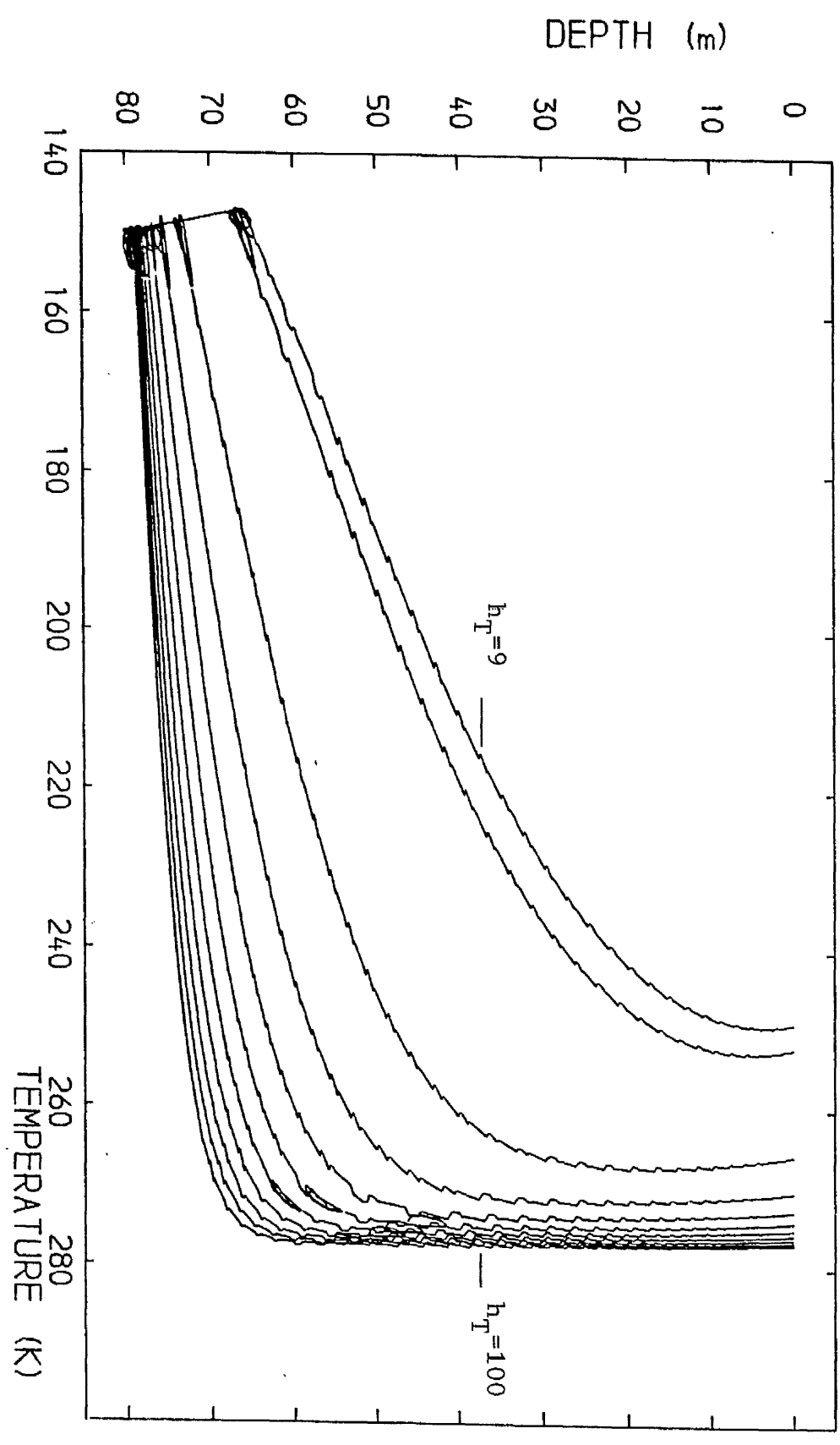

Figure 6.3.2.(b): standard depth and release rate

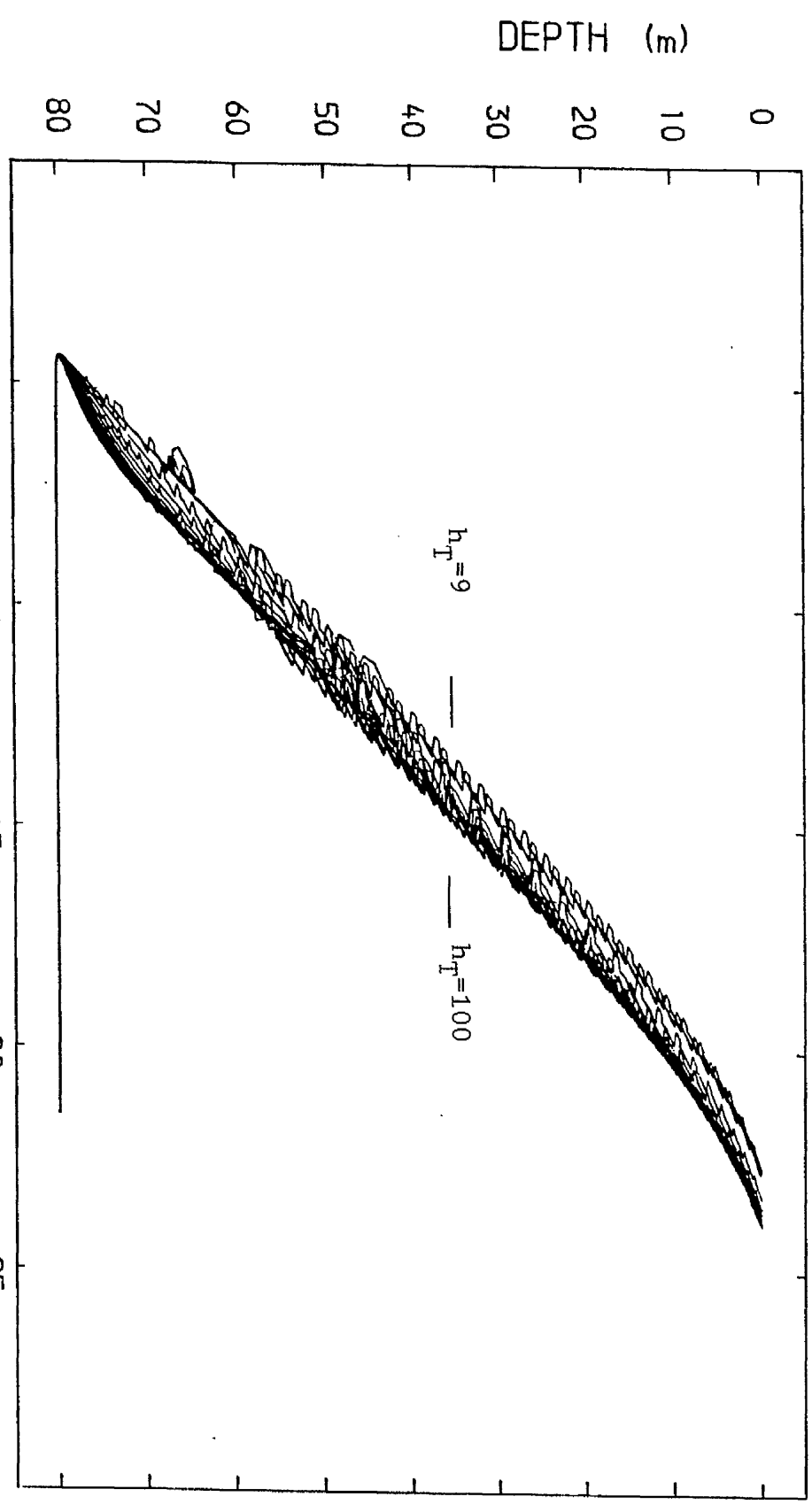

Figure 6.3.2.(c): standard depth and release rate

the temperature for $h_T \geqslant 10$.

Another point to note with regard to the variation in temperature with h_T, is the route the temperature takes from its initial value of 150K to its surface value

(a) For $h_T = 0,1$, the temperature simply falls

(b) For $h_T = 2\text{-}8$, the temperature falls initially, but then rises

(c) For $h_T = 9,10,20$, the temperature varies as in (b) until close to the surface it experiences a slight decrease

(d) For $h_T \geqslant 30$, the temperature rises immediately and continues to its maximum value which it maintains until close to the surface where it undergoes a slight decrease as in (c).

This reflects a comment made in 3.1.

From (3.1.2)

$$c_p \, dT = \delta q + \underbrace{\nu dp}_{\text{negative}}$$

so that

$$\delta q < |\nu dp| \Rightarrow dT < 0$$

$$\delta q > |\nu dp| \Rightarrow dT > 0$$

Hence, for δq small, the temperature will fall.

e.g. for $h_T = 0$, $\delta q = 0$ and so the temperature falls

throughout the rise of the gas.

Cases (b), (c) occurswhen δq is initially $< |vdp|$, but then as the bubbles expand δq increases above $|vdp|$.

Case (d) corresponds to the case when δq is initially $> |vdp|$ and so there is no initial drop in temperature.

The slight drop in temperature experienced close to the surface in cases (c), (d) corresponds to the expansion being so great that $|vdp|$ exceeds δq again.

Having concluded that for $h_T > 40$, the rises were indistinguishable from a depth of around 30m to the surface, the sensitivity analysis for h_T was repeated for a release depth of 30m. The large release rate of 2200 kg/s was retained, with all other input values as in Table 6.2.1.

Table 6.3.2 and Fig. 6.3.3 (a),(b),(c), correspond exactly with Table 6.3.1 and Fig. 6.3.1 (a),(b),(c).

RESULTS AND CONCLUSIONS

Again it can be seen that after initial increases the graphs tend to level off for values of $h_T \geqslant 20$. In the case of the diameter a slight increase can still be detected but it is much less than that observed for values of $h_T < 20$.

Comparing the asymptotic limits on each graph with those for a depth of 80m, that of the velocity is increased, while that of the diameter is decreased and the temperature limit is approximately the same. These may be attributed to the following -

The Temperature limit is the same since it corresponds to the isothermal case with $T = T_{sea}$.

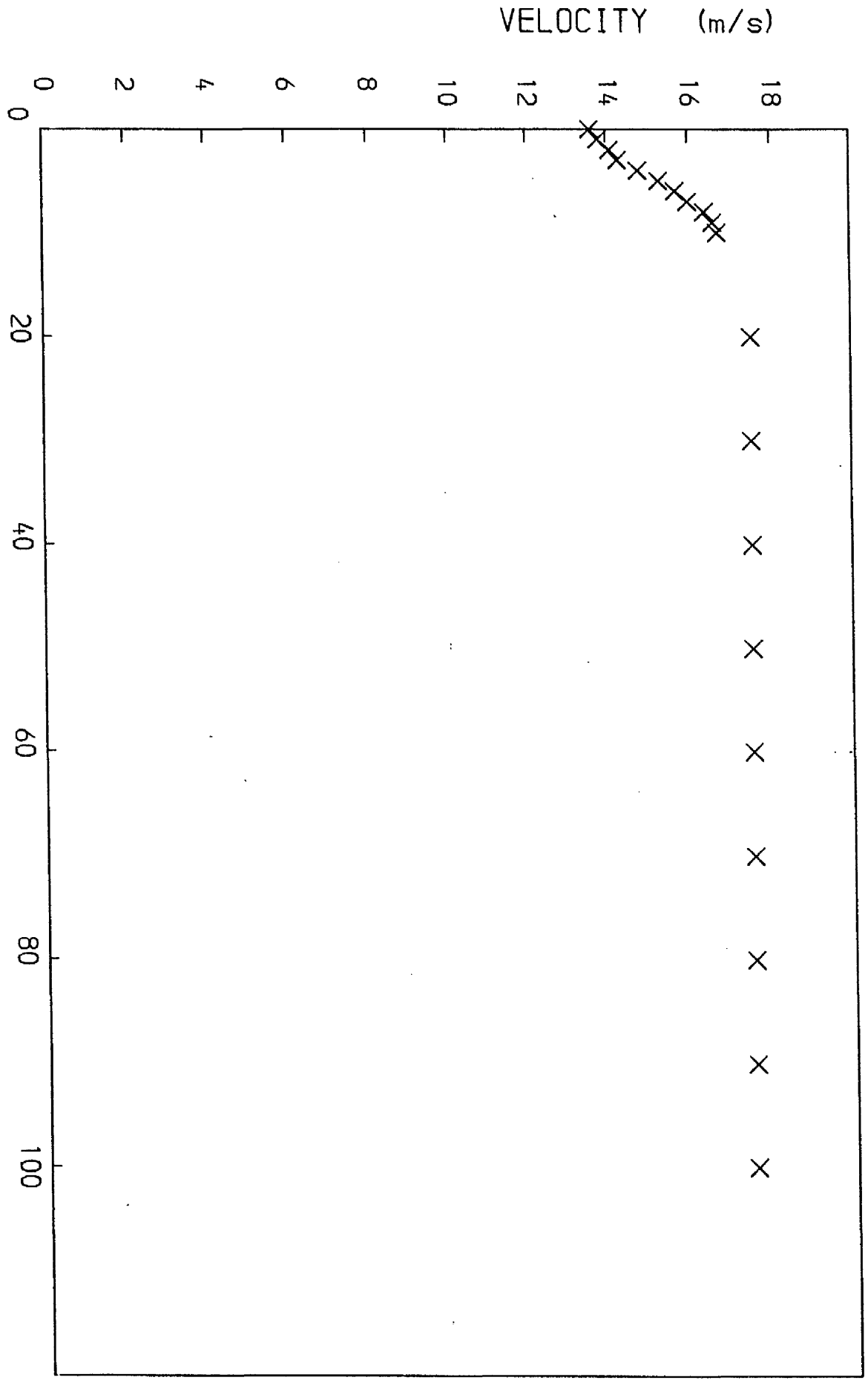

Figure 6.3.3.(a): depth = 30m

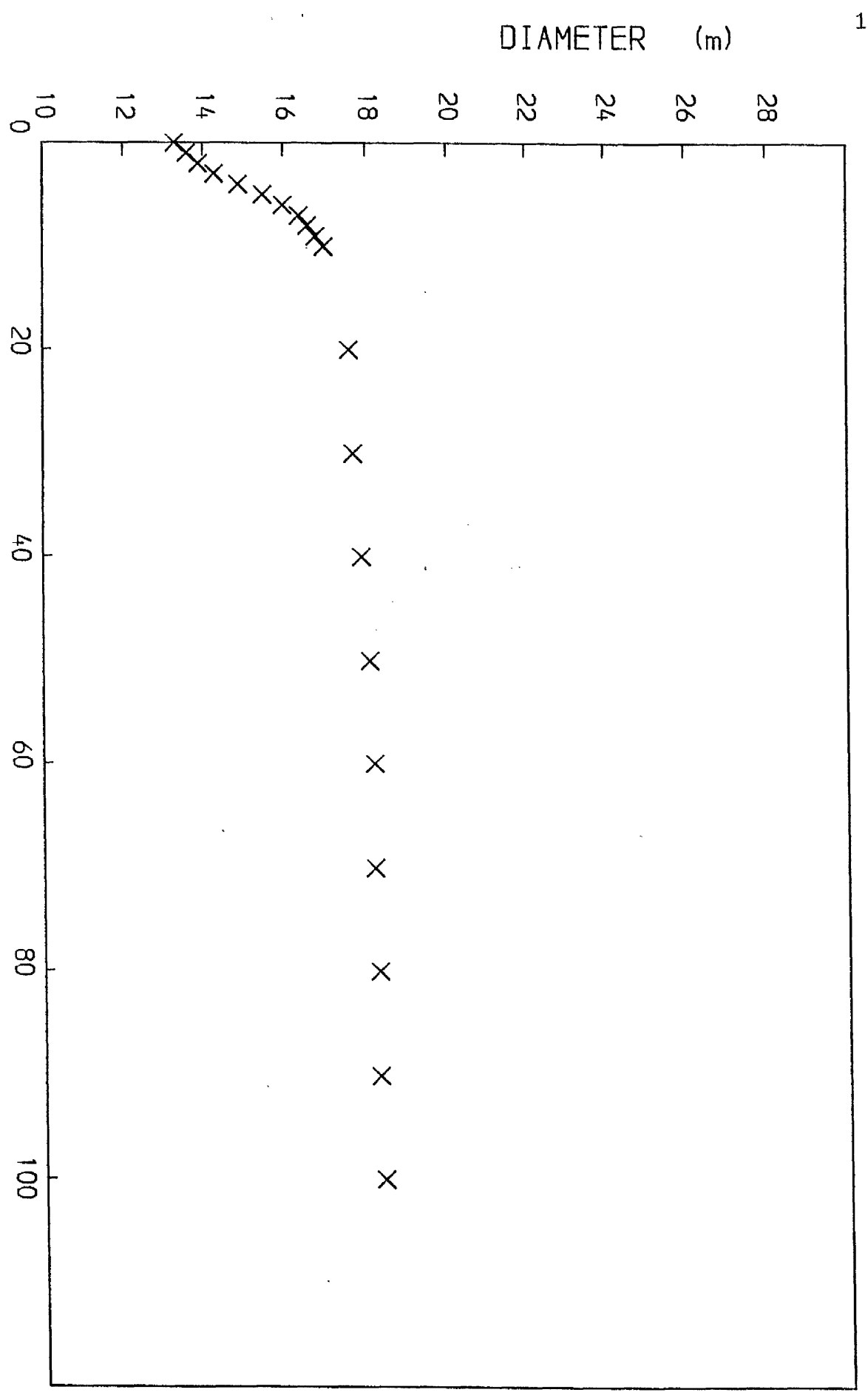
DIAMETER (m)
10
12
14
16
18
20
22
24
26
28
0
20
40
60
80
100
h (W/m²°K)

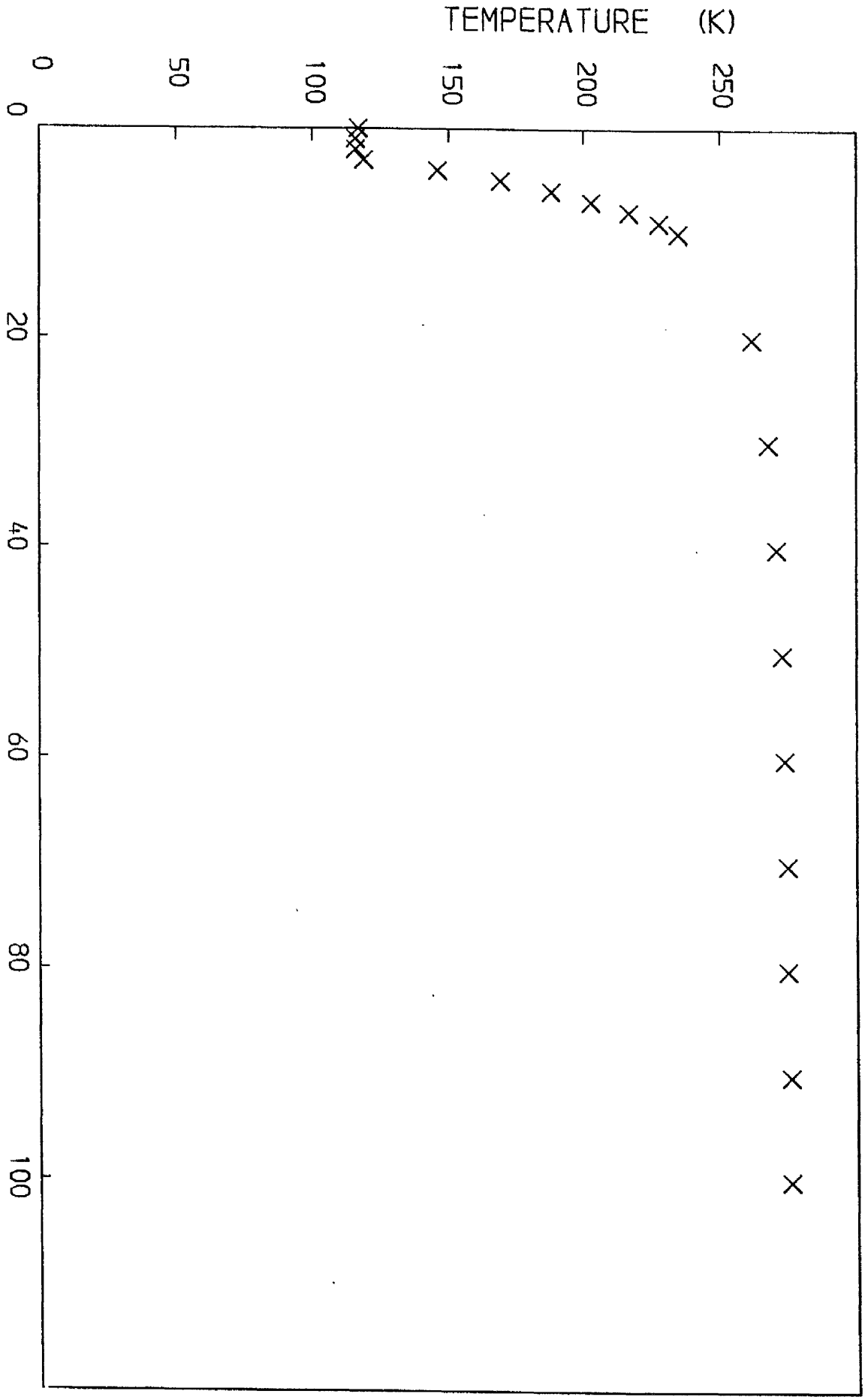

Figure 6.3.3.(c): depth = 30m

The decrease in depth reduces the amount of water entrainment which leads to a decrease in the plume width. With the decrease in entrainment the effective buoyancy force is increased which increases the velocity.

Concentrating on the plateau region graphs corresponding to Fig. 6.3.2 (a),(b) are shown in Fig. 6.3.4 (a),(b), the graph concerning the diameter being omitted as it did not show such interesting characteristics.

As before, the common feature in the two graphs is that the higher h_T is, the more immediate is the change towards the asymptotic limit. Both graphs show a very similar shape to the corresponding one for the 80m depth. In the case of the velocity, the depth of the common point is now 5m and below this the spread is a little more pronounced. In the case of the temperature, for $h_T = 20$ the isothermal rise is only over the last 5m, while for $h_T = 100$ it is over 25m of the the 30m rise.

Finally, the sensitivity analysis was performed once more for a different gas flow rate. Standard conditions are as in Table 6.2.1, except we now have $\dot{m}_{g_o} = 220$, i.e. a decrease by a factor of 10.

An identical set of Tables and graphs to those for the second case were drawn up, and are shown in Table 6.3.3, Fig. 6.3.5 (a),(b),(c) and Fig. 6.3.6(a),(b).

RESULTS

Yet again both the velocity and temperature experience an initial increase with increasing h_T, before levelling off.

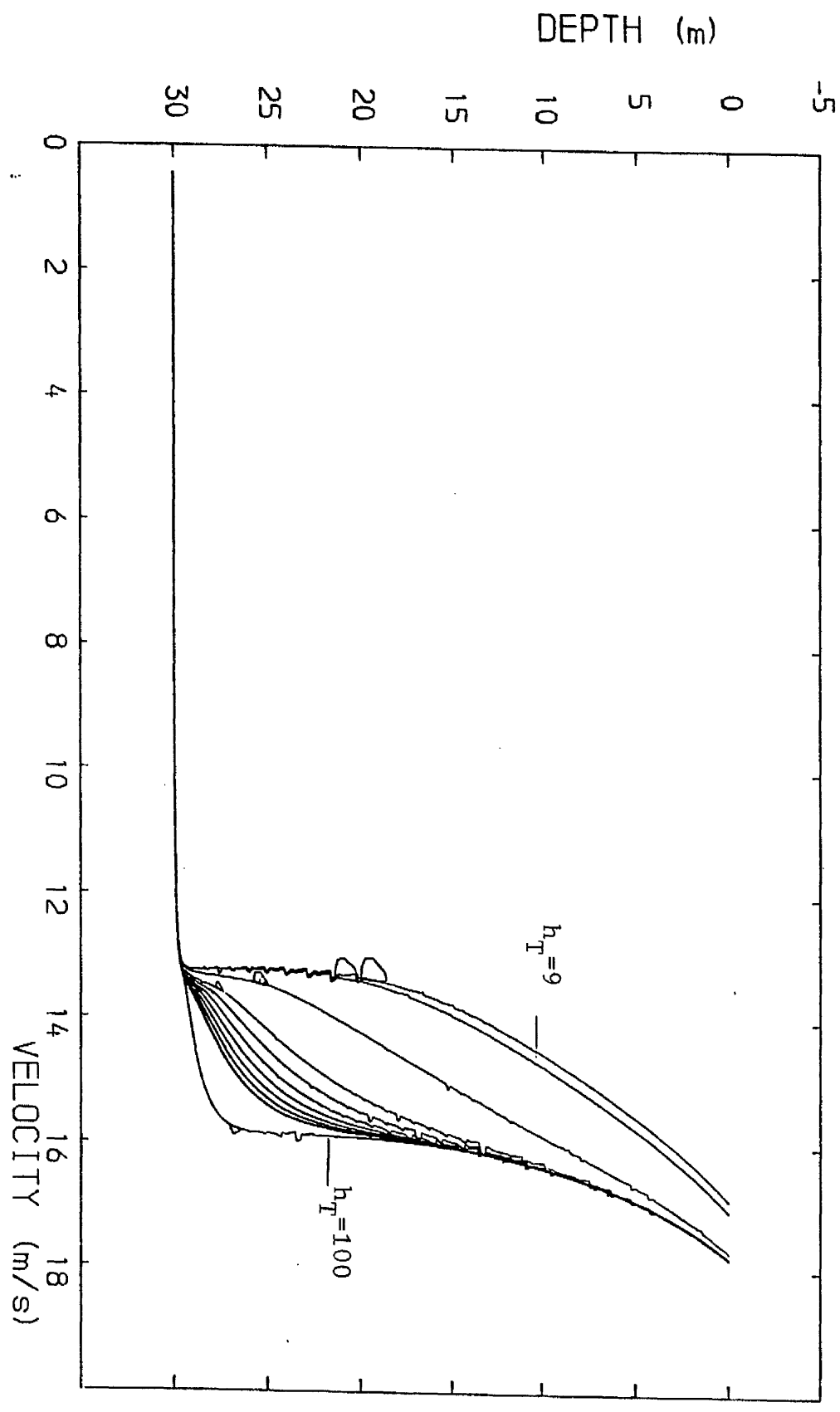

Figure 6.3.4.(a): Depth = 30m

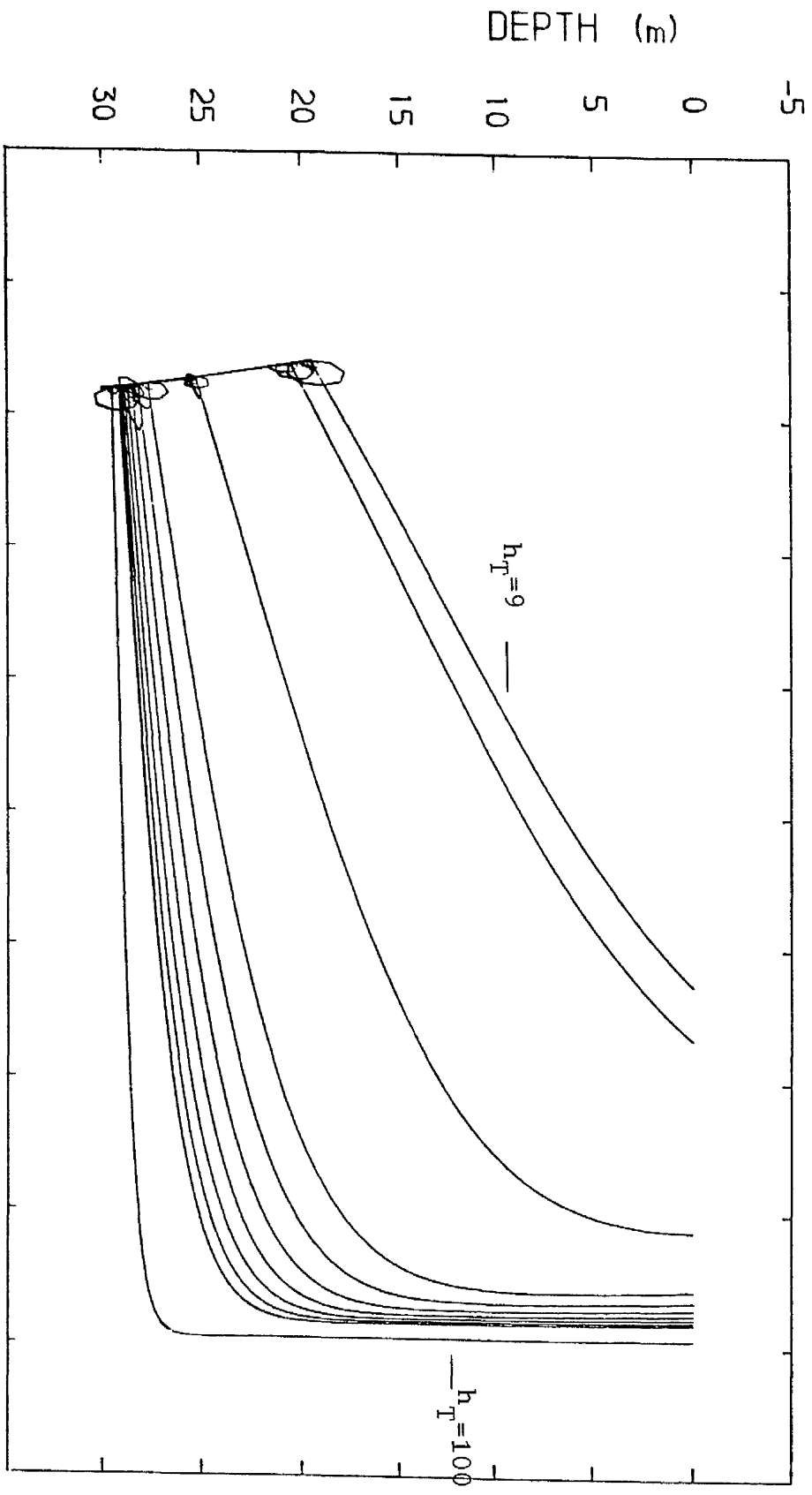

Figure 6.3.4.(b): Depth = 30m

Heat Transfer coeff, h_T [W/m^2K]	Time to rise (s)	Gas Velocity v_g (m/s)	Plume diam. d_{eff} (m)	ξ	ρ_B (kg/m^3)	Void fraction α	Final Temp, T (K)	Final Entropy, S [Cal/mol.K]
0	2.44	13.6	13.3	0.755	2.20	0.531	117	32.2
1	2.42	13.8	13.6	0.836	1.98	0.552	116	33.6
2	2.41	14.1	13.9	0.926	1.79	0.572	116	35.2
3	2.39	14.3	14.3	1.0	1.61	0.591	119	37.0
4	2.37	14.8	14.9	1.0	1.31	0.632	146	38.5
5	2.35	15.3	15.5	1.0	1.14	0.658	169	39.6
6	2.33	15.7	16.0	1.0	1.02	0.676	188	40.4
7	2.31	16.0	16.4	1.0	0.946	0.688	203	41.1
8	2.29	16.4	16.6	1.0	0.889	0.694	217	41.6
9	2.27	16.6	16.8	1.0	0.842	0.699	228	42.0
10	2.25	16.7	17.0	1.0	0.815	0.703	235	42.2
20	2.14	17.5	17.6	1.0	0.734	0.698	262	43.1
30	2.10	17.5	17.7	1.0	0.718	0.689	268	43.3
40	2.07	17.5	17.9	1.0	0.711	0.687	271	43.4
50	2.05	17.5	18.1	1.0	0.706	0.685	273	43.5
60	2.04	17.5	18.2	1.0	0.703	0.684	274	43.6
70	2.03	17.5	18.2	1.0	0.701	0.683	275	43.5
80	2.03	17.5	18.3	1.0	0.699	0.682	275	43.6
90	2.02	17.5	18.3	1.0	0.698	0.682	276	43.6
100	2.02	17.5	18.4	1.0	0.697	0.682	276	43.6

Table 6.3.2 Depth = 30m

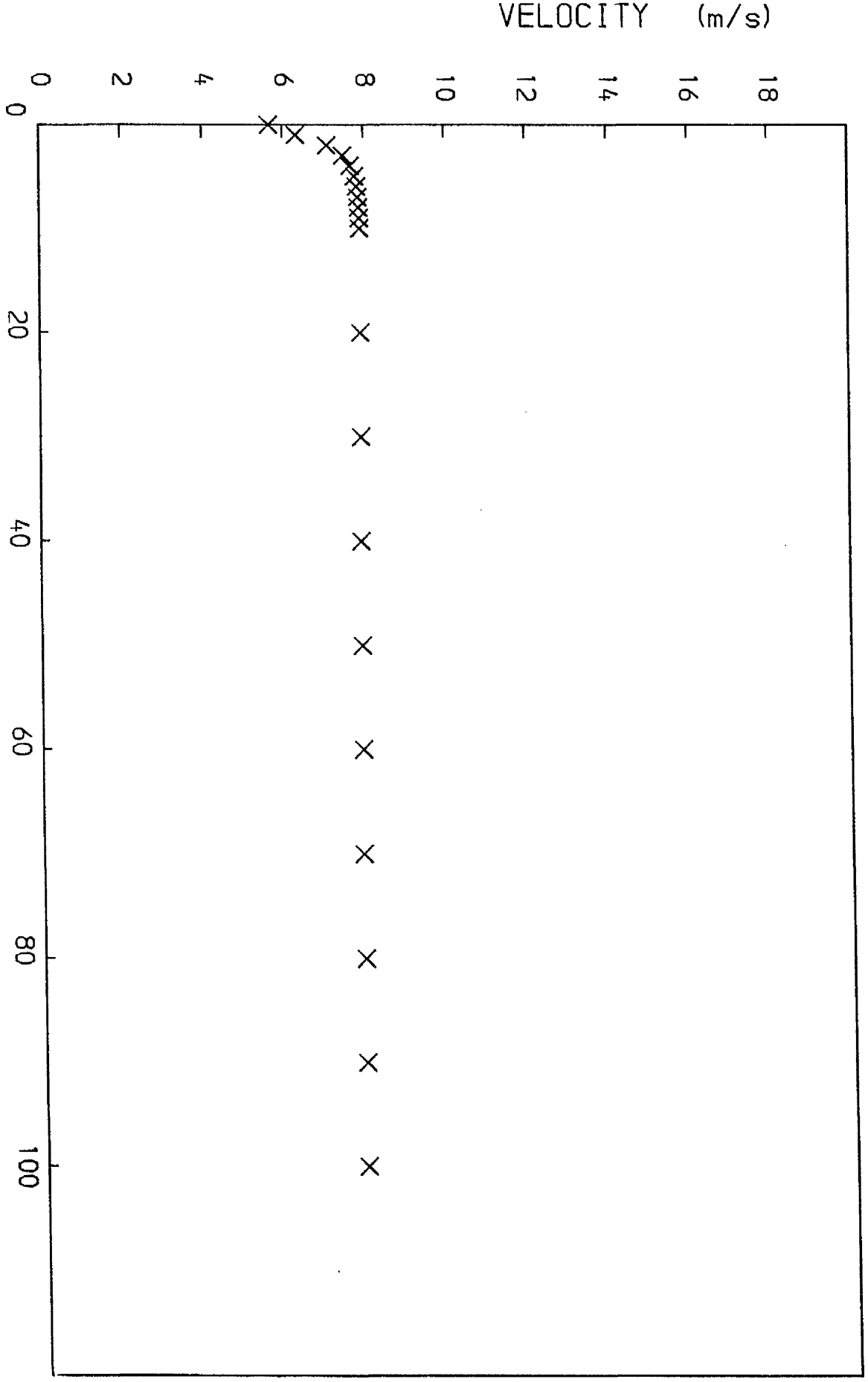

Figure 6.3.5.(a): $\dot{m}_{oc}$ = 220 kg/s

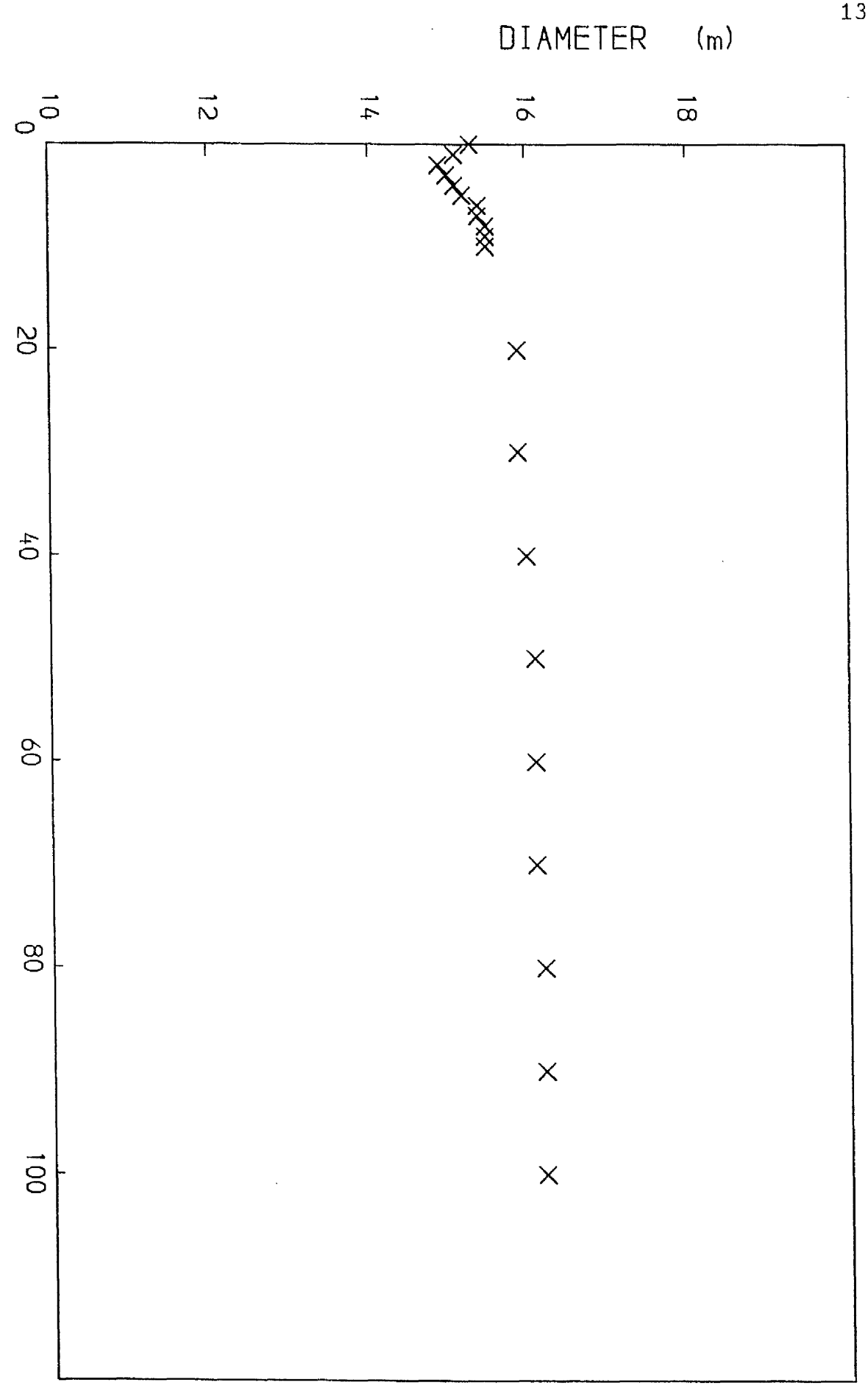

Figure 6.3.5(b): $\dot{m}_g$ = 220 kg/s

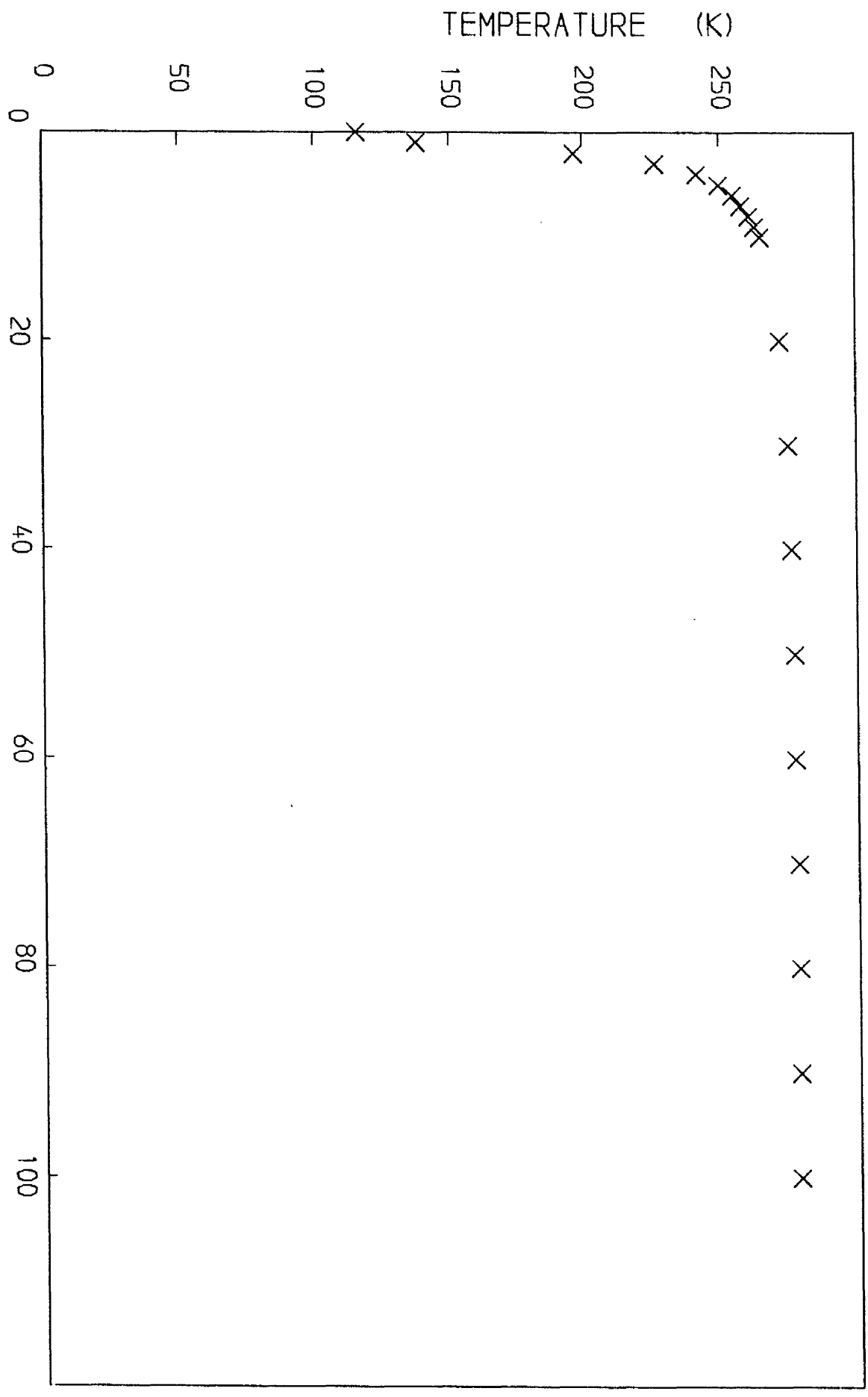

Figure 6.3.5(c) : $\dot{m}$ = 220 kg/s

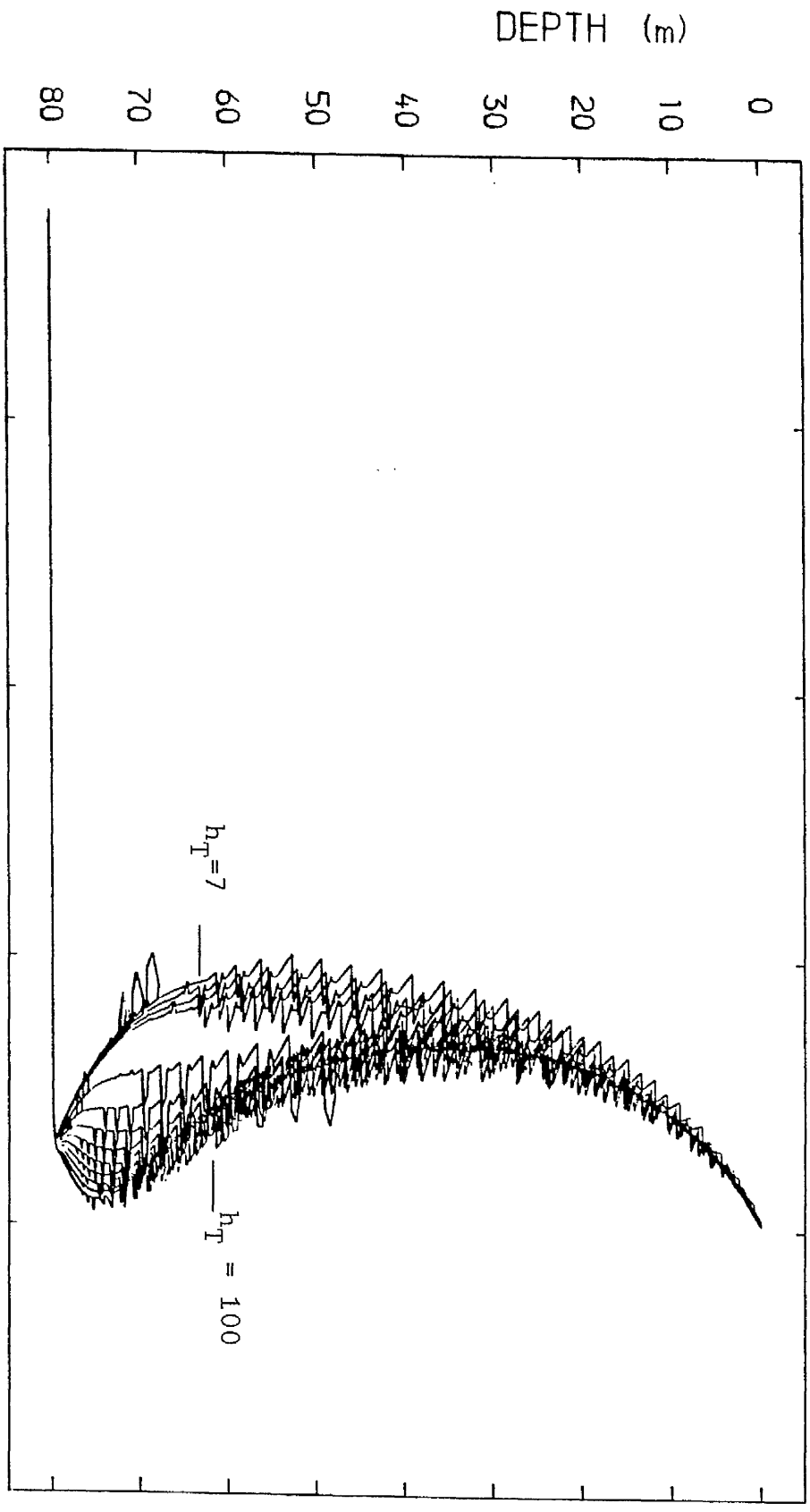

Figure 6.3.6(a): $\dot{m}_{g_o}$ = 220 kg/s

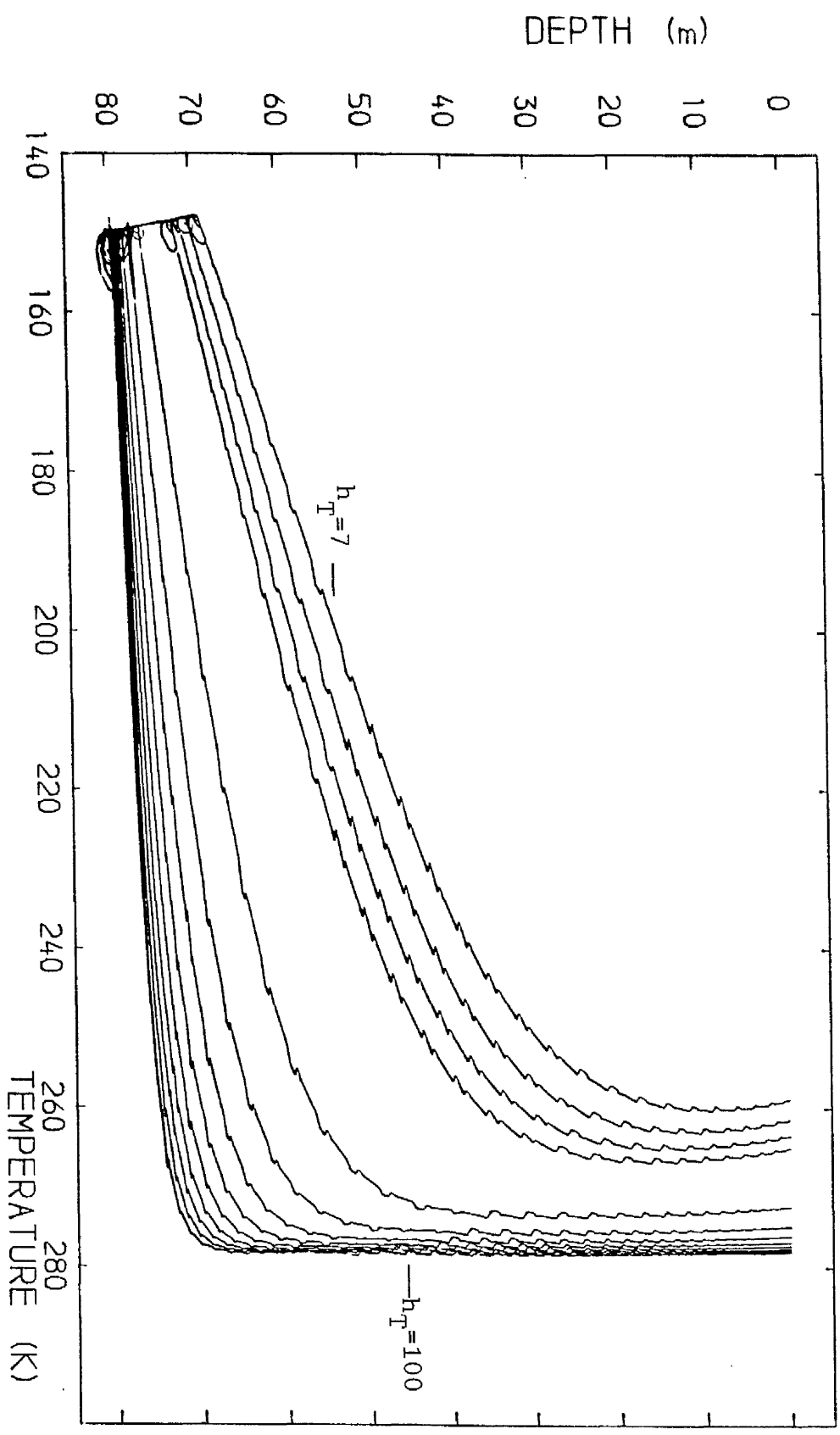

Figure 6.3.6(b): $\dot{m}_{g_o}$ = 220 kg/s

Heat Transfer coeff, h_T [W/m^{2}K]	Time to rise (s)	Gas Velocity v_g (m/s)	Plume diam. d_{eff} (m)	ξ	ρ_B (kg/m^3)	Void Fraction α	Final Temp, T (K)	Final Entropy, S [Cal/mol.K]
0	14.73	5.67	15.3	0.755	2.20	0.0960	116	32.2
1	14.22	6.33	15.1	1.0	1.39	0.139	138	38.0
2	13.65	7.10	14.9	1.0	0.978	0.181	197	40.8
3	13.21	7.49	15.0	1.0	0.847	0.196	227	42.0
4	12.90	7.67	15.1	1.0	0.795	0.201	242	42.6
5	12.66	7.78	15.2	1.0	0.771	0.202	250	42.8
6	12.49	7.83	15.4	1.0	0.756	0.201	255	43.0
7	12.35	7.86	15.4	1.0	0.745	0.202	258	43.1
8	12.24	7.88	15.5	1.0	0.738	0.203	261	43.0
9	12.16	7.89	15.5	1.0	0.733	0.201	263	43.2
10	12.08	7.90	15.5	1.0	0.729	0.202	265	43.3
20	11.74	7.90	15.9	1.0	0.707	0.199	272	43.5
30	11.63	7.89	15.9	1.0	0.701	0.199	275	43.6
40	11.58	7.88	16.0	1.0	0.697	0.196	276	43.5
50	11.56	7.88	16.1	1.0	0.695	0.196	277	43.6
60	11.54	7.88	16.1	1.0	0.694	0.196	277	43.5
70	11.53	7.86	16.1	1.0	0.694	0.197	278	43.7
80	11.52	7.87	16.2	1.0	0.692	0.196	278	43.6
90	11.52	7.87	16.2	1.0	0.691	0.195	278	43.6
100	11.51	7.86	16.2	1.0	0.691	0.195	278	43.6

Table 6.3.3 $\dot{m}_{g_0}$ = 220 kg/s

For the temperature this occurs at $h_T = 20$, but for the velocity the limiting value is reached for $h_T = 7$.

The asymptotic limit for the velocity is much lower than for $\dot{m}_{g_o} = 2200$, caused by the decrease in buoyancy force, while that for the temperature is about the same, due to it again being equivalent to an isothermal rise. Fig. 6.3.5(b) shows that the surface plume diameter is subject to an initial decrease, followed by a steady increase up to $h_T = 20$. After this the graph levels off, but a slight increase is still apparent. Values of the diameter are significantly less than for $\dot{m}_{g_o} = 2200$, which is to be expected with the large drop in the volume of gas at the surface.

Fig. 6.3.6 (a),(b), show trends very similar to the corresponding graphs in the previous cases. For the temperature the large initial spread can be seen at a depth of 75m, $h_T = 20$ gives isothermal conditions from a depth of around 45m while $h_T = 100$ allows this to occur at around 70m below the surface.

For the velocity, since the plateau region in Fig. 6.3.5 (a) begins earlier, fig. 6.3.6(a) involves values of $h_T \geqslant 7$. The spread can clearly be seen at a depth of 75m, gradually decreasing as the gas rises, until at around 25m a point is reached whence the rise is virtually independent of h_T.

To draw some general conclusions, it seems that, for typical depths and release rates of interest to the oil industry, there exists some critical value in the range 20-40 whereby for all values of h_T greater than this critical

value the surface conditions are independent of the heat transfer coefficient and correspond to an isothermal rise. This state is also true over the latter stages of the rise (last 5m for a 30m depth and 25-30m for an 80m depth).

A similar result holds for reduced depths of release or reduced release rates, the critical value being slightly higher in the case of reduced depth and slightly lower for a smaller release rate.

For shallower releases, there is a decrease in the fraction of depth over which isothermal conditions exist. (16% for 30m depth and 31-38% for 80m).

6.4 Sensitivity Analysis of Bubble Size

The investigation into the effect of bubble size on the behaviour of the plume is carried out in two stages.

Stage 1 is as follows:

1. The standard set of conditions as given in Table 6.4.1 are used in the program.

2. The equivalent diameter, d_e, is varied through the values
   0.009, 0.018, 0.036, 0.05, 0.1, 0.15, 0.18, 0.20, 0.25.

3. A non-isothermal expansion is assumed. Due to the fact that the bubble size affects the rise of gas through both the change in heat transfer and change in slip velocity, two separate cases are considered.
   (a) A constant value is assumed for the heat transfer coefficient: $h_T = 8$.

(b) The heat transfer coefficient is assumed to be zero: this removes any heat transfer and means that any variations will be due to changes in the slip velocity.

Comparison of the two cases will then allow us to evaluate the effect of the bubble diameter on the heat transfer within the plume.

Parameter	Standard Values
S_o	32.2
T_{sea}	280
Depth	80
$\dot{m}_{g_o}$	2200
K_1	0.25
K_2	1.0
K_3	1.0
K_4	0.5

Table 6.4.1 Standard values.

RESULTS AND CONCLUSIONS

Tables 6.4.2(a),(b) show surface values of various parameters for each value of d_e in cases (a) and (b). Again concentrating on the temperature, velocity and plume diameter, graphs are drawn of each of these variables against bubble diameter, the results from the two cases being combined on the one graph.

Bubble Size d_e (m)	Slip Velocity v_r (m/s)	Gas Velocity v_g (m/s)	Plume Diam. d_{eff} (m)	ξ	ρ_B (kg/m^3)	Void Fraction α	Final Temp, T (K)	Final Entropy, S [cal/mol/k]
0.009	0.212	14.8	23.1	1.0	0.736	0.477	262	43.8
0.018	0.3	14.6	22.6	1.0	0.790	0.479	244	43.0
0.036	0.424	13.6	21.6	1.0	0.958	0.454	202	42.1
0.05	0.5	13.0	21.1	1.0	1.12	0.423	172	39.8
0.10	0.707	12.0	20.2	0.996	1.67	0.340	116	36.5
0.15	0.866	11.9	19.9	0.909	1.82	0.323	116	35.1
0.18	0.949	11.9	19.9	0.880	1.89	0.315	116	34.6
0.20	1.00	11.8	19.9	0.866	1.92	0.310	116	34.2
0.25	1.12	11.8	19.8	0.843	1.97	0.305	115	33.7

Table 6.4.2(a) h_T = 8 W/m^2/K

Bubble Size d_e (m)	Slip Velocity v_r (m/s)	Gas Velocity v_g (m/s)	Plume Diameter d_{eff} (m)	ξ	ρ_B (kg/m^3)	α	T (K)
0.009	0.212	10.9	19.9	0.756	2.20	0.294	115
0.018	0.3	11.0	19.8	0.756	2.21	0.292	116
0.036	0.424	11.1	19.8	0.756	2.20	0.293	116
0.05	0.5	11.2	19.8	0.755	2.21	0.291	116
0.10	0.707	11.2	19.7	0.756	2.20	0.290	115
0.15	0.866	11.3	19.7	0.756	2.20	0.288	115
0.18	0.949	11.4	19.7	0.757	2.20	0.285	116
0.20	1.00	11.5	19.7	0.756	2.19	0.286	116
0.25	1.12	11.6	19.6	0.756	2.20	0.286	116

Table 6.4.2 (b) $h_T = 0$

These are shown in Figs. 6.4.1(a), (b), (c).

In case (b), with no heat transfer, the graphs show that the gas temperature, plume velocity and plume diameter are virtually invariant under changes in bubble size. Since, as noted, variation in bubble size in case (b) corresponds exactly with variation in slip velocity, these results show that gas temperature, plume velocity and plume diameter are not sensitive to small changes in slip velocity (0.212 to 1.12 m/s for the bubble sizes considered). This is in total agreement with observations of Brevik (1977) and Milgram (1983).

In case (a), where h_T = 8 $W/m^2/^oK$, the effect of increasing the bubble size is to

(i) Decrease the gas temperature

(ii) Decrease the plume velocity

(iii) Decrease the plume diameter

These observations can be explained as follows:

Temperature:

As noted before; for the same volume of gas, larger bubbles reduce the overall surface area available for heat transfer. Reducing the heat transfer reduces the increase in entropy and hence, from equation (3.2.17), reduces the temperature.

Velocity:

The decrease in temperature results in an increase in density which reduces the net upward force and hence,

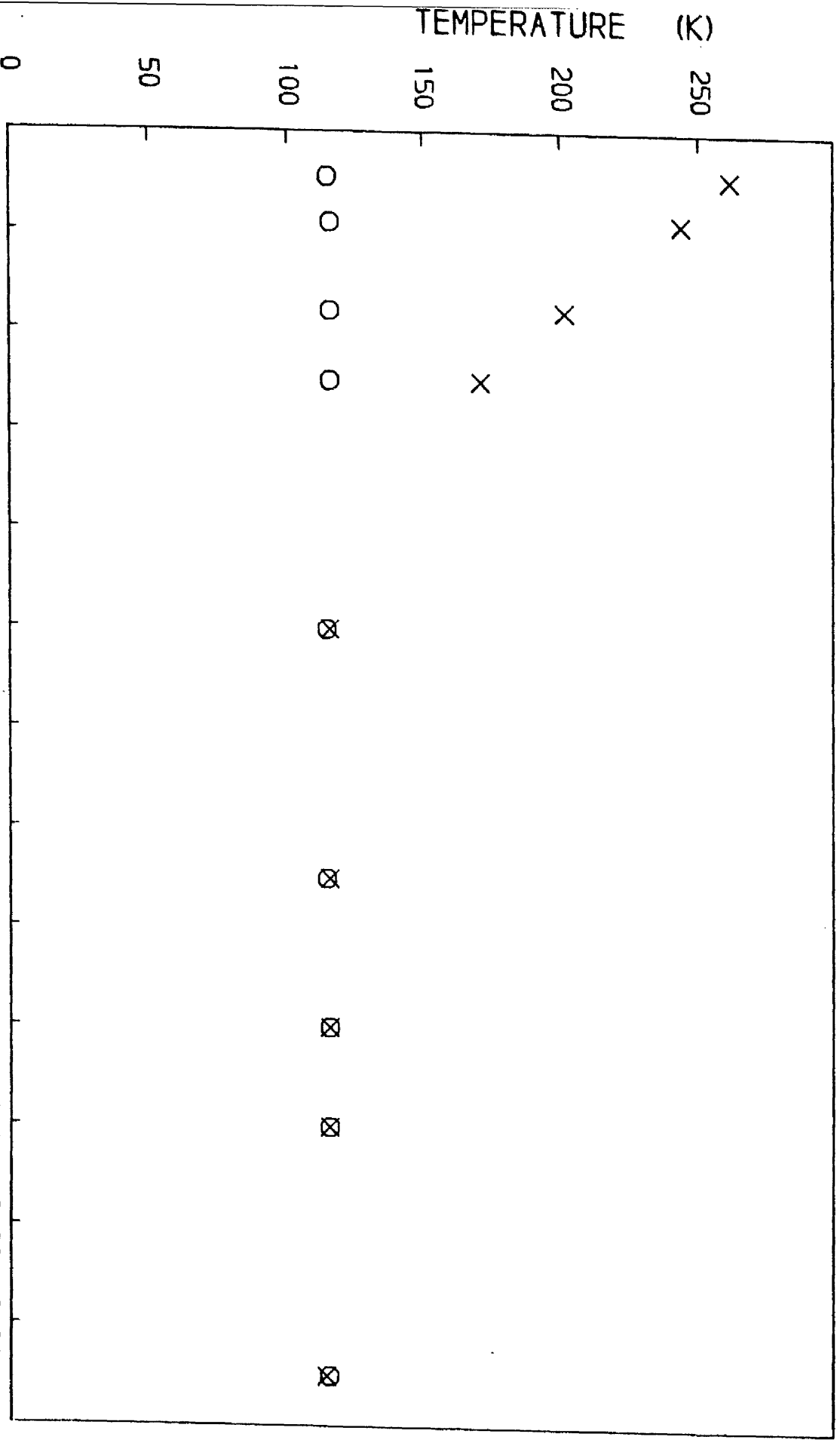

Figure 6.4.1.(a): O - h_T = 0, x - h_T = 8W/m^2°K

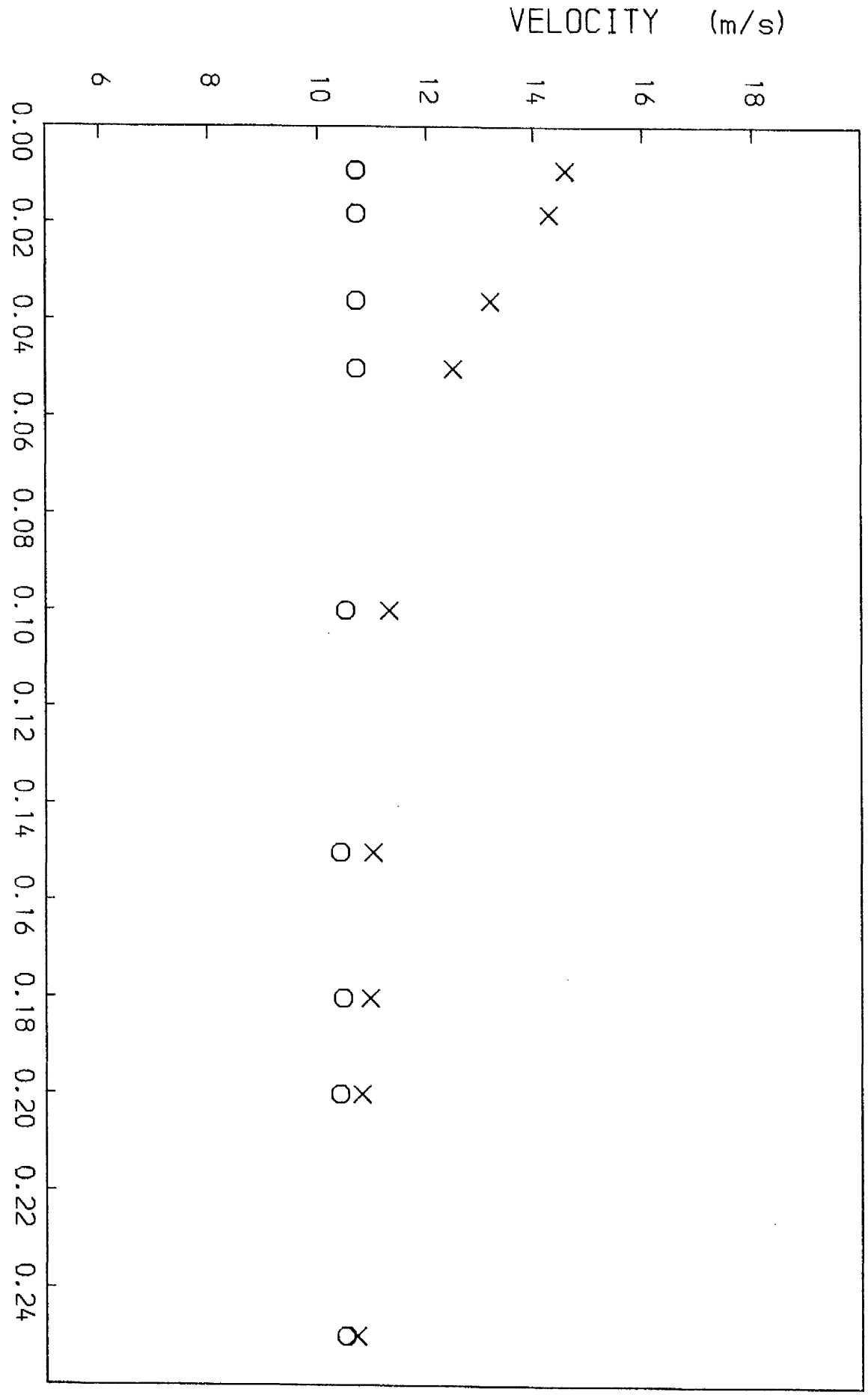
VELOCITY (m/s)
6
8
10
12
14
16
18
0.00
0.02
0.04
0.06
0.08
0.10
0.12
0.14
0.16
0.18
0.20
0.22
0.24
d (m)

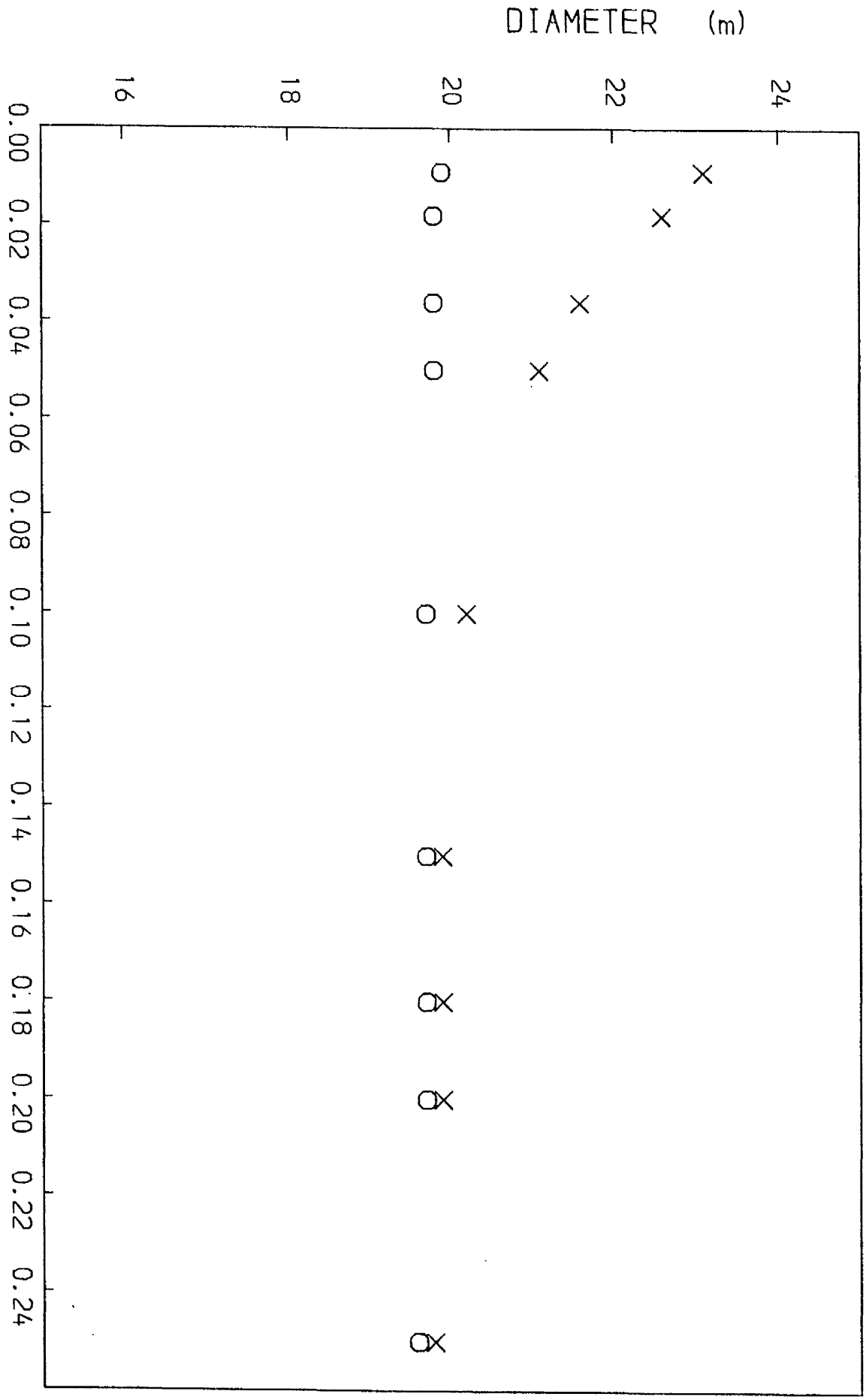

Figure 6.4.1.(c): O - $h_T = 0$, x - $h_T = 8 W/m^2 {}^\circ K$

the velocity.

Diameter:

The increase in gas density reduces its volume which decreases the total cross-sectional area of the plume. There is also a secondary effect. Due to the decrease in velocity there is a drop in the amount of entrained water, which again reduces width of plume.

By comparison of the two cases on each graph we may conclude that the variation in the parameters with changing bubble size can be attributed to its effect on the heat transfer, and that the effect caused by the changing slip velocity is insignificant in comparison.

For values of d_e > 10cm the graphs of case (a) level off at a constant value, which is close to the value obtained in case (b). In the temperature case the values are almost identical, while for the diameter, case (a) values remain approximately 0.2m greater and the velocity ones approximately 0.25 - 0.5 m/s higher.

If it were shown that the correct value for the heat transfer coefficient was 8 $W/m^2/^0K$ (proposed by Smith (1984)) then it could be said that the existence of bubbles of equivalent diameter greater than 10cm would result in the ameliorating effects of the heat transfer being removed.

It is thought, however, that h_T could be far higher than 8.

Stage 2 of the analysis looks more carefully at how the

value of the heat transfer coefficient would affect the dependence on the bubble diameter.

The procedure is as follows:

1. Standard input conditions are as given in Table 6.4.1.

2. Various values for d_e are used, between 0.018 and 2.5m

3. Three separate cases are considered; fixed values for h_T of 150 and 300 $W/m^2/^oK$ and a variable value given by equation (3.4.16).

Figs. 6.4.2 (a), (b), (c), (d) show variation of gas temperature, plume velocity, plume diameter and void fraction with bubble diameter, for varying values of the heat transfer coefficient; the case of $h_T = 0$ also being plotted for comparison purposes.

RESULTS AND CONCLUSIONS

All four graphs show similar trends. For a non-zero value of h_T, the parameters decrease with increasing bubble diameter, but eventually level off at a constant value which is approximately that for $h_T = 0$.

The effect of varying the value of h_T is that the larger h_T is the more slowly the parameter falls to its limiting value.

It can be seen that for a variable heat transfer coefficient which begins at a value of about 300 $W/m^2/^oK$ and falls to around 50 $W/m^2/^oK$, the appropriate quantity falls to its limiting value significantly more quickly than

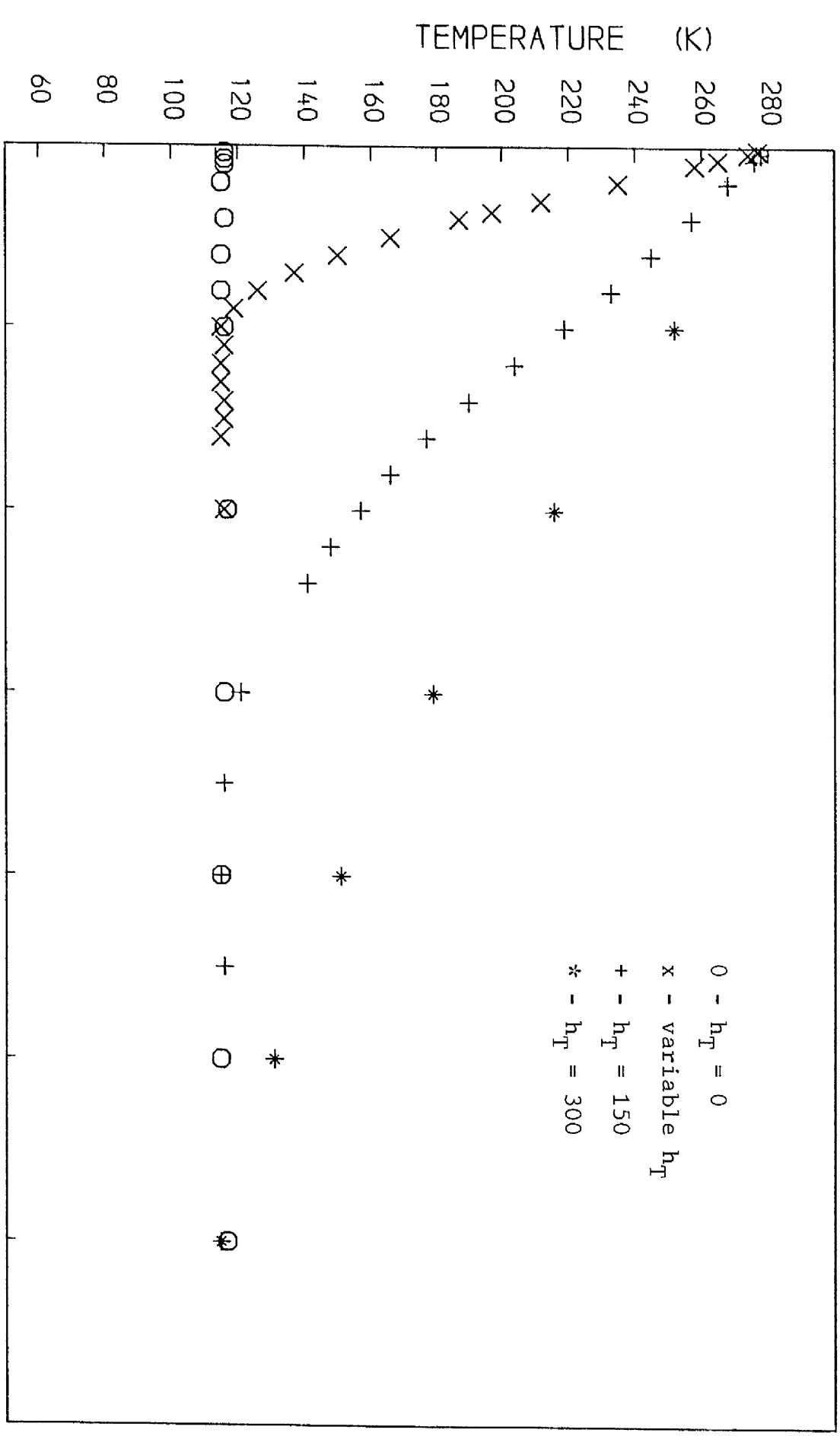
TEMPERATURE (K)
280
260
240
220
200
180
160
140
120
100
80
60
0.0
0.5
1.0
1.5
2.0
2.5
3.0
d_s (m)
0 - h_T = 0
x - variable h_T
+ - h_T = 150
* - h_T = 300

Figure 6.4.2.(a)

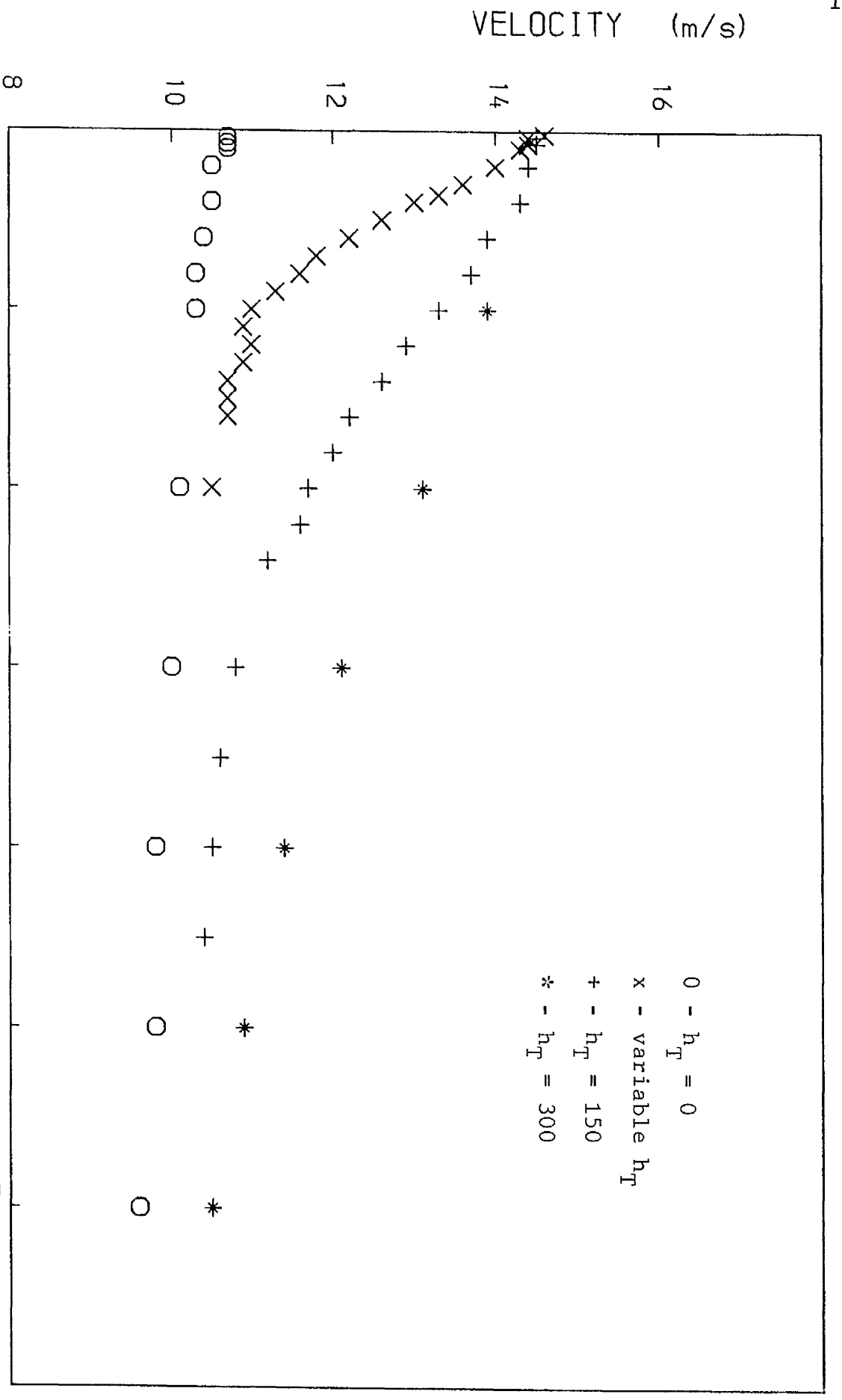
VELOCITY (m/s)
8
10
12
14
16
0.0
0.5
1.0
1.5
2.0
2.5
3.0
d_c (m)
0 - h_T = 0
x - variable h_T
+ - h_T = 150
* - h_T = 300

Figure 6.4.2(b)

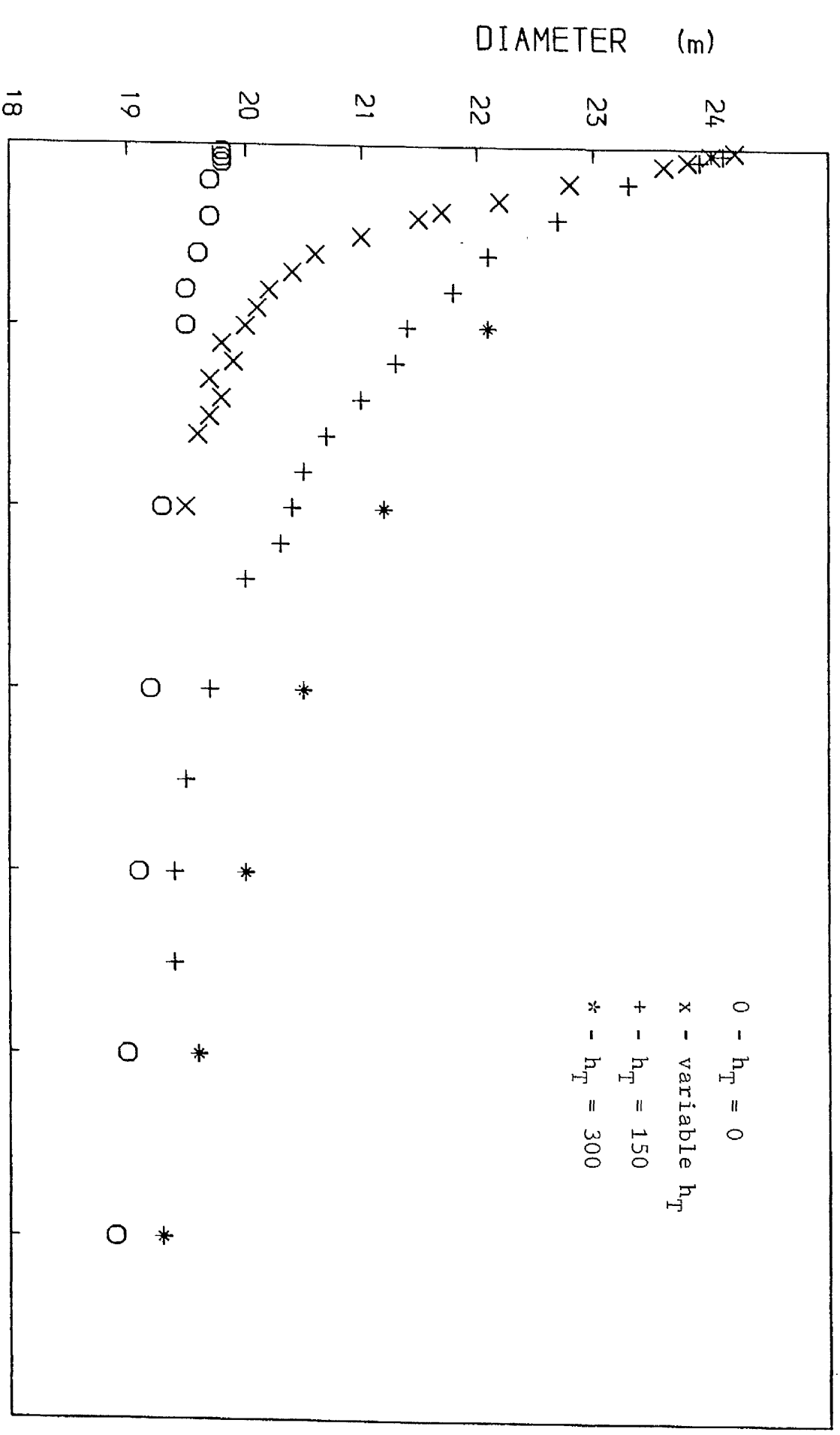
DIAMETER (m)
18
19
20
21
22
23
24
0.0
0.5
1.0
1.5
2.0
2.5
3.0
d (m)
0 - h_T = 0
x - variable h_T
+ - h_T = 150
* - h_T = 300

Figure 6.4.2.(c)

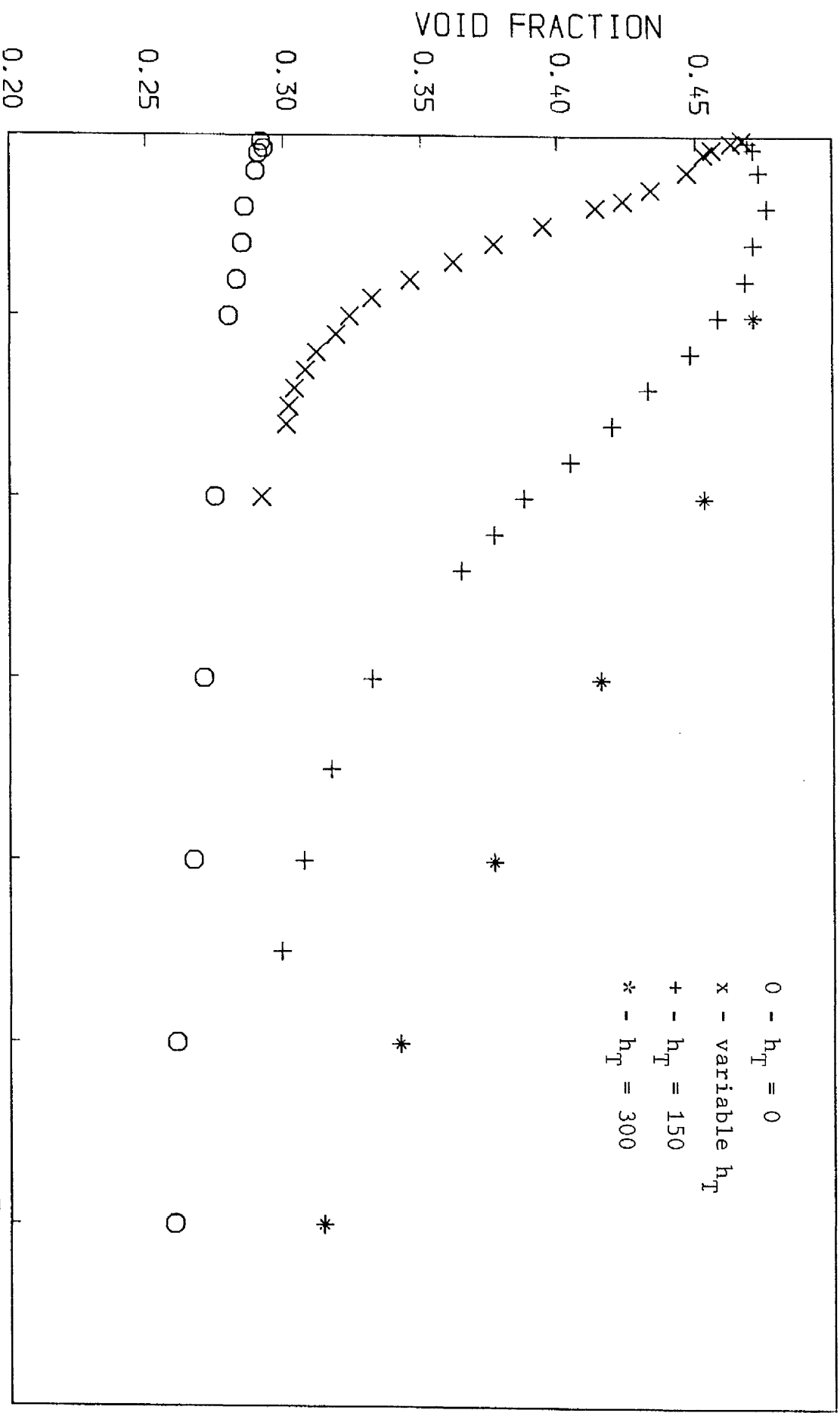
VOID FRACTION
0.20
0.25
0.30
0.35
0.40
0.45
0.0
0.5
1.0
1.5
2.0
2.5
3.0
d (m)
o
0 - h_T = 0
x - variable h_T
+ - h_T = 150
* - h_T = 300

Figure 6.4.2(d)

when h_T = 150 $W/m^2/^oK$.

One of the crucial questions we wish to answer is whether or not the gas will be positively buoyant when reaching the surface. For methane this corresponds to having a temperature of around 170°K.

By considering Fig. 6.4.2(a) we can see that if h_T were as large as 300, then bubble diameters would have to exceed 1.5m before the temperature fell below 170°K but if the variable form is an accurate description of the heat transfer coefficient only bubbles with d_e < 20cm would ensure positively buoyant gas at the surface.

From Fig. 6.4.1(a) for h_T as low as 8 $W/m^2/^oK$, positive buoyancy will be achieved for d_e < 5cm.

Experimental observations predict bubble sizes to be of the order of a few centimetres.

Thus, if the heat transfer coefficient is at least as high as the values given by the variable form of h_T, then it seems fairly likely that the gas will be positively buoyant, but if it is as low as $8W/m^2/^oK$, then the exact size of the bubbles will be necessary before a decision can be reached.

From Fig. 6.4.2.(b) it can be seen that the enhanced velocity which will help to expel the gas into the atmosphere no longer exists for bubble sizes above 0.5m in the variable heat transfer case, while it is present in the cases of higher heat transfer coefficient until d_e is well over 1m.

In terms of the density deficiency which can be measured in terms of the void fraction, α , Fig. 6.4.2(d) shows that the variable form of h_T is more favourable in giving a lower

void fraction for any prescribed bubble size than the higher values of h_T. Overall, large bubbles are desirable in that they reduce the void fraction, but this would have to be weighed against the other adverse effects of increasing d_e.

CHAPTER 7

MASS TRANSFER

7.1 General

In our formulation of the model, it has been assumed that the entire quantity of gas released from the pipeline will be maintained in the plume throughout the rise to the surface. It is known, however, that hydrocarbon gases are soluble in water (e.g. Solubilities of Inorganic and Organic Compounds, Vol. 1 (Binary Systems), Part 1). It is, therefore, possible that a proportion of the gas released would go into solution, which could alter the evolution of the plume and the conditions existing at the surface.

This section concentrates on reformulating the model, taking into account the possibility that some of the gas released may pass into solution.

7.2 Governing Equations

As in Chapter 2, for the case of no mass transfer, in this section we derive a set of conservation equations

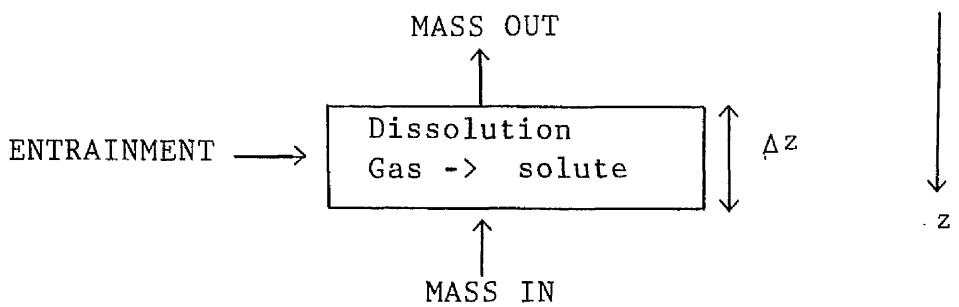

In this case, within the control volume dissolution is permitted, and hence we must have an extra parameter, the solute.

Most symbols are as mentioned in Chapter 2.

CONSERVATION OF MASS

GAS

$m_{g_{out}} = m_{g_{in}}$ - amount of gas dissolved in control volume

and so

$\dot{m}_{g_{out}} = \dot{m}_{g_{in}}$ - rate of mass removal through dissolution

Thus,

$\Delta \dot{m}_g$ = - rate of mass removal through dissolution

$= - k_m(c_i - c_\infty)$ (surface area of gas)

$= - k_m(c_i - c_\infty)$ (no. of bubbles in vol element)$\times$ (S.A. of bubble)

$$= - k_m(c_i - c_\infty) \left(\frac{[\text{vol. in control volume}]}{\text{vol. of bubble}} \right) s_B$$

$$= - k_m(c_i - c_\infty) \left[\frac{\alpha A(-\Delta Z)}{\pi d_e^{\,3}/6} \right] s_B$$

$$= k_m(c_i - c_\infty) \left[\frac{6\alpha A \, \Delta z}{\pi d_e^{\,3}} \right] s_B$$

Taking limit as $\Delta Z \rightarrow 0$

$$\frac{dm_g}{dz} = k_m(c_i - c_\infty) \frac{6\alpha A}{\pi d_e^3} s_B \qquad (7.2.1)$$

where

k_m = mass transfer coeff.

c_i = concentration of dissolved methane at the interface
(= mass of methane dissolved/unit volume of liquid)

c_∞ = mean concentration of dissolved methane in the liquid at a distance from the interface.

s_B = surface area of a single bubble

α = void fraction

A = cross-sectional area of plume

CONCENTRATION

The variation in gas concentration from a bubble to the surrounding liquid may be represented as follows.

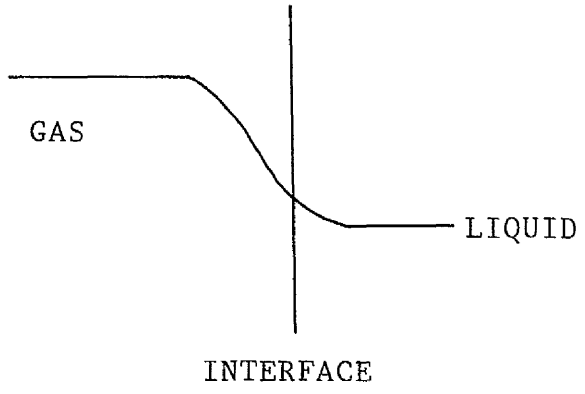

This may be approximated by

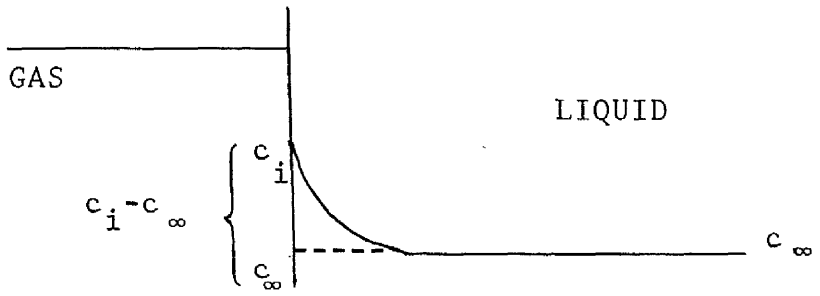

It is the difference $(c_i - c_\infty)$ which is the driving force behind the dissolution.

Now,

$$\dot{m}_g = \rho_g \alpha A v_g \qquad (7.2.2)$$

so that

$$\frac{d\dot{m}_g}{dz} = \rho_g \alpha A \frac{dv_g}{dz} + \rho_g \alpha v_g \frac{dA}{dz} + \rho_g A v_g \frac{d\alpha}{dz} + \alpha A v_g \frac{d\rho_g}{dz}$$

and (7.2.1) becomes

$$\rho_g \alpha A \frac{dv_g}{dz} + \rho_g \alpha v_g \frac{dA}{dz} + \rho_g A v_g \frac{d\alpha}{dz} + \alpha A v_g \frac{d\rho_g}{dz} = k_m (c_i - c_\infty).$$

$$\frac{6\alpha A}{\pi d_e^3} \cdot s_B \qquad (7.2.3)$$

LIQUID

As before (2.2.5)

$$\frac{d\dot{m}_l}{dz} = -K_1 \rho_l v d_{eff} \qquad (7.2.4)$$

we also have,

$$\dot{m}_l = \rho_l(1-\alpha)\, Av \qquad (7.2.5)$$

Combining (7.2.4) and (7.2.5) gives

$$\rho_l(1-\alpha)\, A \frac{dv}{dz} + \rho_l(1-\alpha)\, v \frac{dA}{dz} - \rho_l Av \frac{d\alpha}{dz} + (1-\alpha)\, Av \frac{d\rho_l}{dz}$$

$$= -K_1 \rho_l v \left(\frac{4A}{\pi}\right)^{\frac{1}{2}} \qquad (7.2.6)$$

SOLUTE

The solute refers to the gas which has dissolved in the liquid.

Thus,

$$\dot{m}_{s_{out}} = \dot{m}_{s_{in}} + \text{increase in mass due to dissolution in}$$

control volume, from which follows

$$\dot{m}_{s_{out}} = \dot{m}_{s_{in}} + \text{rate of mass increase due to dissolution}$$

and so

$$\Delta \dot{m}_s = \text{rate of mass increase due to dissolution}$$

$$= -k_m(c_i - c_\infty) \frac{6\alpha A}{\pi d_e^3} \Delta z\, s_B$$

Taking limit as $\Delta z \to 0$ gives

$$\frac{d\dot{m}_s}{dz} = -k_m(c_i - c_\infty) \frac{6\alpha A}{\pi d_e^3} s_B \qquad (7.2.7)$$

Now,

Mass flow rate of solute = c_∞ [volume flow rate of liquid]

giving

$$\dot{m}_s = c_\infty (1-\alpha) Av \qquad (7.2.8)$$

Combining (7.2.7) and (7.2.8) yields

$$c_\infty(1-\alpha)A \frac{dv}{dz} + c_\infty(1-\alpha)v \frac{dA}{dz} - c_\infty Av \frac{d\alpha}{dz} + (1-\alpha)Av \frac{dc_\infty}{dz}$$

$$= -k_m(c_i-c_\infty) \frac{6\alpha A}{\pi d_e^3} s_B \qquad (7.2.9)$$

Combining (7.2.1) and (7.2.7), however, yields

$$\frac{d}{dz} (\dot{m}_g + \dot{m}_s) = 0 \qquad (7.2.10)$$

This implies that

$$\dot{m}_g + \dot{m}_s = \text{constant} = \dot{m}_{g_o} \text{ (initial gas flow rate)} \qquad (7.2.11)$$

Using (7.2.2) and (7.2.8) we have

$$\rho_g \alpha A v_g + c_\infty(1-\alpha) Av = \dot{m}_{g_o}$$

i.e.

$$A[\rho_g \alpha v_g + c_\infty(1-\alpha) v] = \dot{m}_{g_o} \qquad (7.2.12)$$

CONSERVATION OF MOMENTUM

As before we consider a force balance on the control volume, and the fact that

Force = rate of change of momentum

This time,

Downward force = weight of control volume

= g [mass of control volume]

= g [ρ_l(vol. of liquid) + ρ_g(vol. of gas)

+ c_∞(vol. of liquid)]

If we assume that the mass of solute dissolved is small enough to have a negligible effect on the volume of liquid, then

vol. of liquid = $(1-\alpha)\ A\ (-\Delta z)$

vol. of gas = $\alpha A\ (-\Delta z)$

Thus,

$$F_{down} = gA(-\Delta z)\ [(\rho_l + c_\infty)\ (1-\alpha) + \rho_g \alpha] \qquad (7.2.13)$$

Upward Force = Buoyancy

= weight of displaced liquid

$$= g\rho_l\ A\ (-\Delta z) \qquad (7.2.14)$$

Hence,

$\Delta \dot{M}$ = net upward force

$$= -gA\ [\alpha(\rho_l - \rho_g) - (1-\alpha)\ c_\infty]\Delta z \qquad (7.2.15)$$

and taking limit as $\Delta z \to 0$

$$\frac{d\dot{M}}{dz} = -g\ A\ [\alpha\ (\rho_l - \rho_g) - (1-\alpha)\ c_\infty] \qquad (7.2.16)$$

From equations (2.2.33) and (2.2.40), and applying a similar

argument to the solute momentum flux, we can write

$$\begin{aligned} \dot{M}_g &= \dot{m}_g v_g \\ \dot{M}_l &= \dot{m}_l v \\ \dot{M}_s &= \dot{m}_s v \end{aligned} \tag{7.2.17}$$

Thus,

$$\begin{aligned} \frac{d\dot{M}}{dz} &= \frac{d\dot{M}_g}{dz} + \frac{d\dot{M}_l}{dz} + \frac{d\dot{M}_s}{dz} \\ &= v_g \frac{d\dot{m}_g}{dz} + \dot{m}_g \frac{dv_g}{dz} + v\left[\frac{d\dot{m}_l}{dz} + \frac{d\dot{m}_s}{dz}\right] + (\dot{m}_l + \dot{m}_s)\frac{dv}{dz} \end{aligned} \tag{7.2.18}$$

If we make similar assumptions about the gas velocity, namely,

$$v_g = K_3 v + v_r \tag{7.2.19}$$

$$\frac{dv_r}{dz} = 0 \tag{7.2.20}$$

then, (7.2.18) becomes

$$\begin{aligned} \frac{d\dot{M}}{dz} &= (K_3 v + v_r)\frac{d\dot{m}_g}{dz} + K_3 \dot{m}_g \frac{dv}{dz} + v\left[\frac{d\dot{m}_l}{dz} + \frac{d\dot{m}_s}{dz}\right] + (\dot{m}_l + \dot{m}_s)\frac{dv}{dz} \\ &= (K_3 v + v_r)\frac{d\dot{m}_g}{dz} + v\left[\frac{d\dot{m}_l}{dz} + \frac{d\dot{m}_s}{dz}\right] + (K_3 \dot{m}_g + \dot{m}_l + \dot{m}_s)\frac{dv}{dz} \end{aligned}$$

Using (7.2.1), (7.2.4), (7.2.5), (7.2.7) and (7.2.11), and assuming $(1 - K_3) c_\infty \ll \rho_l$ leaves us with

$$\frac{dM}{dz} = [(K_3-1)v+v_r]k_m(c_i-c_\infty)\frac{6\alpha A}{\pi d_e}{}_3\, s_B - \frac{2K_1\rho_l}{\sqrt{\pi}} v^2 A^{\frac{1}{2}} + (K_3\dot{m}_{g_o} + \rho_l(1-\alpha)Av)\frac{dv}{dz} \qquad (7.2.21)$$

Finally, combining (7.2.21) with (7.2.16) we obtain

$$[(K_3-1)v+v_r]k_m(c_i-c_\infty)\frac{6\alpha A}{\pi d_e}{}_3\, s_B - \frac{2K_1\rho_l}{\sqrt{\pi}} v^2 A^{\frac{1}{2}} + (K_3\dot{m}_{g_o} + \rho_l(1-\alpha)Av)\frac{dv}{dz}$$
$$= -gA[\alpha(\rho_l-\rho_g) - (1-\alpha)c_\infty] \qquad (7.2.22)$$

Letting

$$k_m(c_i-c_\infty)\frac{6\alpha A}{\pi d_e}{}_3 s_B = \Phi \qquad (7.2.23)$$

(7.2.22) may be rewritten

$$[K_3\dot{m}_{g_o} + \rho_l(1-\alpha)Av]\frac{dv}{dz} = -gA[\alpha(\rho_l-\rho_g)-(1-\alpha)c_\infty]$$
$$+ \frac{2K_1\rho_l}{\sqrt{\pi}} v^2 A^{\frac{1}{2}} - \Phi[(K_3-1)v + v_r]$$

yielding

$$\frac{dv}{dz} = \frac{-gA[\alpha(\rho_l-\rho_g)-(1-\alpha)c_\infty] + \frac{2K_1}{\sqrt{\pi}}\rho_l v^2 A^{\frac{1}{2}} - \Phi[(K_3-1)v+v_r]}{[K_3\dot{m}_{g_o} + \rho_l(1-\alpha)Av]} \qquad (7.2.24)$$

Equation (7.2.12) may be solved to give c_∞,

$$c_\infty = \begin{cases} \dfrac{\dot{m}_{g_o} - \rho_g \alpha A v_g}{(1-\alpha)vA} & \alpha \neq 1 \\ 0 & \alpha = 1, \text{ under assumption} \\ & \alpha = 1 \text{ only at very beginning,} \\ & \text{when no gas has dissolved.} \end{cases} \qquad (7.2.25)$$

Substituting for $(1-\alpha)\, c_\infty$ in (7.2.24) gives

$$\frac{dv}{dz} = \frac{-g\left[\alpha A(\rho_1 - \rho_g) - \left\{\frac{\dot{m}_{g_o} - \rho_g \alpha v_g A}{v}\right\}\right] + \frac{2K_1}{\sqrt{\pi}}\rho_1 v^2 A^{\frac{1}{2}} - \Phi[(K_3-1)v+v_r]}{[K_3\dot{m}_{g_o} + \rho_1(1-\alpha)\, Av]}$$

$$= \frac{-g[\alpha A\rho_1 - \alpha A\rho_g - \frac{\dot{m}_{g_o}}{v} + \frac{\rho_g \alpha A(K_3 v+v_r)}{v}] + \frac{2K_1}{\sqrt{\pi}}\rho_1 v^2 A^{\frac{1}{2}} - \Phi[(K_3-1)v+v_r]}{[K_3\dot{m}_{g_o} + \rho_1\,(1-\alpha)\, Av]}$$

$$= \frac{-g/v[\alpha A\rho_1 v - \dot{m}_{g_o} + \alpha A\rho_g\{(K_3-1)v+v_r\}] + \frac{2K_1}{\sqrt{\pi}}\rho_1 v^2 A^{\frac{1}{2}} - \Phi[(K_3-1)v+v_r]}{[K_3\dot{m}_{g_o} + \rho_1\,(1-\alpha)\, Av]}$$

$$= \frac{-g/v[\alpha A\{\rho_1 v + \rho_g[(K_3-1)v+v_r]\} - \dot{m}_{g_o}] + \frac{2K_1}{\sqrt{\pi}}\rho_1 v^2 A^{\frac{1}{2}} - \Phi[(K_3-1)v+v_r]}{[K_3\dot{m}_{g_o} + \rho_1(1-\alpha)\, Av]} \qquad (7.2.26)$$

To summarise, we have the following set of equations, making use of (7.2.19), (7.2.20)

GAS (7.2.3)

$$K_3\rho_g\alpha A\frac{dv}{dz} + \rho_g\alpha(K_3v+v_r)\frac{dA}{dz} + \rho_g A(K_3v+v_r)\frac{d\alpha}{dz} + \alpha A(K_3v+v_r)\frac{d\rho_g}{dz} = \Phi. \qquad (7.2.27)$$

LIQUID (7.2.6) (assuming ρ_1 is constant)

$$(1-\alpha)\,A\frac{dv}{dz} + (1-\alpha)\,v\frac{dA}{dz} - Av\frac{d\alpha}{dz} = \frac{-2K_1}{\sqrt{\pi}}\,vA^{\frac{1}{2}} \qquad (7.2.28)$$

SOLUTE (7.2.12)

$$[c_\infty(1-\alpha)\,v + \rho_g\alpha(K_3v+v_r)]\,A = \dot{m}_{g_o} \qquad (7.2.29)$$

MOMENTUM (7.2.26)

$$\frac{dv}{dz} = \frac{-g/v[\alpha A\{\rho_1 v+\rho_g[(K_3-1)v+v_r]\}-\dot{m}_{g_o}]+\frac{2K_1}{\sqrt{\pi}}\rho_1 v^2A^{\frac{1}{2}}-\Phi[(K_3-1)v+v_r]}{[K_3\dot{m}_{g_o} + \rho_1(1-\alpha)\,Av]} \qquad (7.2.30)$$

Rewriting (7.2.27) and (7.2.28),

$$\rho_g(K_3v+v_r)[\alpha\frac{dA}{dz} + A\,\frac{d\alpha}{dz}] = \Phi - \alpha A(K_3v+v_r)\frac{d\rho_g}{dz} - K_3\rho_g\alpha A\,\frac{dv}{dz} \qquad (7.2.31)$$

$$v\,[\,(1-\alpha)\,\frac{dA}{dz} - A\frac{d\alpha}{dz}\,] = \frac{-2K_1}{\sqrt{\pi}}\,vA^{\frac{1}{2}} - (1-\alpha)\,A\,\frac{dv}{dz} \qquad (7.2.32)$$

Adding v x (7.2.31) to $\rho_g(K_3v+v_r)$x(7.2.32) gives

$$\rho_g v(K_3v+v_r)\,\frac{dA}{dz} = \Phi v - \frac{2K_1}{\sqrt{\pi}}\rho_g v(K_3v+v_r)A^{\frac{1}{2}} - \alpha\,Av(K_3v+v_r)\,\frac{d\rho_g}{dz} - \rho_g[AK_3v+(1-\alpha)\,v_r]\,\frac{dv}{dz} \qquad (7.2.33)$$

Subtracting $\alpha\rho_g(K_3v+v_r)$ x (7.2.32) from (1-α) v x (7.2.31) gives

$$\rho_g v(K_3 v+v_r)A\frac{d\alpha}{dz} = (1-\alpha)\, v\Phi + \frac{2K_1}{\sqrt{\pi}}\alpha\rho_g v(K_3 v+v_r)A^{\frac{1}{2}} - \alpha(1-\alpha)\, Av(K_3 v+v_r)\frac{d\rho_g}{dz} + \rho_g \alpha(1-\alpha)Av_r\frac{dv}{dz} \qquad (7.2.34)$$

i.e.

$$\frac{dA}{dz} = \frac{\Phi v - \frac{2K_1}{\sqrt{\pi}}\rho_g v(K_3 v+v_r)A^{\frac{1}{2}} - \alpha Av(K_3 v+v_r)\frac{d\rho_g}{dz} - \rho_g A[K_3 v+(1-\alpha)v_r]\frac{dv}{dz}}{\rho_g v(K_3 v+v_r)} \qquad (7.2.35)$$

and

$$\frac{d\alpha}{dz} = \frac{(1-\alpha)v\Phi + \frac{2K_1}{\sqrt{\pi}}\alpha\rho_g v(K_3 v+v_r)A^{\frac{1}{2}} - \alpha(1-\alpha)Av(K_3 v+v_r)\frac{d\rho_g}{dz} + \rho_g \alpha(1-\alpha)Av_r\frac{dv}{dz}}{\rho_g Av(K_3 v+v_r)} \qquad (7.2.36)$$

Throughout this derivation, ρ_g has been used to denote the density of the gas. In reality, as noted before, the gas may exist in both liquid and vapour phase and ρ_B is used to denote the mean density of the bubbles, while ρ_{g_g} will refer to the vapour phase alone. If the entropy is greater than the saturation entropy, all the gas in the bubbles will be in the vapour phase and ρ_B will equal ρ_{g_g}

Rewriting equations (7.2.29), (7.2.30), (7.2.35) and (7.2.36) gives the system.

$$[c_\infty(1-\alpha)\ v + \rho_B\alpha(K_3v+v_r)]A = \dot{m}_{g_o} \tag{7.2.37}$$

$$\frac{dv}{dz} = \frac{-g/v[\alpha A\{\rho_l v+\rho_B[(K_3-1)v+v_r]\} - \dot{m}_{g_o}]+ \frac{2K_1}{\sqrt{\pi}}\rho_l v^2 A^{\frac{1}{2}} - \Phi[(K_3-1)v+v_r]}{[K_3\dot{m}_{g_o} + \rho_l(1-\alpha)\ Av]} \tag{7.2.38}$$

$$\frac{dA}{dz} = \Phi v - \frac{2K_1}{\sqrt{\pi}}\rho_B v(K_3v+v_r)A^{\frac{1}{2}} - \alpha Av(K_3v+v_r)\frac{d\rho_B}{dz} - \rho_B A[K_3v+(1-\alpha)v_r]\frac{dv}{dz}}{\rho_B v(K_3v+v_r)} \tag{7.2.39}$$

$$\frac{d\alpha}{dz} = (1-\alpha)v\ \Phi + \frac{2K_1}{\sqrt{\pi}}\alpha\rho_B v(K_3v+v_r)A^{\frac{1}{2}} - \alpha(1-\alpha)Av(K_3v+v_r)\ \frac{d\rho_B}{dz} + \rho_B\alpha(1-\alpha)\cdot Av_r\ \frac{dv}{dz}}{\rho_B Av(K_3v+v_r)} \tag{7.2.40}$$

with Φ given by (7.2.23)

Equations (7.2.37) to (7.2.40), therefore, give a system of four equations in the five unknowns A,v,α, c_∞ and ρ_B, assuming that the values of K_1, K_3,ρ_l, $\dot{m}_{g_o}$ and v_r may all be prescribed. Calculation of Φ requires knowledge of the parameters k and c_i, which will be discussed in the following two sections.

To resolve the closure problem use is made of the following constitutive equations for the density.

1. From Chapter 3 we have the expression for the mean bubble density.

$$\rho_B = \frac{\rho_{g_g}\rho_{g_l}}{\xi\rho_{g_l} + (1-\xi)\rho_{g_g}} \tag{7.2.41}$$

with

$$\xi = \begin{cases} \dfrac{2S - 3.5\ 1nz - 29}{50 - 61nz} & S < S_{sat} \\ 1 & S \geqslant S_{sat} \end{cases} \tag{7.2.42}$$

2. Equation (3.3.5) gives an equation for the gas density, derived from the ideal gas law

$$\rho_{g_g} = \frac{10^4 \hat{M}_z}{RT} \tag{7.2.43}$$

Hence, assuming ρ_{g_l} constant,

$$\frac{d\rho_B}{dz} = \frac{\rho_{g_l} \frac{d\rho_{g_g}}{dz}\left[\xi\rho_{g_l} + (1-\xi)\rho_{g_g}\right] - \rho_{g_l}\rho_{g_g}\left[\rho_{g_l}\frac{d\xi}{dz} + (1-\xi)\frac{d\rho_{g_g}}{dz} - \rho_{g_g}\frac{d\xi}{dz}\right]}{\left[\xi\rho_{g_l} + (1-\xi)\rho_{g_g}\right]^2}$$

$$= \rho_{g_l} \left[\xi \rho_{g_l} \frac{d\rho_{g_g}}{dz} - \rho_{g_g} (\rho_{g_l} - \rho_{g_g}) \frac{d\xi}{dz} \right]$$

$$\frac{}{[\xi \rho_{g_l} + (1-\xi) \rho_{g_g}]^2} \qquad (7.2.44)$$

Also,

$$\frac{d\xi}{dz} = \frac{(2 \frac{dS}{dz} - \frac{3.5}{z})(50-6 \ln z) - (2S-3.5 \ln z - 29)(\frac{-6}{z})}{(50 - 6 \ln z)^2}$$

$$= \frac{(100 - 12 \ln z) \frac{dS}{dz} + (\frac{12S - 349}{z})}{(50 - 6 \ln z)^2} \quad (S < S_{sat}) \qquad (7.2.45(a))$$

$$\frac{d\xi}{dz} = 0 \qquad S \geqslant S_{sat} \qquad (7.2.45(b))$$

and,

$$\frac{d\rho_{g_g}}{dz} = \frac{10^4 \hat{M}}{RT} - \frac{10^4 \hat{M} z}{RT^2} \frac{dT}{dz}$$

$$= \frac{10^4 \hat{M}}{RT} \left[1 - \frac{z}{T} \frac{dT}{dz}\right] \qquad (7.2.46)$$

From equation (3.2.17), (3.2.18)

$$T = \exp \left\{ \frac{S'}{8} + \frac{\ln z}{3.65} - 0.457 \right\} \qquad (7.2.47)$$

with

$$S' = \max (S, S_{sat})$$

Thus,

$$\frac{dT}{dz} = \left(\frac{1}{8}\frac{dS'}{dz} + \frac{1}{3.65\ z}\right) T \qquad (7.2.48)$$

which can be substituted into (7.2.46) to give

$$\frac{d\rho_{g_g}}{dz} = \frac{10^4 \hat{M}}{RT}\left[1 - \left(\frac{z}{8}\frac{dS'}{dz} + \frac{1}{3.65}\right)\right]$$

$$= \frac{\rho_{g_g}}{z}\left[\frac{2.65}{3.65} - \frac{z}{8}\frac{dS'}{dz}\right] \qquad (7.2.49)$$

Finally, there are two expressions for $\frac{dS'}{dz}$;

From (3.2.19)

$$S_{sat} = \frac{158 - 5\ln z}{4} \qquad (7.2.50)$$

$$\Rightarrow \quad \frac{dS_{sat}}{dz} = -\frac{5}{4z} \qquad (7.2.51)$$

From (3.4.4)

$$\frac{dS}{dz} \simeq \frac{\Delta S}{\Delta z} = \frac{-6\varepsilon}{\pi \rho_B d_e (K_3 v + v_r)} \left(\frac{0.016}{4.1863}\right) h_T \left(\frac{T_{sea}}{T} - 1\right) \quad (7.2.52)$$

with ε as given in (3.4.3), and h_T is given as before by

$$h_T = \begin{cases} \frac{1.13}{\sqrt{1-\alpha}} \left[\frac{\rho_B v_r \, k \, c_p}{d_e} \right]^{\frac{1}{2}} & \alpha \leqslant 0.9 \\ \text{UCONS} & \alpha > 0.9 \end{cases} \quad (7.2.53)$$

There are two separate situations

(i) $S \geqslant S_{sat}$

$\varepsilon = 1$, $\rho_B = \rho_{g_g}$, $S' = S$

Thus, from (7.2.49)

$$\frac{d\rho_B}{dz} = \frac{\rho_B}{z} \left[\frac{2.65}{3.65} - \frac{z}{8} \frac{dS}{dz} \right] \quad (7.2.54)$$

with

$\frac{dS}{dz}$ given by (7.2.52)

(ii) $S < S_{sat}$

$S' = S_{sat}$

From (7.2.49) and (7.2.51)

$$\frac{d\rho_{g_g}}{dz} = \frac{\rho_{g_g}}{z} \left[\frac{2.65}{3.65} + \frac{5}{32} \right] \quad (7.2.55)$$

(7.2.41) may be rewritten to give

$$\rho_{g_g} = \frac{\xi \rho_{g_1} \rho_B}{[\rho_{g_1} - (1-\xi)\rho_B]} \qquad (7.2.56)$$

which may then be used along with (7.2.55), (7.2.45(a)) and (7.2.52) in (7.2.44) to yield an expression for

$$\frac{d\rho_B}{dz}$$

As with the case of no mass transfer, it is more convenient to define h, the height above release by

$$h = z_o - z \text{ (so that } z = z_o - h) \qquad (7.2.57)$$

which leads to

$$\frac{d}{dh} = -\frac{d}{dz} \qquad (7.2.58)$$

Our final system of equations may then be written, instead of equations (7.2.38) - (7.2.40), as

$$\frac{dv}{dh} = \frac{g/v\ [\alpha A\{\rho_1 v + \rho_B[(K_3-1)v+v_r]\} - \dot{m}_{g_o}] - \frac{2K_1}{\sqrt{\pi}} \rho_1 v^2 A^{\frac{1}{2}} + \Phi[(K_3-1)v+v_r]}{[K_3 \dot{m}_{g_o} + \rho_1(1-\alpha)\,Av]} \qquad (7.2.59)$$

$$\frac{dA}{dh} = \frac{\frac{2K_1}{\sqrt{\pi}} \rho_B v(K_3 v+v_r)A^{\frac{1}{2}} - \Phi v - \alpha Av(K_3 v+v_r)\frac{d\rho_B}{dh} - \rho_B A[K_3 v+(1-\alpha)v_r]\frac{dv}{dh}}{\rho_B v(K_3 v+v_r)} \qquad (7.2.60)$$

$$\frac{d\alpha}{dh} = \frac{-2K_1}{\sqrt{\pi}} \frac{\alpha\rho_B v(K_3 v+v_r)A^{\frac{1}{2}}-(1-\alpha)\ v\Phi-\alpha(1-\alpha)Av(K_3 v+v_r)\frac{d\rho_B}{dh}+\rho_B\ (1-\alpha).\ Av_r\frac{dv}{dh}}{\rho_B Av(K_3 v+v_r)} \qquad (7.2.61)$$

while (7.2.37) is unchanged

$$[\ c_\infty(1-\alpha)v + \rho_B\alpha(K_3 v+v_r)]\ A = \dot{m}_{g_o}$$

Those corresponding to the density equations become

(i) $S \geqslant S_{sat}$

$$\frac{d\rho_B}{dh} = \frac{-\rho_B}{(z_o-h)}\left[\frac{2.65}{3.65} + \frac{(z_o-h)}{8}\frac{dS}{dh}\right] \qquad (7.2.62)$$

$$\frac{dS}{dh} = \frac{6\varepsilon}{\pi\rho_B d_e(K_3 v+v_r)}\left(\frac{0.016}{4.186}\right) h_T\left(\frac{T_{sea}}{T}-1\right) \qquad (7.2.63)$$

(ii) $S < S_{sat}$

$$\frac{d\rho_{g_g}}{dh} = \frac{-\rho_{g_g}}{(z_o-h)}\left[\frac{2.65}{3.65} + \frac{5}{32}\right] \qquad (7.2.64)$$

$$\rho_{g_g} = \frac{\xi\rho_{g_l}\rho_B}{[\rho_{g_l} - (1-\xi)\rho_B]} \qquad (7.2.65)$$

$$\frac{d\xi}{dh} = \frac{[100 - 12\ln(z_o - h)]\frac{dS}{dh} + \left(\frac{349-12S}{z_o-h}\right)}{[50 - 6\ln(z_o-h)]^2} \qquad (7.2.66)$$

$\frac{dS}{dh}$ as above (7.2.63)

$$\frac{d\rho_B}{dh} = \frac{\rho_{g_1}[\rho_{g_1}\xi\frac{d\rho_{g_g}}{dh} - \rho_{g_g}(\rho_{g_1} - \rho_{g_g})\frac{d\xi}{dh}]}{[\xi\rho_{g_1} + (1-\xi)\rho_{g_g}]^2} \qquad (7.2.67)$$

INITIAL CONDITIONS

Following the arguments of the case without mass transfer, we assume that initially the entire cross section of the plume is occupied by gas, giving the conditions

$$A_o = \frac{\dot{m}_{g_o}}{\rho_{B_o}(K_3 v_o + v_r)} \qquad (7.2.68)$$

$$\alpha_o = 1 \qquad (7.2.69)$$

and we shall assume

$$v_o = K_4 v_r \qquad K_4 = 0(0.5) \qquad (7.2.70)$$

In this system we also require ρ_{B_o}, S_o

Using equations (3.3.5) and (3.3.31)

$$\rho_{B_o} = \frac{\rho_{g_1}\left[\frac{10^4 \hat{M}z_o}{R\,T_o}\right]}{\xi_o \rho_{g_1} + (1-\xi)\left[\frac{10^4 \hat{M}z_o}{RT_o}\right]} \qquad (7.2.71)$$

where T_o, ξ_o depend on S_o, S_{sat_o}

Finally,

S_o = initial pipeline entropy of Gas, unless rise is isothermal when S_o is calculated from the temperature of the gas by changing around (3.2.17) (7.2.72)

7.3 Mass Transfer Coefficient

In a manner entirely analagous to that used to define the Heat Transfer coefficient, (Leclair & Hamielec, 1971), the following expression is used as a starting point

$$Sh = C\,Re^{\frac{1}{2}}\,Sc^{\frac{1}{2}} \qquad (7.3.1)$$

where $$C = \frac{1.13}{\sqrt{1-\alpha}} \qquad (7.3.2)$$

and the Sherwood number, Sh, the Reynolds number, Re, and the Schmidt number, Sc, are defined by,

$$Sh = \frac{d_e k_m}{D} \qquad (7.3.3.a,b,c)$$

$$Re = \frac{\rho_l v_r d_e}{\mu} \qquad Sc = \frac{\mu}{\rho_l D}$$

The symbols are as defined previously, except for D which is the Diffusivity.

This then reduces to

$$k_m = C \left[\frac{D v_r}{d_e} \right]^{\frac{1}{2}} \tag{7.3.4}$$

Due to the form of the expression for C, there is again the problems of a singularity at $\alpha = 1$. As before, the solution employed is to use a constant value for k_m until α has fallen to 0.9.

This constant value is chosen to be that obtained from (7.3.4) for $\alpha = 0.9$.

In our case k_m is a function of α alone. By having a fixed bubble size, we have dictated that d_e and v_r are constant throughout the rise. D is a function of the sea temperature, but again this is kept constant and hence so is D. D is expressed as a cubic function of the sea temperature by curve fitting data points quoted in Witherspoon & Bonoli, 1969 and the required value for $T_{sea} = 280$ is then calculated giving $D = 0.97 \times 10^{-9}\ m^2/s$.

Thus, the actual expression used in the model is given by (7.3.4), where

$$C = \begin{cases} \dfrac{1.13}{\sqrt{1-\alpha}} & \alpha \leqslant 0.9 \\ 3.57 & \alpha > 0.9 \end{cases} \tag{7.3.5}$$

7.4 Interfacial concentration

We firstly consider the well known statement of Henry's Law (see e.g. Balzhiser & Samuels (1977))

$$p_i = H_i x_i \tag{7.4.1}$$

where

p_i = partial pressure of constituent i
(= total pressure when only 1 constituent)

x_i = molal concentration

At a given temperature, H_i is a constant, reflecting the variation of p_i with x_i, but H_i varies with temperature.

Where the solvent is water, we may write

$$x_i = \frac{m_i/\hat{M}_i}{m_i/\hat{M}_i + m_w/\hat{M}_w} \tag{7.4.2}$$

under the assumption of a weak solution,

$$m_i/\hat{M}_i \ll m_w/\hat{M}_w \tag{7.4.3}$$

and

$$x_i \simeq \frac{m_i}{\hat{M}_i} \cdot \frac{\hat{M}_w}{m_w} \tag{7.4.4}$$

Using the fact that $\hat{M}_w = 0.018$, and that the interfacial concentration is the mass of solution per unit volume of solvent, (7.4.4) reduces to

$$x_i = \frac{0.018}{\hat{M}_i \rho_w} . c_i \qquad (7.4.5)$$

We now introduce the Bunsen Absorption Coefficient β_N which may be defined by the following statement (Seidell, 1941)

β_N is the volume of gas (reduced to 0°C and 760mm) dissolved by 1 volume of the liquid when the partial pressure of the gas is 760mm.

Linked to the Bunsen Absorption coefficient, is the solubility Expression, l, which is defined as (Seidell, 1941)

l is the ratio of the volume of gas absorbed at any pressure and temperature to the volume of the absorbing liquid.

It differs from β_N in that the volume of gas is not reduced to 0°C and 760mm, and thus l is the volume of gas dissolved by unit volume of solvent at the temperature of the experiment.

Clearly, for a single constituent,

$$\begin{aligned} c_i &= l . \rho_g \\ l &= l(T) \end{aligned} \qquad (7.4.6)$$

Returning, however, to the Bunsen Absorption coefficient, the following is true

$$C_R = \beta_N . \rho_{g_R} \qquad (7.4.7)$$

where the subscripts i have been dropped since there is only one constituent, namely the methane, and the subscript R refers to the reduced conditions.

From (7.4.5) and (7.4.7) we can write

$$x_R = \frac{0.018}{\hat{M}_g \rho_w} \beta_N \rho_{g_R} \tag{7.4.8}$$

Returning to Henry's Law, at any given temperature

$$H = \frac{p_R}{x_R} = \frac{p_R}{\beta_N} \cdot \frac{\hat{M}_g}{0.018} \cdot \frac{\rho_w}{\rho_{g_R}} \tag{7.4.9}$$

and, using equations (7.4.1), (7.4.5) and (7.4.9), we can express the interfacial concentration, at this temperature, by

$$c_i = \frac{p}{p_R} \rho_{g_R} \beta_N \tag{7.4.10}$$

where $$\beta_N = \beta_N (T) \tag{7.4.11}$$

By use of the ideal gas law (3.3.3) we can write

$$\frac{p}{\rho_g T} = \frac{p_R}{\rho_{g_R} T_R} \tag{7.4.12}$$

Substituting this into (7.4.10) leads to

$$l_i = \rho_g \frac{T}{T_R} \beta_N (T) \tag{7.4.13}$$

Use of (3.3.5) translates this into

$$l_i = \frac{10^4 \hat{M}z}{RT_R} \beta_N(T) \tag{7.4.14}$$

Comparison of (7.4.6) and (7.4.13) shows the relationship between β_N and l, as noted in Seidell (1941), which is

$$1 = \left(\frac{T}{T_R}\right)^{\beta_N} \qquad (7.4.15)$$

The Bunsen Absorption Coefficient may be expressed as a function of temperature and salinity, (Yamamoto et al. (1976)), as follows:

$$\ln\beta_N = A_1+A_2(100/T)+A_3(T/100)+S_1[B_1+B_2(T/100)+B_3(T/100)^2] \qquad (7.4.16)$$

where

$$\begin{aligned} A_1 &= -67.1962 \\ A_2 &= 99.1624 \\ A_3 &= 27.9015 \\ B_1 &= -0.072909 \\ B_2 &= 0.041674 \\ B_3 &= -0.0064603 \end{aligned} \qquad (7.4.17)$$

and S_1 is the salinity, measured in parts per thousand.

No mention is made as to whether T refers to the temperature of the methane or the water, the two presumably being assumed to be equal.

This is not true, however, in our model and so a choice must be made as to the exact definition of T. Equation (7.4.16) is only valid for a temperature range -2°C to 30°C and salinity range 0-40 parts per thousand, so it was decided to assume that the temperature to be used was that of the water. Use of the gas temperature would lead to values far lower than -2°C and (7.4.16) would not be appropriate to evaluate β_N.

7.5 Variation in Basic Model

The model is essentially the same as that detailed in Section 4.

The main difference is that the system of ordinary differential equations has been increased to five from the existing three. The two additions relate to the bubble density, ρ_B, and the void fraction, α.

The equation describing the variation in area now refers to the total cross-sectional area of the plume, rather than just the area of the water.

The set of equations to be integrated now consists of (7.2.59) - (7.2.61), (7.2.63) and either (7.2.62) or (7.2.67) which are rewritten as follows:

$$\frac{dA}{dh} = \frac{\frac{2K_1}{\sqrt{\pi}}\rho_B v(K_3 v+v_r)A^{\frac{1}{2}} - \phi v - \alpha A v(K_3 v+v_r)\frac{d\rho_B}{dh} - \rho_B A[K_3 v+(1-\alpha)v_r]\frac{dv}{dh}}{\rho_B v(K_3 v+v_r)} \qquad (7.5.1)$$

$$\frac{dv}{dh} = \frac{g/v[\alpha A\{\rho_1 v+\rho_B[(K_3-1)v+v_r]\}-\dot{m}_{g_o}] - \frac{2K_1}{\sqrt{\pi}}\rho_1 v^2 A^{\frac{1}{2}} + \phi[(K_3-1)v+v_r]}{[K_3\dot{m}_{g_o} + \rho_1(1-\alpha)Av]} \qquad (7.5.2)$$

$$\frac{d\rho_B}{dh} = \begin{cases} -\frac{\rho_B}{(z_e-h)}\left[\frac{2.65}{3.65} + \frac{(z_e-h)}{8}\frac{dS}{dh}\right] & S \geq S_{sat} \\ \frac{\rho_{g_1}\left[\rho_{g_1}\xi\frac{d\rho_{g_g}}{dh} - \rho_{g_g}(\rho_{g_1}-\rho_{g_g})\frac{d\xi}{dh}\right]}{\left[\xi\rho_{g_1} + (1-\xi)\rho_{g_g}\right]^2} & S < S_{sat} \end{cases} \qquad (7.5.3)$$

$$\frac{d\alpha}{dh} = \frac{-2K_1}{\sqrt{\pi}}\frac{\alpha\rho_B v(K_3 v+v_r)A^{\frac{1}{2}} - (1-\alpha)v\Phi - \alpha(1-\alpha)Av(K_3 v+v_r)\frac{d\rho_B}{dh} + \rho_B\alpha(1-\alpha)Av_r\frac{dv}{dh}}{\rho_B Av(K_3 v+v_r)} \qquad (7.5.4)$$

$$\frac{dS}{dh} = \frac{6\varepsilon_s}{\pi\rho_B d_e(K_3 v+v_r)}\left(\frac{0.016}{4.1868}\right)h_T\left(\frac{T_{sea}}{T}-1\right) \qquad (7.5.5)$$

In this case the extra equations necessary for closure consist of (7.2.23), (7.2.25), (7.3.4), (7.3.5), (7.4.13), (7.4.16), (7.2.42), (7.2.43), (7.2.50), (7.2.53) plus, in the case of $S < S_{sat}$, (7.2.64) - (7.2.66).

Again a set of initial conditions must be prescribed at $h_o = 0$, and these are given by (7.2.68) - (7.2.72), while the standard parameters are as in Table 4.2.1

The main changes in the numerical procedure are then

(a) ρ_B is no longer calculated from ρ_{g_g} and ξ, rather it is determined by the integration and ρ_{g_g} is then calculated according to equation (7.2.65).

(b) α is also determined by the integration, rather than being calculated separately.

The additional procedures carried out at each step are as follows.

1. Calculation of the Bunsen Absorption Coefficient, β_N, from (7.4.16), (7.4.17).

2. Calculation of the Mass Transfer Coefficient, k_m, via (7.3.4), (7.3.5) where the constant D is given the value calculated in section 7.3.

3. Calculation of the Interfacial concentration, c_i, by use of eqn. (7.4.13).

4. Calculation of the bulk concentration, c_∞, (7.2.25) which, in conjunction with c_i allows evaluation of the mass transfer rate, Φ .

REDUCTION OF SECOND MODEL TO FIRST MODEL

Although the two systems of equations seem very different, for consistency the second system should reduce to the first in the absence of mass transfer.

The assumption of no mass transfer means that the RHS of (7.2.1) is zero, i.e. $\Phi = 0$.

Using this fact in (7.2.59) - (7.2.61) leaves us with the set of equations.

$$\frac{dv}{dh} = \frac{g/v[\alpha A\{\rho_1 v+\rho_B[(K_3-1)v+v_r]\} - \dot{m}_{g_o}] - \frac{-2K_1}{\sqrt{\pi}}\rho_1 v^2 A^{\frac{1}{2}}}{[K_3\dot{m}_{g_o} + \rho_1(1-\alpha)Av]} \qquad (7.5.6)$$

$$\frac{dA}{dh} = \frac{\frac{2K_1}{\sqrt{\pi}}\rho_B v(K_3v+v_r)A^{\frac{1}{2}} - \alpha Av(K_3v+v_r)\frac{d\rho_B}{dh} - \rho_B A[K_3v+(1-\alpha)v_r]\frac{dv}{dh}}{\rho_B v(K_3v+v_r)} \qquad (7.5.7)$$

$$\frac{d\alpha}{dh} = \frac{-\frac{2K_1}{\sqrt{\pi}}\alpha\rho_B v(K_3 v+v_r)A^{\frac{1}{2}} - \alpha(1-\alpha)Av(K_3 v+v_r)\frac{d\rho_B}{dh} + \rho_B\alpha(1-\alpha)Av_r\frac{dv}{dh}}{\rho_B Av(K_3 v+v_r)} \qquad (7.5.8)$$

We also have the following relationship

$$A_1 = (1-\alpha)\,A \qquad (7.5.9)$$

and so

$$\frac{dA_1}{dz} = (1-\alpha)\frac{dA}{dz} - A\frac{d\alpha}{dz} \qquad (7.5.10)$$

Substituting from (7.5.7), (7.5.8), leads to

$$\frac{dA_1}{dz} = \frac{\frac{2K_1}{\sqrt{\pi}}\rho_B v(K_3 v+v_r)A^{\frac{1}{2}} - \rho_B(1-\alpha)A(K_3 v+v_r)\frac{dv}{dh}}{\rho_B v(K_3 v+v_r)} \qquad (7.5.11)$$

which can be written more simply as

$$\frac{dA_1}{dz} = \frac{2K_1}{\sqrt{\pi}}A^{\frac{1}{2}} - \frac{(1-\alpha)A}{v}\frac{dv}{dh} \qquad (7.5.12)$$

By use of (7.5.6) plus the relations

$$A = A_1 + A_g \qquad (7.5.13)$$

$$A_g = \frac{\dot{m}_{g_o}}{\rho_B(K_3 v+v_r)} = \alpha A \qquad (7.5.14)$$

(7.5.12) may finally be written as

$$\frac{dA_1}{dh} = \frac{2K_1}{\sqrt{\pi}} \frac{(2\rho_1 vA_1 + K_3\dot{m}_{g_o})[A_1+\frac{\dot{m}_{g_o}}{\rho_B(K_3v+v_r)}]^{\frac{1}{2}} - g(\rho_1-\rho_B)A_1\frac{\dot{m}_{g_o}}{\rho_B v(K_3v+v_r)}}{(K_3\dot{m}_{g_o} + \rho_1 vA_1)} \qquad (7.5.15)$$

which is exactly (2.2.74) with $K_2 = 1$

Similarly, using (7.5.13), (7.5.14) in (7.2.6) yields (2.2.75), with $K_2 = 1$

From equation (7.2.60), (7.2.61)

$$\frac{1}{\alpha}\frac{d\alpha}{dh} = \frac{-1}{A}\frac{dA}{dh} - \frac{1}{\rho_B}\frac{d\rho_B}{dh} - \frac{K_3}{(K_3v+v_r)}\frac{dv}{dh} \qquad (7.5.16)$$

This can then be solved to give

$$\alpha A \rho_B (K_3v+v_r) = \text{const} \qquad (7.5.17)$$

Using the initial conditions at $h = 0$, we have

$$\text{const} = \dot{m}_{g_o}$$

and thus, in general

$$\alpha = \frac{\dot{m}_{g_o}}{\rho_B A(K_3v+v_r)}$$

$$= \frac{\dot{m}_{g_o}}{\rho_B(K_3v+v_r)\left[A_1+\dot{m}_{g_o/\rho_B(K_3v+v_r)}\right]}$$

$$= \frac{\dot{m}_{g_o}}{[\rho_B A_1 (K_3 v + v_r) + \dot{m}_{g_o}]} \qquad (7.5.18)$$

which is exactly the definition of α in the first model ($K_2 = 1$) (2.2.79).

With these simplifications, there is no longer any need to define $\frac{d\rho_B}{dh}$ explicitly.

7.6 Consideration of the Term $\frac{d\rho_B}{dh}$

In the initial model, neglecting mass transfer, it was possible to formulate the system of equations without specific mention of $\frac{d\rho_B}{dh}$.

In the more complicated system arising from the inclusion of the possibility of mass transfer, this is no longer possible, and the term $\frac{d\rho_B}{dh}$ appears explicitly in (7.2.60), (7.2.61). Over a small increment in h, this term is likely to be small, and the question was raised as to whether this term could be neglected, thus simplifying greatly the system of equations and returning the calculation of ρ_B to that used in the first model.

By considering equation (7.2.60) (7.2.61) in the special case of no mass transfer ($\phi = 0$), they may be rewritten in the form of (7.5.16), and then rearranged slightly to give

$$\frac{1}{\alpha}\frac{d\alpha}{dh} + \frac{1}{\rho_B}\frac{d\rho_B}{dh} + \frac{K_3}{(K_3 v + v_r)}\frac{dv}{dh} + \frac{1}{A}\frac{dA}{dh} = 0 \qquad (7.6.1)$$

which may then be solved as before, to give

$$\alpha A \rho_B (K_3 v + v_r) = \text{const.} \qquad (7.6.2)$$

Evaluating at $h = 0$, gives

$$1.\ \frac{\dot{m}_{g_o}}{\rho_{B_o}(K_3 v_o + v_r)}\ \rho_{B_o}(K_3 v_o + v_r) = \text{const.} \qquad (7.6.3)$$

In other words

$$\text{const} = \dot{m}_{g_o} \qquad (7.6.4)$$

and hence,

$$\alpha = \frac{\dot{m}_{g_o}}{\rho_B A (K_3 v + v_r)} \qquad (7.6.5)$$

which is exactly the equation used for calculation of α in the first model (assuming $K_2 = 1$)

By choosing to neglect the term $\frac{d\rho_B}{dh}$ in eqns (7.2.60), (7.2.61), they may be combined to give

$$\frac{dA}{dh} = -\frac{A}{\alpha}\frac{d\alpha}{dh} - \frac{K_3 A}{(K_3 v + v_r)}\frac{dv}{dh} \qquad (7.6.6)$$

which can be rearranged to give

$$\frac{1}{\alpha}\frac{d\alpha}{dh} + \frac{K_3}{(K_3 v + v_r)}\frac{dv}{dh} + \frac{1}{A}\frac{dA}{dh} = 0 \qquad (7.6.7)$$

Solving this yields

$$\alpha A(K_3 v + v_r) = \text{const} \qquad (7.6.8)$$

Again evaluating this expression at h = 0, we have

$$\text{const} = \frac{\dot{m}_{g_o}}{\rho_{B_o}} \qquad (7.6.9)$$

which means that

$$\alpha = \frac{\dot{m}_{g_o}}{\rho_{B_o} A(K_3 v + v_r)} \qquad (7.6.10)$$

Comparison of (7.6.5) and (7.6.10) shows that (7.6.10) gives an erroneous expression for α, and as the gas rises, and ρ_B decreases, (7.6.10) would predict too low a value for α, which in turn would affect the values of A,v.

We can, therefore, conclude that it is not permissible to neglect the term $\frac{d\rho_B}{dh}$ from the second system of equations.

7.7 Effect of Mass Transfer

To assess the effect of allowing the possibility of mass transfer a number of runs were made, at varying depths and release rates, with the second model, each run being

made under two conditions:

(i) Allowance made for mass transfer by dissolution of methane in the water.

(ii) By setting the mass transfer coefficient to zero, the mass transfer is neglected.

Table 7.7.1 shows surface values of v_g, d_{eff}, T, and α for cases (i) and (ii) at each depth and release rate: for each the upper set of figures relate to case (ii), while the lower set refer to case (i).

CONCLUSIONS

The results show that the effect of allowing mass transfer is to

(a) decrease gas velocity

(b) decrease width of plume

(c) decrease the void fraction

while there is no effect on the temperature of the gas. The inclusion of mass transfer does not affect the values greatly, especially at shallow depths and low release rates, but the general trends are as would be expected.

Dissolution of the gas means that there is a smaller volume of gas, which will decrease the buoyancy force and lead to a smaller velocity. There will be a two-fold effect on the plume width. Decrease in gas present plus a slight decrease in amount of water entrainment due to smaller

Depth	20					40					60					80				
$\dot{m}^{(m)}_{g_o}$	v_g	d_{eff}	T	α	$\dot{m}_{g_o}$	v_g	d_{eff}	T	α	$\dot{m}_{g_o}$	v_g	d_{eff}	T	α	$\dot{m}_{g_o}$	v_g	d_{eff}	T	α
500	13.3	10.7	275	0.600	500	11.9	13.2	275	0.440	500	10.8	15.6	275	0.344	500	9.98	18.1	275	0.278
	13.3	10.7	275	0.599		11.8	13.1	275	0.437		10.7	15.6	275	0.339		9.87	18.1	275	0.272
1000	15.6	13.2	275	0.673	1000	14.1	15.6	274	0.526	1000	13.0	18.0	274	0.431	1000	12.1	20.4	274	0.362
	15.5	13.1	275	0.672		14.1	15.6	274	0.524		12.9	17.9	274	0.427		12.0	20.3	274	0.357
2000	18.2	16.5	275	0.737	2000	16.7	18.9	274	0.608	2000	15.5	21.2	274	0.520	2000	14.5	23.5	274	0.452
	18.1	16.4	275	0.736		16.6	18.9	274	0.606		15.4	21.1	274	0.516		14.4	23.4	274	0.447
3000	19.8	18.9	274	0.770	3000	18.3	21.3	274	0.652	3000	17.1	23.6	273	0.569	3000	16.1	25.8	273	0.505
	19.8	18.9	274	0.769		18.3	21.3	274	0.650		17.0	23.5	273	0.566		16.0	25.7	273	0.500

Table 7.7.1: Effect of mass transfer at varying depths and release rates.

velocity will both lead to a decrease in plume width. The second of these two effects will be far less significant and hence the void fraction, being predominantly affected by the change in gas volume, will also decrease.

By comparing values of α in Table 7.7.1 it can be seen that the mass transfer has increasing effect as the depth increases, and at a fixed depth, the effect varies directly with the release rate.

Finally, to check that case (ii) was equivalent to the first model, the set of runs was repeated using the first model. Table 7.7.2 shows the results: the upper set of figures referring to the second model (case (ii)), while the lower set refer to the first model.

It can be seen that the figures are identical.

Depth (m)	20					40					60					80				
$\dot{m}_{g_o}$	v_g	d_{eff}	T	α	$\dot{m}_{g_o}$	v_g	d_{eff}	T	α	$\dot{m}_{g_o}$	v_g	d_{eff}	T	α	$\dot{m}_{g_o}$	v_g	d_{eff}	T	α
500	13.3	10.7	275	0.600	500	11.9	13.2	275	0.440	500	10.8	15.6	275	0.344	500	9.98	18.1	275	0.278
	13.3	10.7	275	0.600		11.9	13.2	275	0.440		10.8	15.6	275	0.344		9.98	18.1	275	0.278
1000	15.6	13.2	275	0.673	1000	14.1	15.6	274	0.526	1000	13.0	18.0	274	0.431	1000	12.1	20.4	274	0.362
	15.6	13.2	275	0.673		14.1	15.6	274	0.526		13.0	18.0	274	0.431		12.1	20.4	274	0.362
2000	18.2	16.5	275	0.737	2000	16.7	18.9	274	0.608	2000	15.5	21.2	274	0.520	2000	14.5	23.5	274	0.452
	18.2	16.5	275	0.737		16.7	18.9	274	0.608		15.5	21.2	274	0.520		14.5	23.5	274	0.452
3000	19.8	18.9	274	0.770	3000	18.3	21.3	274	0.652	3000	17.1	23.6	273	0.569	3000	16.1	25.8	273	0.505
	17.8	18.9	274	0.770		18.3	21.3	274	0.652		17.1	23.6	273	0.569		16.1	25.8	273	0.505

Table 7.7.2 Comparison of two models (no mass transfer)

CHAPTER 8

CONCLUSIONS

By means of a control volume argument the conservation equations for an unconfined bubble plume in non-stratified surroundings are established. These equations are identical to those obtained by simplification of the general conservation equations of mass and momentum for the gas and liquid phases.

No assumption is made as to the liquid velocity and void fraction profiles; instead "equivalent" values are used. A correlation between these and the corresponding values from Gaussian profiles is made.

Thermodynamic relations are used to allow for a non-isothermal rise of gas through the water and various expressions for the heat transfer coefficient are discussed. Numerical values and empirical formulae used all relate to methane, the major constituent of the gas under consideration.

By combining the dynamics and thermodynamics a general mathematical model is obtained which is then solved numerically. This model describes the main part of the rise through the water. This is, in fact, the second of four

separate stages necessary to describe completely the history of the escaping gas. Brief comments are made on the other three stages.

Comparison of the present model with experimental results shows that for relatively low flow rates of air the model will give reasonable predictions of plume characteristics.

Experimental data on high release rates of low temperature gas does not appear to be available. Further work in this area, where the initial stages of the plume formation are likely to be important, is needed. The accuracy of the initial conditions for phase two which have been assumed could then be assessed and any necessary adjustments made.

Sensitivity analysis for the heat transfer coefficient, h_T shows that once the heat transfer coefficient exceeds some critical value (in the range 20-40 $W/m^2°K$) the surface conditions are independent of this coefficient and resemble those of an isothermal rise. Variation does occur as to the depth at which the gas achieves these isothermal characteristics.

This study also shows that positive buoyancy is achieved by the gas for all values of h_T above a second critical value (this time of the order of 5 $W/m^2°K$).

Sensitivity analysis for the "equivalent" bubble diameter, d_e, shows that in the absence of heat transfer the surface conditions are virtually independent of bubble size. This also means that the model is not sensitive to changes in the slip velocity. In the presence of heat transfer from the surrounding water, increasing the bubble size reduces the

warming effect. For d_e greater than some critical value the effect of the heat transfer is cancelled out, this value depending on the heat transfer coefficient assumed. (From 0.1m for h_T = 8W/m^2°K to values of the order of a few metres for h_T = 300 W/m^2°K).

As to the buoyancy of the gas at the surface; for h_T = 300 W/m^2°K the gas will be positively buoyant if d_e does not exceed 1.5m. If the variable form of the heat transfer coefficient derived is assumed bubbles over 0.2m in diameter would result in the gas being negatively buoyant while for h_T = 8W/m^2°K this would occur for d_e greater than 0.05m.

An extension to the model allows for the possibility of mass transfer caused by the dissolution of the gas in the sea-water. An expression for the mass transfer coefficient is derived in a manner similar to that employed for the heat transfer coefficient. On comparison with the initial model, the presence of mass transfer results in a decrease in gas velocity, plume width and void fraction while the temperature of the gas is unchanged.

At this stage of development there remains unanswered the question of the effect of using a richer gas, e.g. a typical composition might be

C_1	62.28%
C_2	17.74%
C_3	14.29%
IC_4	0.85%

/.....

NC_4	2.23%
IC_5	0.11%
NC_5	0.11%
N_2	0.28%
CO_2	2.11%

where C_1 - C_5 denote Methane, Ethane, Propane, Butane and Pentane, N_2 is Nitrogen and CO_2, Carbon Dioxide.

In place of the numerical values and curve-fitted expressions used in Chapter 3 for thermodynamic properties, use of the computer program in conjunction with one of the property generating programs available would allow evaluation of such properties for any given gas composition.

As depths of interest get deeper the question of hydrate formation will become important. The depths quoted in the literature (Topham (1984a,b)), however, refer to ambient pressure. In our case there is a large pressure drop at the point of escape giving rise to a significant temperature drop which could make hydrate formation an important consideration at much shallower depths. I believe, therefore, that further study in this area would be beneficial.

There is a need for accurate experiments to determine the heat transfer coefficient. There is some available evidence, e.g. L'Ecuyer, but experimental results relating to heat transfer are rare, especially for hydrocarbon gases.

APPENDIX A RISE OF SPHERICAL-CAP BUBBLES

The following consideration of the speed of rise of a spherical-cap bubble is based on the arguments of Batchelor (1967) and Davies & Taylor (1950).

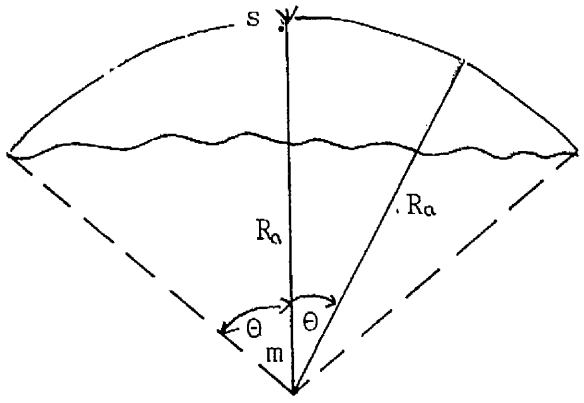

For small gas bubbles of volumes less than about $6 \times 10^{-10} m^3$ rising through water, the effect of surface tension is sufficiently strong to keep the bubble approximately spherical. As the volume increases, the bubble becomes oblate due to the variation of pressure in the water over the surface of the bubble, and for volumes above about 5×10^{-6} m^3, for which surface tension effects are negligible, the bubble has a spherical cap shape. The vertical motion is approximately steady and the front surface is steady, smooth and closely spherical while the rear face is jagged and irregular.

By considering the steady flow near the stagnation point, s, on the forward face, with axes fixed relative to the bubble, we use Bernoulli's theorem for a streamline at the bubble surface.

Outside the bubble,

$$p + \rho g R_\alpha \cos\theta + \frac{1}{2}\rho u_s^2 = p_o + \rho g R_\alpha \qquad (A1)$$

where the subscript s refers to evaluation on surface of bubble, and the subscript o relates to the stagnation point.

If we let an overbar denote conditions inside the bubble, then corresponding to (A1) we can write

$$\bar{p} + \bar{\rho} g R_\alpha \cos\theta + \frac{1}{2}\bar{\rho}\,\bar{u}_s^2 = \bar{p}_o + \bar{\rho}\, g R_\alpha \qquad (A2)$$

Subtracting,

$$(p - \bar{p}) + (\rho - \bar{\rho})\, g R_\alpha \cos\theta + (\tfrac{1}{2}\rho u_s^2 - \tfrac{1}{2}\bar{\rho}\,\bar{u}_s^2) = (p_o - \bar{p}_o) + (\rho - \bar{\rho}) g R_\alpha$$

By making the assumption that the variation of the dynamic pressure inside the bubble, $\frac{1}{2}\bar{\rho}\,\bar{u}_s^2$, is small compared with that outside, we have $(p-\bar{p}) + (\rho - \bar{\rho}) g R_\alpha \cos\theta + \frac{1}{2}\rho u_s^2 = (p_o - \bar{p}_o) + (\rho - \bar{\rho}) g R_\alpha$

or,

$$(p-\bar{p}) + \tfrac{1}{2}\rho u_s^2 = (p_o - \bar{p}_o) + g R_\alpha (\rho - \bar{\rho})(1 - \cos\theta) \qquad (A3)$$

The pressure difference must be uniform, implying

$$p - \bar{p} = p_o - \bar{p}_o \qquad (A4)$$

and thus reducing (A4) to

$$\tfrac{1}{2} u_s^2 = g R_\alpha \frac{(\rho - \bar{\rho})}{\rho}(1 - \cos\theta) \qquad (A5)$$

Since it is not possible to calculate the flow round a spherical cap shaped body, but evidence shows that the detached boundary layer lies roughtly on the same sphere as the forward face of the bubble, u_s was calculated from the flow round a sphere in an inviscid fluid, moving with speed $\hat{U}$, giving

$$u_s = \frac{3}{2}\hat{U}\sin\Theta \qquad (A6)$$

Equating the two expressions for u_s leads to

$$\hat{U}^2 = \frac{8}{9} gR_\alpha\left(\frac{\rho-\bar{\rho}}{\rho}\right)\left[\frac{1-\cos\Theta}{\sin^2\Theta}\right] \qquad (A7)$$

For Θ small $\quad \frac{1-\cos\Theta}{\sin^2\Theta} \rightarrow \frac{1}{2}$

so that, near the stagnation point

$$\hat{U} = \frac{2}{3}\sqrt{gR_\alpha\left(\frac{\rho-\bar{\rho}}{\rho}\right)} \qquad (A8)$$

Expressing R in terms of the equivalent diameter, d_e, (see Appendix F)

$$R_\alpha = \frac{d_e}{\left[2(1-\cos\Theta_m)^2\,(2+\cos\Theta_m)\right]^{\frac{1}{3}}} \qquad (A9)$$

Thus,

$$\hat{U} = \frac{2}{3}\sqrt{g\left(\frac{\rho-\bar{\rho}}{\rho}\right)\frac{}{[2(1-\cos\theta_m)^2(2+\cos\theta_m)]^{\frac{1}{3}}}} \qquad \text{(A10)}$$

For a typical value of $\theta_m = 50°$ this reduces to

$$\hat{U} = 0.712\sqrt{g\left(\frac{\rho-\bar{\rho}}{\rho}\right)d_e} \qquad \text{(A11)}$$

Experimentally, Davies & Taylor (1950) found that

$\hat{U} = 2.48\ V^{1/6}$, where V is the volume of the bubble

which translates into

$$\hat{U} = 2.23\sqrt{d_e} = \sqrt{4.96d_e} \qquad \text{(A12)}$$

It is based on this figure that the present model assumes a value of $\sqrt{5d_e}$

APPENDIX B GAS DISCHARGE

This appendix contains some well known theory which is included for completeness.

1. Velocity of Sound in an Ideal Gas

If we consider a disturbance set up by the movement of a piston at the end of a tube. A wave travels down the tube with sonic velocity, c. After the passage of the wave the properties of the gas have changed by an infinitesimal amount and the gas is moving with velocity du towards the wave front.

By considering the wave front as a control surface, the First Law of Thermodynamics may be written (Van Wylen & Sonntag (1978)) as

$$\hat{h} + c^2/2 = (\hat{h}+d\hat{h}) + \frac{(c-du)^2}{2}$$

where $\hat{h}$ denotes the specific enthalpy.
To leading order, this implies

$$d\hat{h} - c\,du = 0 \qquad (B.1)$$

From the continuity equation, for a tube of cross-sectional area A,

$$\rho A c = (\rho + d\rho)\, A\, (c-du)$$

and so, again to leading order

$$c\,d\rho - \rho du = 0 \tag{B.2}$$

Using the thermodynamic relation

$$Tds = d\hat{h} - \frac{dp}{\rho} \tag{B.3}$$

and assuming the process is isentropic (ds = 0) (B.1) may be rewritten as

$$\frac{dp}{\rho} - c\,du = 0 \tag{B.4}$$

which may then be combined with (B.2) to give

$$\left(\frac{\partial p}{\partial \rho}\right)_s = c^2 \tag{B.5}$$

For an ideal gas undergoing an isentropic change of state, assuming a constant specific heat we also have the relation

$$\left(\frac{\partial p}{\partial \rho}\right)_s = \gamma \frac{p}{\rho} \tag{B.6}$$

where γ is the ratio of specific heats.

Combining (B.5) and (B.6) and making use of the Ideal gas law, leaves us with

$$c^2 = \gamma rT \tag{B.7}$$

where T is the temperature, and r is the gas constant

2. Reversible, Adiabatic, One-Dimensional, Steady Flow of an Ideal Gas through a nozzle

Letting the subscript o denote stagnation conditions, the First Law gives

$$\hat{h} + \frac{u^2}{2} = \hat{h}_o \qquad (B.8)$$

Using the thermodynamic relations

$$\hat{h} = c_{p_o} T \qquad (B.9)$$

$$c_{p_o} = \frac{r\gamma}{\gamma - 1} \qquad (B.10)$$

(B.8) may be rewritten as

$$u^2 = \frac{2\gamma r T}{\gamma - 1}\left(\frac{T_o}{T} - 1\right) \qquad (B.11)$$

Combining with (B.7) and rearranging

$$\frac{T_o}{T} = 1 + \frac{(\gamma - 1)}{2} M^2 \qquad (B.12)$$

where $M' = \frac{u}{c}$ is the Mach number

For an isentropic process

$$\left(\frac{T_o}{T}\right)^{\gamma/\gamma - 1} = \frac{p_o}{p} \qquad \left(\frac{T_o}{T}\right)^{1/\gamma - 1} = \frac{\rho_o}{\rho} \qquad (B.13(a),(b))$$

leading to

$$\frac{p_o}{p} = \left[1 + \frac{(\gamma-1)}{2} M^2\right]^{\gamma/(\gamma-1)} \qquad (B.14)$$

$$\frac{\rho o}{\rho} = \left[1 + \frac{(\gamma-1)}{2} M^2\right]^{1/(\gamma-1)} \qquad (B.15)$$

At the throat of the nozzle, necessarily

$$M' = 1$$

and so, denoting by * the conditions at the throat,

$$\frac{T^*}{T_o} = \frac{2}{\gamma+1}$$

$$\frac{p^*}{p_o} = \left(\frac{2}{\gamma+1}\right)^{\gamma/\gamma-1} \qquad (B.16(a),(b),(c))$$

$$\frac{\rho^*}{\rho_o} = \left(\frac{2}{\gamma+1}\right)^{1/\gamma-1}$$

These ratios are frequently referred to as the critical temperature, critical pressure and critical density ratios: and can be found in tables

3. Mass Flow Rate of an Ideal Gas through an Isentropic nozzle

The mass flow rate per unit area can be written

$$\frac{\dot{m}}{A} = \rho u = \frac{pu}{rT}\sqrt{\frac{\gamma T_o}{\gamma T_o}}$$

$$= \frac{pu}{\sqrt{\gamma r T}}\sqrt{\frac{\gamma}{r}}\sqrt{\frac{T_o}{T}}\sqrt{\frac{1}{T_o}}$$

$$= \frac{pM'}{\sqrt{T_o}}\sqrt{\frac{\gamma}{r}}\sqrt{1 + \frac{\gamma-1}{2}M^2} \quad \text{(by use of (B.7) and (B.12))}$$

Use of (B.14) leads to

$$\frac{\dot{m}}{A} = \frac{p_o}{\sqrt{T_o}}\sqrt{\frac{\gamma}{r}} \cdot \frac{M'}{\left[1+\frac{\gamma-1}{2}M^2\right]^{\frac{\gamma+1}{2(\gamma-1)}}} \qquad \text{(B.17)}$$

At the throat, $M' = 1$ and (B.17) reduces to

$$\frac{\dot{m}}{A^*} = \frac{p_o}{\sqrt{T_o}}\sqrt{\frac{\gamma}{r}} \cdot \frac{1}{\left(\frac{\gamma+1}{2}\right)^{\frac{\gamma+1}{2(\gamma-1)}}} \qquad \text{(B.18)}$$

4. Note on Maximum flow rates

Effect of the back pressure, p_B, which is the pressure outside the nozzle exit.

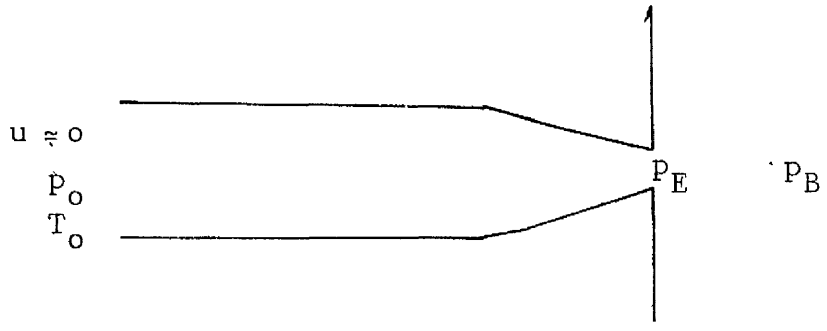

(a) when $\frac{p_B}{p_o} = 1$, there is no flow; $\frac{p_E}{p_o} = 1$

(b) If p_B is lowered but $\frac{p_B}{p_o}$ > critical pressure ratio, then $\dot{m}$ has a certain value and $p_E = p_B$ (exit Mach number is less than 1)

(c) If p_B is lowered to the critical pressure ratio, $p_E = p_B$ and the exit Mach number is 1.

(d) Further decrease in p_B will not increase $\dot{m}$, p_E remains constant at the critical pressure and the exit Mach number is 1. The drop in pressure from p_E to p_B occurs outside the nozzle exit. Under such conditions the nozzle is said to be choked, which means that for given stagnation conditions the nozzle is passing the maximum possible mass flow.

In the case of interest in this thesis, it is not the back pressure which is varying, but the stagnation pressure p_o which is decreasing with time.

This affects two things

(1) The mass flow rate

(2) The speed of exit of the gas

For a given stagnation pressure, p_o, the gas will be at sonic velocity so long as the back pressure is less than or equal to the critical pressure for this p_o.

For γ = 1.3 (value for methane), the critical pressure ratio is

$$\frac{p^*}{p_o} = 0.5457 \qquad (B.19)$$

which implies the critical pressure is 0.5457 p_o. Therefore,

Flow will be at sonic velocity so long as

$$p_B \leqslant 0.5457\ p_o$$

i.e. $p_o \geqslant \frac{p_B}{0.5457}$

Once $p_o < \frac{p_B}{0.5457}$, the exit velocity will be less than sonic.

Although the speed of exit of the gas will remain at sonic velocity until the stagnation pressure falls below $\frac{1}{0.5457}$ times the back pressure, the mass flow rate will not remain at a constant value during this time, but will decrease with the decreasing p_o, according to (B.18).

For methane,

γ = 1.3

r = 0.51835×10^3

and (B.18) becomes

$$\frac{\dot{m}}{A^*} = 0.0293 \frac{p_o}{\sqrt{T_o}} \qquad \text{(B.20)}$$

APPENDIX C AVERAGE DENSITY AND VELOCITY OF TWO-PHASE BUBBLES

The concept of continuum theories is comprehensively explored by Atkin & Craine (1976a,b). In less detail, the general formulation adopted here is that discussed by Soo (1976).

Following his method, it is assumed that for a mixture of two phases, a particle in each phase exists at every point of the mixture.

DENSITY

We have for the mass of the bubble, in terms of the mass of the two phases,

$$m_B = m_{g_l} + m_{g_g} \tag{C.1}$$

or, dividing by the volume of the mixture, V_B,

$$\rho_B = \rho'_{g_l} + \rho'_{g_g} \tag{C.2}$$

where the densities on the RHS refer to their values within the mixture.

We require, however, to express ρ_B in terms of the densities which each phase would have existing as a separate entity; ρ_{g_g} and ρ_{g_l}

Then,

$$m_{g_g} = \rho_{g_g} V_g \tag{C.3}$$

$$m_{g_l} = \rho_{g_l} V_l \qquad (C.4)$$

and

$$\rho_B = \frac{m_B}{V_g + V_l}$$

$$= \frac{m_B}{m_{g_g}/\rho_{g_g} + m_{g_l}/\rho_{g_l}}$$

$$= \frac{m_B \rho_{g_g} \rho_{g_l}}{m_{g_g} \rho_{g_l} + m_{g_l} \rho_{g_g}}$$

i.e.

$$\rho_B = \frac{\rho_{g_g} \rho_{g_l}}{\xi \rho_{g_l} + (1-\xi)\rho_{g_g}} \qquad (C.5)$$

where,

$$\xi = \frac{m_{g_g}}{m_B} = \text{fraction of gas in vapour phase}$$

VELOCITY

By writing the momentum of the mixture as

$$m_B v_B = m_{g_g} v_{g_g} + m_{g_l} v_{g_l} \qquad (C.6)$$

where the terms v_B, $v_{g_g} + v_{g_l}$ denoted the velocities of the mixture, the gas phase and the liquid phase, respectively

Hence the mean velocity of the two-phase mixture may be written as

$$v_B = \frac{m_{g_g} v_{g_g} + m_{g_l} v_{g_l}}{m_B}$$

$$= \xi v_{g_g} + (1-\xi) v_{g_l} \qquad (C.7)$$

If, however, we assume that both phases move with the same velocity i.e.

$$v_{g_g} = v_{g_l} = v_g \qquad (C.8)$$

then,

$$v_B = v_g \qquad (C.9)$$

APPENDIX D

MEAN AND FLUCTUATING COMPONENTS OF VELOCITY

Letting u = instantaneous liquid velocity

$\bar{u}$ = average value over the time liquid is present

$\tilde{u}$ = fluctuating component

Then,

$$u = \bar{u} + \tilde{u} \tag{D.1}$$

and

$$\bar{u} = \frac{1}{\Delta t_1} \int_{\Delta t_1} u \, dt \tag{D.2}$$

Thus,

$$\overline{u^2} = \frac{1}{\Delta t_1} \int_{\Delta t_1} u^2 \, dt$$

$$= \frac{1}{\Delta t_1} \int_{\Delta t_1} (\bar{u}^2 + 2\bar{u}\tilde{u} + \tilde{u}^2) \, dt$$

$$= \frac{1}{\Delta t_1} \int_{\Delta t_1} \bar{u}^2 dt + \frac{1}{\Delta t_1} \int_{\Delta t_1} 2\bar{u}\,(u-\bar{u}) \, dt + \frac{1}{\Delta t_1} \int_{\Delta t_1} \tilde{u}^2 \, dt$$

$$= \frac{1}{\Delta t_1} \cdot \bar{u}^2 \cdot \Delta t_1 + \frac{1}{\Delta t_1} \cdot 2\bar{u} \int_{\Delta t_1} u \, dt - \frac{1}{\Delta t_1} \cdot 2\bar{u}^2 \cdot \Delta t_1 + \frac{1}{\Delta t_1} \int_{\Delta t_1} \tilde{u}^2 \, dt$$

$$= \bar{u}^2 + 2\,\bar{u}^2 - 2\bar{u}^2 + \overline{\tilde{u}^2} \qquad (D.3)$$

$$= \bar{u}^2 + \overline{\tilde{u}^2}$$

APPENDIX E: RELATIONSHIP BETWEEN GAUSSIAN AND TOPHAT PROFILES

The present model is based on Top Hat profiles for the velocity and gas fraction, while Sjoen (1983) concentrates on Gaussian profiles.

If Top Hat values are identified by the subscript T, and Gaussian by the subscript G, then there exists the following:

Top Hat: The plume has average upward velocity w_T, and radius b_T.

The gas fraction has a value α_T, averaged across the plume to a radius $\lambda_T b_T$

So,

w_T, b_T and α_T are functions of the height z, but independent of the radial distance r_α.

Gaussian: Here the upward velocity is denoted by

$$w = w_G e^{-r_\alpha^2/b_G^2} \qquad (E.1)$$

where w_G = centre line value, and

b_G = characteristic plume radius

and the gas fraction

$$\alpha = \alpha_G e^{-r_\alpha^2/\lambda_G^2 b_G^2} \qquad (E.2)$$

where α_G = centre line value, and

$\lambda_G b_G$ = characteristic radius of the bubble-containing part of the plume.

It is possible to compare various quantities, calculated using both Top Hat and Gaussian distributions, namely gas

volume flux, gas cross-sectional area, liquid mass flux, liquid momentum flux and liquid entrainment.

GAS VOLUME FLUX

Gaussian

$$G = \int_0^\infty 2\pi r_a \alpha\ (w+w_r)dr_a$$

$$= \pi\alpha_G\ w_G \int_0^\infty 2r_a\ e^{-r_a^2/b_G^2(1+1/\lambda_G^2)}dr_a + \pi\alpha_G w_r \int_0^\infty 2r_a e^{-r_a^2/\lambda_G^2 b_G^2}\ dr_a$$

$$= \pi\alpha_G\ w_G\ \frac{b_G^2}{1+1/\lambda_G^2} + \pi\alpha_G\ w_r\ \lambda_G^2\ b_G^2$$

$$= \pi\alpha_G\ b_G^2\lambda_G^2 w_G\left(\frac{}{1+\lambda_G^2} + w_r\right). \qquad \text{E.3}$$

Top Hat

$$G = \int_0^\infty 2\pi r_a\ \alpha_T\ (w_T + v_r)\ dr_a$$

$$= 2\pi\alpha_T w_T \int_0^{\min(\lambda_T b_T, b_T)} r_a dr_a + 2\pi\alpha_T v_r \int_0^{\lambda_T b_T} r_a\ dr_a$$

$$= \pi\alpha_T\ w_T\ \min\ (\lambda_T^2 b_T^2,\ b_T^2) + \pi\alpha_T\ v_r\ \lambda_T^2 b_T^2$$

$$= \begin{cases} \pi\alpha_T \, b_T^2 \, \lambda_T^2 \, (w_T + v_r) & \lambda_T \leqslant 1 \\ \pi\alpha_T \, b_T^2 \, \lambda_T^2 \, \left(\dfrac{w_T}{\lambda_T^2} + v_r \right) & \lambda_T > 1 \end{cases} \qquad \text{(E.4)}$$

LIQUID MASS FLUX

Gaussian

$$\dot{m}_l = \rho_l \int_0^\infty 2\pi r_a (1-\alpha) \, w \, dr_a$$

$$= \rho_l \int_0^\infty 2\pi r_a \left(1 - \alpha_G e^{-r_a^2/\lambda_G^2 b_G^2}\right) w_G \, e^{-r_a^2/b_G^2} \, dr_a$$

$$= 2\pi\rho_l w_G \left[\int_0^\infty r_a e^{-r_a^2/b_G^2} \, dr_a - \alpha_G \int_0^\infty r_a e^{-r_a^2/b_G^2 \left(\frac{1+1/\lambda_G^2}{}\right)} \, dr_a \right]$$

$$= \pi\rho_l w_G \left(b_G^2 - \frac{\alpha_G b_G^2}{1+1/\lambda_G^2} \right)$$

$$= \pi\rho_l w_G b_G^2 \left(1 - \frac{\alpha_G}{1+1/\lambda_G^2} \right) \qquad \text{(E.5)}$$

Top Hat

$$\dot{m}_l = \rho_l \int_0^\infty 2\pi r_a (1-\alpha_T) \, w_T \, dr_a$$

$$= 2\pi\rho_l w_T \left[\int_0^{b_T} r_a\, dr_a - \alpha_T \int_0^{\min(\lambda_T b_T, b_T)} r_a\, dr_a \right]$$

$$= \pi\rho_l w_T \left[b_T^2 - \alpha_T \min(\lambda_T^2 b_T^2, b_T^2) \right]$$

$$= \begin{cases} \pi\rho_l w_T b_T^2 (1 - \lambda_T^2 \alpha_T) & \lambda_T \leq 1 \\ \pi\rho_l w_T b_T^2 (1 - \alpha_T) & \lambda T > 1 \end{cases} \qquad (E.6)$$

LIQUID MOMENTUM FLUX

Gaussian

$$\dot{M}_l = \rho_l \int_0^\infty 2\pi r_a (1-\alpha) w^2\, dr_a$$

$$= \pi\rho_l w_G^2 \left[\int_0^\infty 2 r_a e^{-r_a^2/b_G^2} dr_a - \alpha_G \int_0^\infty 2 r_a e^{-r_a^2/b_G^2(2+1/\lambda_G^2)} dr_a \right]$$

$$= \pi\rho_l w_G^2 \left(b_G^2/2 - \frac{\alpha_G b_G^2}{2+1/\lambda_G^2} \right)$$

$$= \frac{\pi\rho_l w_G^2 b_G^2}{2} \left(1 - \frac{\alpha_G}{1+\frac{1}{2}\lambda_G^2} \right) \qquad (E.7)$$

Top Hat

$$\dot{M}_l = \rho_l \int_0^\infty 2\pi r_a (1-\alpha_T) w_T^2\, dr_a$$

$$= 2\pi\rho_l w_T^2 \left[\int_0^{b_T} r_a\, dr_a - \alpha_T \int_0^{\min(\lambda_r b_T, b_T)} r_a\, dr_a \right]$$

$$= 2\pi\rho_1 w_T^2 \left[b_{T/2}^2 - \alpha_{T/2} \min (\lambda_T^2 b_T^2, b_T^2) \right]$$

$$= \begin{cases} \pi\rho_1 w_T^2 b_T^2 (1-\lambda_T^2 \alpha_T) & \lambda_T \leq 1 \\ \pi\rho_1 w_T^2 b_T^2 (1-\alpha_T) & \lambda_T > 1 \end{cases} \qquad (E.8)$$

GAS CROSS-SECTIONAL AREA

Gaussian

$$A_g = \int_0^\infty 2\pi r_a \alpha \, dr_a$$

$$= \pi\alpha_G \int_0^\infty 2r_a e^{-r_a^2/\lambda_G^2 b_G^2} \, dr_a$$

$$= \pi\alpha_G \lambda_G^2 b_G^2 \qquad (E.9)$$

Top Hat

$$A_g = \int_0^\infty 2\pi r_a \alpha_T \, dr_a$$

$$= \pi\alpha_T \int_0^\infty 2r_a \, dr_a$$

$$= \pi\alpha_T \lambda_T^2 b_T^2 \qquad (E.10)$$

LIQUID ENTRAINMENT

This is related to the liquid mass increase equation

Gaussian

$$\frac{d\dot{m}_l}{dz} = -2\pi\rho_l \beta_G w_G b_G \qquad (E.11)$$

Top Hat

$$\frac{d\dot{m}_l}{dz} = -2\pi\rho_l \beta_T w_T b_T \qquad (E.12)$$

where β is the entrainment parameter

Comparisons between certain parameters of the two profiles may be made by equating a number of the previous expressions.

By equating the liquid mass and momentum fluxes, and dividing the equation relating to momentum by that relating to mass

$$\frac{w_G^2 b_G^2 \left(1 - \frac{\alpha_G}{1+\frac{1}{2}\lambda_G^2}\right)}{2 \quad w_G b_G^2 \left(1 - \frac{\alpha_G}{1+1/\lambda_G^2}\right)} = \frac{w_T^2 b_T^2}{w_T b_T^2} \qquad \forall \lambda_T$$

which may be rearranged to see that

$$w_G = 2w_T \left[\frac{1+2\lambda_G^2}{1+\lambda_G^2} \cdot \frac{1+\lambda_G^2(1-\alpha_G)}{1+2\lambda_G^2(1-\alpha_G)}\right] \qquad \forall \lambda_T \qquad (E.13)$$

For negligible gas fraction, $1 - \alpha_G \simeq 1$, and the above equation reduces to

$$w_G = 2\, w_T \tag{E.14}$$

which is the well known result, as quoted in Fanneløp & Sjøen (1980).

Equating the mass fluxes

$$w_G\, b_G^{\,2} \left[1 - \frac{\alpha G}{1+1/\lambda_G^{\,2}} \right] = w_T b_T^{\,2} [1-\min(\lambda_T^{\,2},1)\alpha_T]$$

Substitution for w_T gives

$$w_G b_G^{\,2} \left[1 - \frac{\alpha G}{1+1/\lambda_G^{\,2}} \right] = b_T^{\,2} [1-\min(\lambda_T^{\,2},1)\alpha_T] \cdot \frac{w_G}{2} \left[\frac{1+\lambda_G^{\,2}}{1+2\lambda_G^{\,2}} \right] \left[\frac{1+2\lambda_G^{\,2}(1-\alpha_G)}{1+\lambda_G^{\,2}(1-\alpha_G)} \right]$$

which may be solved for b_G to obtain

$$b_G = \frac{b_T}{\sqrt{2}} \left[\frac{1+\lambda_G^{\,2}}{1+\lambda_G^{\,2}(1-\alpha_G)} \right] \left[\frac{1+2\lambda_G^{\,2}(1-\alpha_G)}{1+2\lambda_G^{\,2}} \right]^{\frac{1}{2}} \cdot [1-\min(\lambda_T^{\,2},1)\alpha_T]^{\frac{1}{2}} \tag{E.15}$$

Again, for negligible gas fraction, the equation reduces to

$$b_G = \frac{b_T}{\sqrt{2}} \tag{E.16}$$

as expected.

Using the equations relating to the momentum fluxes yields an identical result.

Equating the gas cross-sectional areas yields

$$\alpha_G \lambda_G^2 b_G^2 = \alpha_T \lambda_T^2 b_T^2$$

Substituting for b_G^2, and rearranging, we find

$$\bar{\alpha}_G = \frac{2\alpha_T \lambda_T^2}{\lambda_G^2(1-\mu^2\alpha_T)}\left[\frac{1+\lambda_G^2(1-\alpha_G)}{1+\lambda_G^2}\right]^2\left[\frac{1+2\lambda_G^2}{1+2\lambda_G^2(1-\alpha_G)}\right] \qquad (E.17)$$

$$\mu^2 = \min(\lambda_T^2, 1)$$

and, for negligible gas fraction

$$\alpha_G = 2\frac{\lambda_T^2}{\lambda_G^2}\alpha_T. \qquad (E.18)$$

Finally, equating entrainment rates

$$\beta_G w_G b_G = \beta_T w_T b_T$$

and this leads to

$$\beta_G = \frac{\beta_T}{\sqrt{2(1-\mu^2\alpha_T)}}\left[\frac{1+2\lambda_G^2(1-\alpha_G)}{1+2\lambda_G^2}\right]^{\frac{1}{2}} \qquad (E.19)$$

so that for $\alpha_G, \alpha_T, \ll 1$

$$\beta_G = \frac{\beta_T}{\sqrt{2}} \qquad (E.20)$$

It is possible to write equations (E.13), (E.15), (E.17), (E.19)

in a different form

$$\frac{w_G}{w_T} = 2\left[1 + \frac{\lambda_G^2 \alpha_G}{[1+\lambda_G^2][1+2\lambda_G^2(1-\alpha_G)]}\right] \qquad (E.21)$$

$$\frac{b_G}{b_T} = \frac{1}{\sqrt{2}}\left[\frac{1+\lambda_G^4\left\{\alpha_G(1-\alpha_G)+[1+2\lambda_G^2(1-\alpha_G)][\alpha_G-\mu^2\alpha_T(1+1/\lambda_G^2)^2]\right\}}{[1+2\lambda_G^2][1+\lambda_G^2(1-\alpha_G)]^2}\right]^{\frac{1}{2}} \qquad (E.22)$$

$$\frac{\alpha_G}{\alpha_T} = \frac{2\lambda_T^2}{\lambda_G^2}\left[1+\lambda_G^2\alpha_G\left[\frac{\mu^2\{1+\lambda_G^4+2\lambda_G^6(1-\alpha_G)\}}{+(\mu^2-\lambda_T^2)\{2\lambda_G^2(2-\alpha_G)+4\lambda_G^4(1-\alpha_G)\}}\right]\right] \qquad (E.23)$$

$$\frac{\beta_G}{\beta_T} = \frac{1}{\sqrt{2}}\left[1 + \frac{\mu^2\alpha_T[1+2\lambda_G^2(1-\frac{\alpha_G}{\mu^2\alpha_T})]}{(1+2\lambda_G^2)(1-\mu^2\alpha_T)}\right]^{\frac{1}{2}} \qquad (E.24)$$

from which the simplified forms for $\alpha_G, \alpha_T \ll 1$ can easily be seen.

Equation (E.21) shows that the effect of allowing a non-negligible gas fraction is to increase the ratio w_G/w_T for all values of λ, α($\alpha < 1$)

The ratios b_G/b_T and β_G/β_T, however, will show an increase or decrease depending on the values of λ, α .

For α_G/α_T , if $\lambda_T \leqslant 1$ there will be an increase, but for $\lambda_T > 1$ it will depend on λ, α

Returning to (E.21), if we let

$$f(\lambda_G) = \frac{\lambda_G^2 \alpha_G}{[1+\lambda_G^2]\,[1+ 2\lambda_G^2(1-\alpha_G)]} \tag{E.25}$$

Then, by differentiating and rearranging

$$f'(\lambda_G) = \frac{2\lambda_G\alpha_G[1-2\lambda_G^4(1-\alpha_G)]}{[1+\lambda_G^2]^2[1+2\lambda_G^2(1-\alpha_G)]^2} \tag{E.26}$$

Hence, $f'(\lambda_G) = 0$ when $\lambda_G\alpha_G\,[1-2\lambda_G^4(1-\alpha_G)] = 0$

This requires $\lambda_G = 0$ or $\alpha_G = 0$, or

$$\lambda_G^4 = \frac{1}{2(1-\alpha_G)} \tag{E.27}$$

Since gas is present, the first two solutions are not possible so that the third must hold.

In fact, for $\lambda_G^2 < \frac{1}{\sqrt{2(1-\alpha_G)}}$, $f'(\lambda_G) > 0$ (E.28)

and so $f(\lambda_G)$ increases with λ_G,

while for $\lambda_G^2 > \frac{1}{\sqrt{2(1-\alpha_G)}}$, $f'(\lambda_G) < 0$,

and $f(\lambda_G)$ decreases with λ_G. (E.29)

As $\alpha_G \to 0$, $\dfrac{1}{\sqrt{2(1-\alpha_G)}} \to \dfrac{1}{\sqrt{2}}$, (E.30)

and it can be noted that $f(\lambda_G)$ increases with λ_G so long as $\lambda_G^2 < 1/\sqrt{2}$, i.e. so long as $\lambda_G < 0.841$

For $\alpha_G \neq 0$, $\dfrac{1}{\sqrt{2(1-\alpha_G)}} > \dfrac{1}{\sqrt{2}}$ (E.31)

and hence, $f(\lambda_G)$ increases with λ_G for $\lambda_G > \lambda_{G_{crit}}$ where $\lambda_{G_{crit}} > 0.841$

Using this information in (E.21), we can say that for $\alpha_G \neq 0$, the effect on the ratio w_G/w_T will be to increase its value above 2, and this increase will be dependent on λ_G (assuming effect of λ_G dominates effect of varying α_G) in such a way that it is directly proportional to λ_G for all values of $\lambda_G > \lambda_{G_{crit}}$ where $\lambda_{G_{crit}} > 0.841$.

Due to the complicated nature of the expressions, similar analysis was not applied to the other ratios. For comparison purposes in each of the four ratios the simplified version obtained for $\alpha_G, \alpha_T \to$ was used

i.e. $\dfrac{w_G}{b_T} = 2$, $\dfrac{b_G}{b_T} = \dfrac{1}{\sqrt{2}}$, $\dfrac{\alpha_G}{\alpha_T} = \dfrac{2\lambda_T^2}{\lambda_G^2}$, $\dfrac{\beta_G}{\beta_T} = \dfrac{1}{\sqrt{2}}$

(E.32(a),(b),(c),(d))

AVERAGE GAS VELOCITY

By considering equations (E.3) and (E.4) it can be seen that for a Gaussian profile the average gas velocity may be written

$$v_g = \frac{1}{1+\lambda_G^2} + w_r \qquad \text{(E.33)}$$

while for a Top Hat profile, the equivalent expression is

$$v_g = \begin{cases} w_T + v_r & \lambda_T \leqslant 1 \\ \frac{w_T}{\lambda_T 2} + v_r & \lambda_T > 1 \end{cases} \qquad \text{(E.34)}$$

We shall only consider $\lambda_T \leqslant 1$, so the second alternative is not applicable.

Comparing (E.33) and (E.34) with equation (2.2.37) it follows that, assuming $w_r = v_r$, $w_T = v$ and $w_G = 2w_T$,

$$K_3 = \begin{cases} \frac{2}{1+\lambda_G^2} & \text{Gaussian profile} \\ 1 & \text{Top Hat Profile} \end{cases} \qquad \text{(E.35)}$$

For the purpose of comparing results in 4.6 a special case of (E.22) is considered.

Assumptions: $\lambda_T = 1$ (E.36(a),(b),(c))

$\lambda_G < 1$

$\alpha_T = \frac{\lambda_G^2 \alpha_G}{2K}$, where by previous discussion

$K \geqslant 1$

Equation (E.22) may then be rewritten as

$$\frac{b_G}{b_T} = \frac{1}{\sqrt{2}} \left[1 + \frac{\lambda_G^4 \, g(\lambda_G)}{[1+2\lambda_G^2][1+\lambda_G^2(1-\alpha_G)]^2} \right]^{\frac{1}{2}} \qquad (E.37)$$

where

$$g(\lambda_G) = \alpha_G(1-\alpha_G)+[1+2\lambda_G^2(1-\alpha_G)] \left[\alpha_G - \frac{\lambda_G^2 \alpha_G}{2K} \left(1+\frac{1}{\lambda_G^2}\right)^2\right] \qquad (E.38)$$

This reduces to

$$g(\lambda_G) = \alpha_G \left[(1-1/K) + (1-1/K)(1-\alpha_G) + 2(1-1/K)\, \lambda_G^2(1-\alpha_G) - \frac{\lambda_G^2}{2K} - \frac{\lambda_G^4}{K}(1-\alpha_G) - \frac{1}{2K\lambda_G^2}\right] \qquad (E.39)$$

Clearly, for $K = 1$, $g(\lambda_G) < 0$, but for non-negligible gas fraction $K > 1$, and the sign of $g(\lambda_G)$ is not so obvious.

If we consider the term

$$\left[2(1-1/K) - \frac{\lambda_G^2}{K}\right] \lambda_G^2(1-\alpha_G), \qquad (E.40)$$

this is less than zero so long as

$$K < 1 + \frac{\lambda_G^2}{2} \qquad (E.41)$$

In this case

$$(1-1/K) + (1-1/K)(1-\alpha_G) - \frac{\lambda_G^2}{2K} - \frac{1}{2K\lambda_G^2}$$

In this case

$$(1-1/K) + (1-1/K)(1-\alpha_G) - \frac{\lambda_G^2}{2K} \quad - \frac{1}{2K\lambda_G^2}$$

$$< \left(1 - \frac{2}{2+\lambda_G^2}\right) - \frac{\lambda_G^2}{2+\lambda_G^2} + \left(1 - \frac{2}{2+\lambda_G^2}\right)(1-\alpha_G) - \frac{1}{\lambda_G^2(2+\lambda_G^2)}$$

$$= \left(1 - \frac{2}{2+\lambda_G^2}\right)(1-\alpha_G) - \frac{1}{\lambda_G^2(2+\lambda_G^2)}$$

$$< 1 - \frac{2}{2+\lambda_G^2} \quad \frac{1}{\lambda_G^2(2+\lambda_G^2)}$$

$$= - \frac{1}{\lambda_G^2(2+\lambda_G^2)} (1 - \lambda_G^4)$$

< 0 , since $\lambda_G < 1$

Thus, $g(\lambda_G) < 0$ and the result is a decrease in the ratio $b_{G/}b_T$ for values of K greater than 1 but less than $1 + \lambda_G^2/2$.

Using equation (E.36(c)) we can say that $g(\lambda_G) < 0$

$$\text{if} \quad \frac{\alpha_G}{\alpha_T} < 1 + \frac{2}{\lambda_G^2} = \begin{cases} 5.08 & \lambda_G = 0.7 \\ 6.37 & \lambda_G = 0.61 \\ 4.65 & \lambda_G = 0.74 \\ 4.20 & \lambda_G = 0.79 \end{cases} \qquad \text{(E.42)}$$

APPENDIX F: SURFACE AREA OF SPHERICAL CAP IN THE FORM $SA = d_e^2$

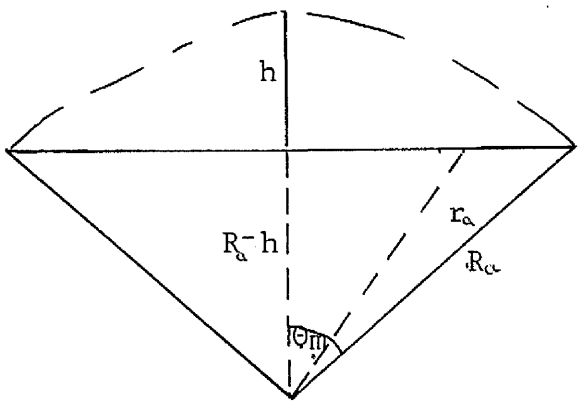

The volume of this spherical cap may be calculated from

$$V = 2\pi \int_0^{\Theta_m} \int_{\frac{R_a-h}{\cos\Theta}} r_a^2 \sin\Theta \; dr_a \, d\Theta$$

to give

$$V = \pi h^2 (R_a - h/3) \qquad (F.1)$$

The surface area of this spherical cap may be calculated from

$$S.A. = \int_0^{2\pi} \int_0^{\Theta_m} R_a^2 \sin\Theta \, d\Theta \, d\phi + \pi [R_a^2 - (R_a - h)^2]$$

to give

$$S.A. = \pi h (4R_a - h) \qquad (F.2)$$

It is also easily verified that

$$h = R_a(1 - \cos\Theta_m) \qquad (F.3)$$

Substituting (F.3) into (F.1) and (F.2) leads to

$$V = \frac{\pi R_a^3}{3}(1 - \cos\Theta_m)^2(2 + \cos\Theta_m) \qquad (F.4)$$

$$S.A. = \pi R_a^2 (1 - \cos\Theta_m)(3 + \cos\Theta_m) \qquad (F.3)$$

We wish, however, to relate everything to the "equivalent" diameter d_e, defined by

$$V = \frac{\pi d_e^3}{6} \qquad (F.6)$$

If we express the surface area as

$$S.A. = \varepsilon d_e^2 \qquad (F.7)$$

then

$$\frac{V}{S.A.} = \frac{\pi d_e}{6\varepsilon} \qquad (F.8)$$

which, from (F.4) and (F.2) may be equated to

$$\frac{V}{S.A.} = \frac{R_a(1 - \cos\Theta_m)(2 + \cos\Theta_m)}{3(3 + \cos\Theta_m)} \qquad (F.9)$$

to give

$$\varepsilon = \frac{\pi d_e}{2R_a}\,\frac{(3 + \cos\Theta_m)}{(1-\cos\Theta_m)(2 + \cos\Theta_m)} \qquad (F.10)$$

Finally, from (F.4) and (F.6), we have

$$R_a = \frac{d_e}{2^{\frac{1}{3}}(1-\cos\theta_m)^{\frac{2}{3}}(2+\cos\theta_m)^{\frac{1}{3}}} \qquad (F.11)$$

This may be substituted into (F.10) to give

$$\varepsilon_a = \frac{\pi(3 + \cos\theta_m)}{[4(1- \cos\theta_m)(2+\cos\theta_m)^2]^{\frac{1}{3}}} \qquad (F.12)$$

APPENDIX G: SAMPLE OUTPUT

The program is run for the standard set of values as given in Table 6.2.1.

The variable form of the heat transfer coefficient is used and mass transfer is accounted for.

Figure G1 shows a sample output with values printed at 5m intervals.

Figures G2, G3 and G4 are plots of velocity, diameter and temperature against depth respectively.

Figure G.1

```
RUNNING OF PROGRAM ..... GAS.ESCAPE


GAS CONCERNED IS ... METHANE

CONSTANTS

 WATER DENSITY ..................  0.1000E+04 KG/CU.M
 GAS DENSITY-LIQUID PHASE .....  0.3376E+03 KG/CU.M

PARAMETERS

 INPUT DEPTH ....................  0.8000E+02 M
 GAS CONDITION IN PIPE ........  0.3220E+02 CAL/MOL/K
 HEAT TRANSFER COEFFICIENT ....  0.3000E+03 W/K/SQ.M
 SEA TEMPERATURE ................  0.2800E+03 K
 MOLECULAR WEIGHT OF GAS ......  0.1600E-01 KG/MOL
 VOLUME INJECTION RATE ........  0.1637E+03 CU.M/S
 VOL. INJECTION RATE (ATM.PRES.) 0.1473E+04 CU.M/S
 MASS INJECTION RATE ............  0.2200E+04 KG/S
 INITIAL BUBBLE DENSITY .......  0.1344E+02 KG/CU.M
 INITIAL BUBBLE DIAMETER ......  0.1800E-01 M
 SLIP VELOCITY ..................  0.3000E+00 M/S
 ENTRAINMENT COEFF., C1 ........0.2500E+00

CONDITIONS

1.    VARIABLE HEAT TRANSFER COEFF. USED
2.    MASS TRANSFER ACCOUNTED FOR
```

TIME (S)	DEPTH (M)	VELOCITY (M/S)	DIAMETER (M)	TEMP (K)	ENTROPY (CAL/MOL.K)	MASS TR (KG/S/M)	DENSITY (KG/CU.M)	ALPHA
0.000E+00	0.800E+02	0.450E+00	0.215E+02	0.150E+03	0.322E+02	0.767E-01	0.134E+02	0.100E+01
0.404E+00	0.750E+02	0.131E+02	0.671E+01	0.276E+03	0.389E+02	0.312E-01	0.593E+01	0.793E+00
0.788E+00	0.700E+02	0.129E+02	0.773E+01	0.278E+03	0.391E+02	0.191E-01	0.553E+01	0.652E+00
0.118E+01	0.650E+02	0.127E+02	0.875E+01	0.278E+03	0.392E+02	0.136E-01	0.519E+01	0.551E+00
0.158E+01	0.600E+02	0.125E+02	0.977E+01	0.278E+03	0.394E+02	0.104E-01	0.485E+01	0.479E+00
0.198E+01	0.550E+02	0.124E+02	0.108E+02	0.278E+03	0.395E+02	0.82?E-02	0.450E+01	0.427E+00
0.238E+01	0.500E+02	0.123E+02	0.118E+02	0.278E+03	0.397E+02	0.669E-02	0.416E+01	0.388E+00
0.279E+01	0.450E+02	0.123E+02	0.128E+02	0.278E+03	0.399E+02	0.555E-02	0.381E+01	0.359E+00
0.320E+01	0.400E+02	0.123E+02	0.138E+02	0.277E+03	0.401E+02	0.464E-02	0.347E+01	0.339E+00
0.360E+01	0.350E+02	0.123E+02	0.149E+02	0.277E+03	0.403E+02	0.395E-02	0.312E+01	0.325E+00
0.401E+01	0.300E+02	0.124E+02	0.159E+02	0.277E+03	0.406E+02	0.336E-02	0.278E+01	0.317E+00
0.441E+01	0.250E+02	0.125E+02	0.169E+02	0.277E+03	0.408E+02	0.287E-02	0.243E+01	0.315E+00
0.481E+01	0.200E+02	0.127E+02	0.180E+02	0.276E+03	0.412E+02	0.244E-02	0.209E+01	0.319E+00
0.520E+01	0.150E+02	0.130E+02	0.191E+02	0.276E+03	0.416E+02	0.205E-02	0.174E+01	0.330E+00
0.558E+01	0.100E+02	0.134E+02	0.204E+02	0.276E+03	0.420E+02	0.169E-02	0.140E+01	0.353E+00
0.594E+01	0.500E+01	0.139E+02	0.218E+02	0.275E+03	0.426E+02	0.130E-02	0.105E+01	0.391E+00
0.629E+01	0.000E+00	0.148E+02	0.239E+02	0.274E+03	0.435E+02	0.852E-03	0.703E+00	0.459E+00

```
IFAIL= 0
 TOLR= 0.1000E-04

END OF LISTING OF FILE :GAMV06.GRAPH(1,*,1).Z2(1) FOR USER :GAMV06 AT 1986/10/24__09:23:15

*****************************************************************************************************************************
```

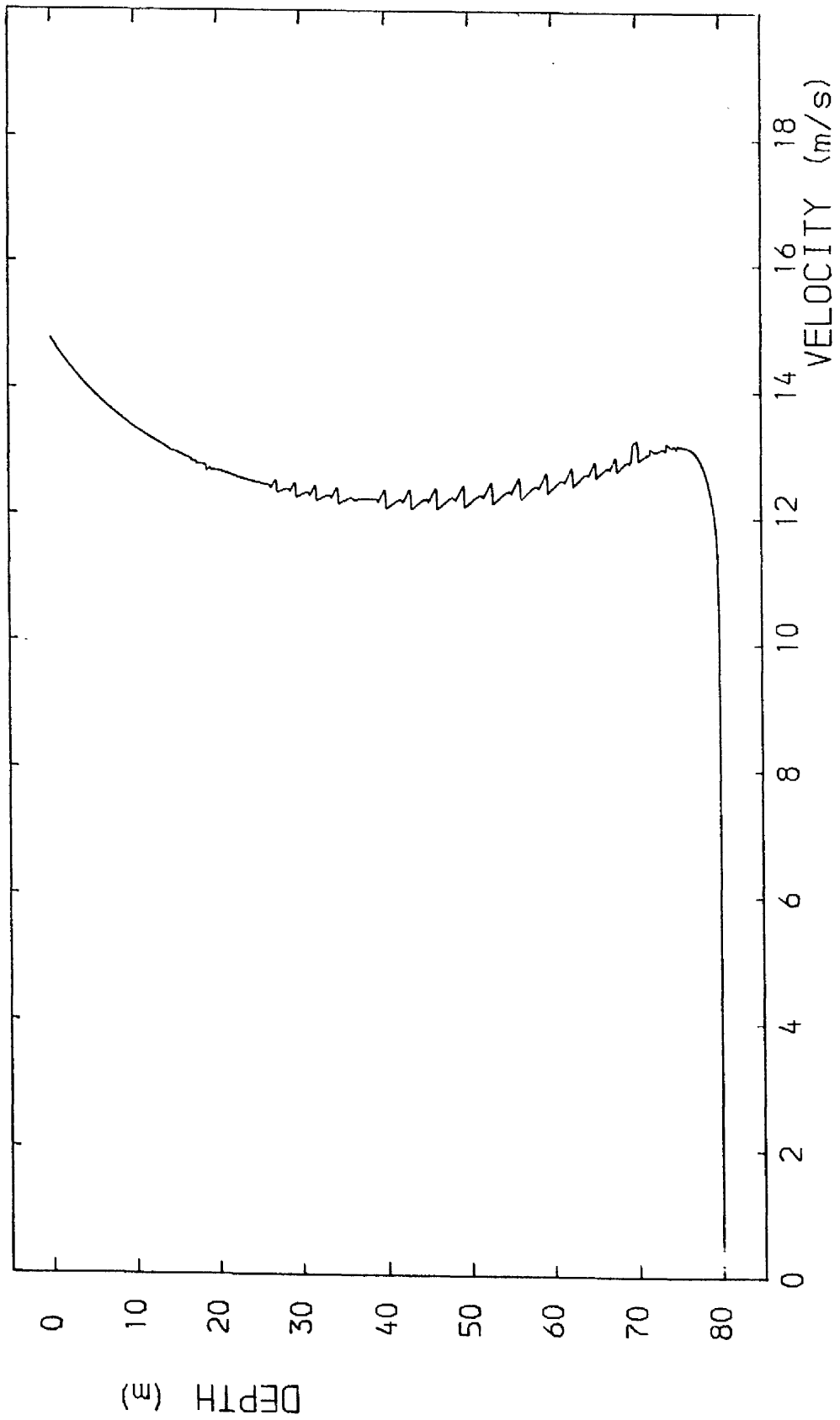

Figure G.2

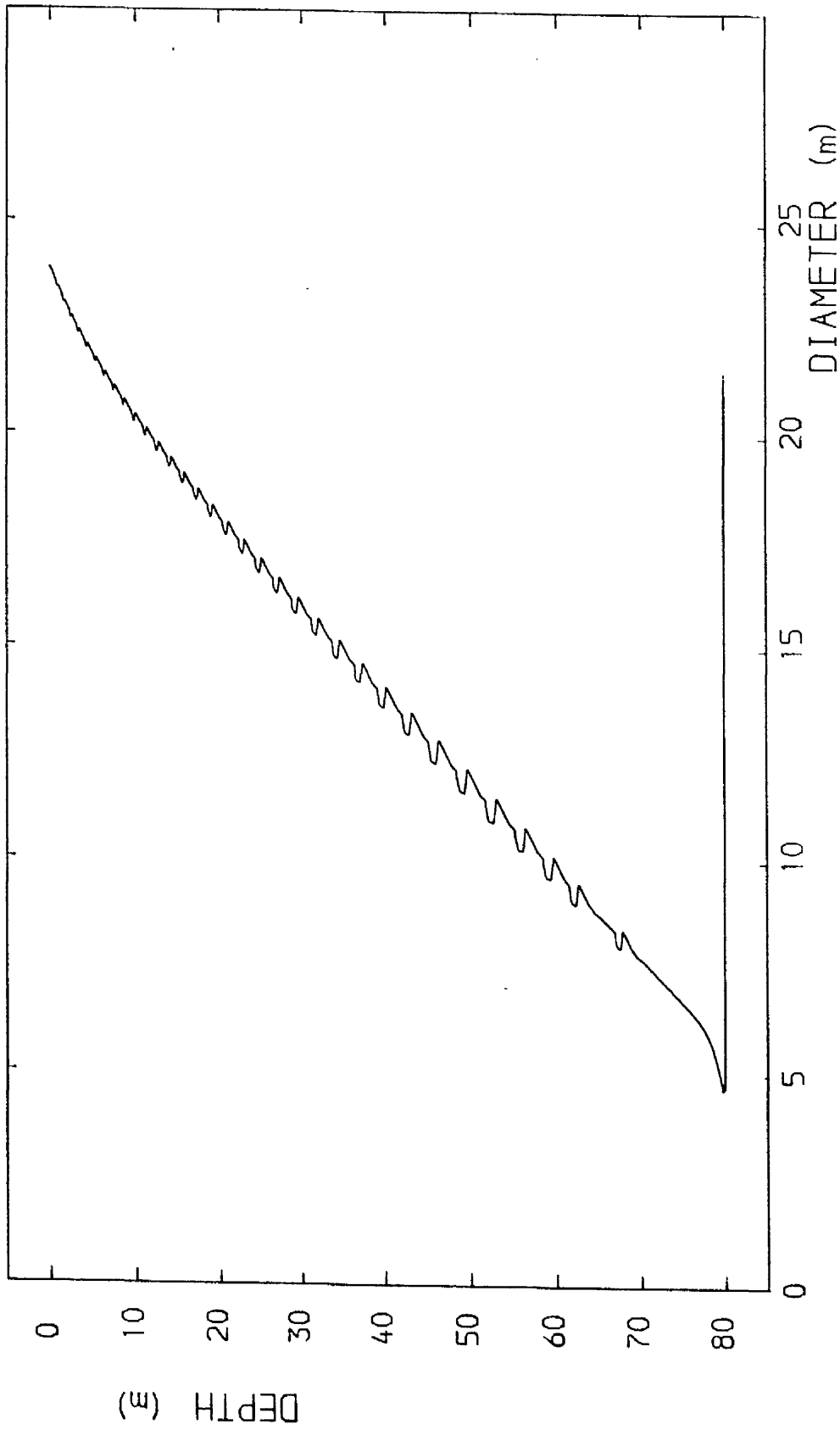

Figure G.3

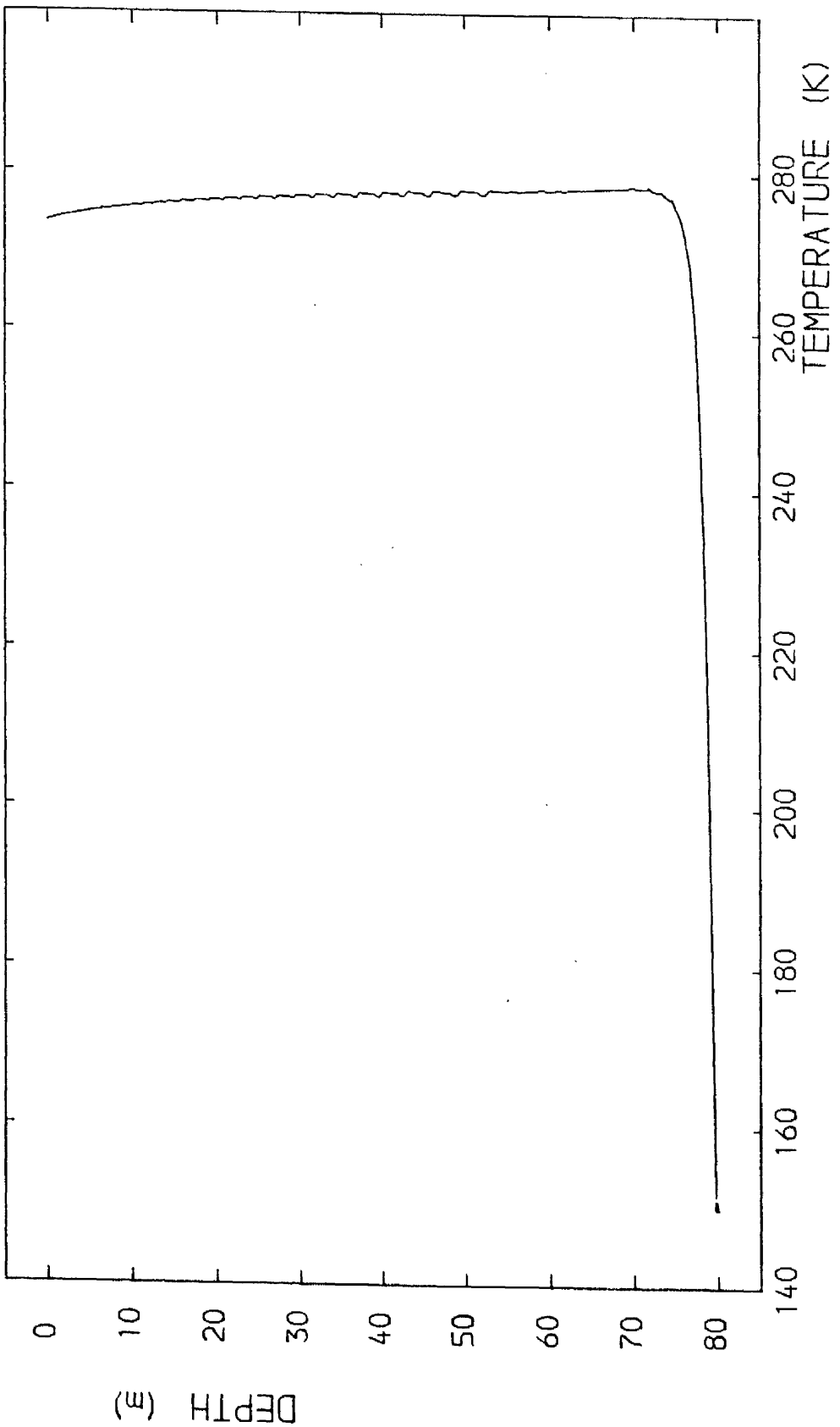
DEPTH (m)
0
10
20
30
40
50
60
70
80
140
160
180
200
220
240
260
280
TEMPERATURE (K)

Figure G.4

REFERENCES

Atkin, R.J. and Craine, R.E. (1976 a) Continuum Theories of Mixtures: Basic Theory and Historical Development. Quarterly Journal of Mechanics and Applied Mathematics, Vol. 229, part 2, 209-244.

Atkin, R.J. and Craine, R.E. (1976b) Continuum Theories of Mixtures: Applications. J. Inst. Maths Applics., 17, 153-207.

Batchelor, G.K. (1967) An Introduction to Fluid Dynamics. Cambridge University Press.

Balzhiser, R.E. and Samuels, M.R. (1977) Engineering Thermodynamics. U.S.A.: Prentice-Hall, Inc.

Brevik, I. (1977) Two-Dimensional Air-Bubble Plume. Proc. ASCE. J. Waterways, Harbours, Coastal Eng. Div., 103, 101-115.

Butterworth, D. and Hewitt, G.F. (1977) Two-phase Flow and Heat Transfer. Oxford University Press.

Cederwall, K. and Ditmars, J.D. (1970) Analysis of Air-bubble plumes. California Inst. Tech. Rep. no. KH-R-24.

Chesters, A.K., Van Doorn, M. and Goossens, L.H.J. (1980) A general model for unconfined bubble plumes from extended sources. Int. J. Multiphase Flow, 6, 499-521.

Clift, R., Grace, J. and Weber, M.E. (1978) Bubbles, Drops and Particles. Academic Press.

Collins, R. (1966) A second approximation for the velocity of a large gas bubble rising in an infinite liquid. J. Fluid Mech., 25, 469-480.

Cornwell, K. (1977) The Flow of Heat. Wokingham: Van Nostrand Reinhold.

Davies, R.M. and Taylor, G.I. (1950) The mechanics of large bubbles rising through extended liquids and through liquids in tubes. Proc. Roy. Soc. A., 200, 375-390.

Fanneløp T.K. and Sjøen, K. (1980) Hydrodynamics of Underwater Blowouts. A.I.A.A. 18th Aerospace Sciences Meeting, Pasadena, Paper AIAA-80-0219.

Fazal, R. and Milgram, J.H. (1980) The structure of gas-liquid plumes above blowouts. 80-12. Mass.Inst. of Tech., Dept. Ocean Engineering

Goossens, L.H.J. (1979) Reservoir destratification with bubble columns Ph.D. thesis, U. Delft: Delft University Press.

Haaland, S.E. (1979) Mathematical Modelling of Bubble Plumes. Rep.no. IFAG B-122 , Division of Aero - and Gas Dynamics, The Norwegian Inst. of Tech.

Haberman, W.L. and Morton, R.K. (1954) An experimental study of bubbles moving in liquids. Proc. ASCE, 80, separate no. 387.

Havens, J.A. and Spicer, T.O. (1985) Development of an Atmospheric Dispersion model for heavier-than-air gas mixtures. vol. I. (no title), vol II: Laboratory calm air heavy gas dispersion experiments, vol III: DEGADIS user's manual, prepared for the U.S. Dept. of Transportation, U.S. Coast Guard.

Hussain, N.A. and Siegel, R. (1976) Liquid Jet Pumped by Rising Gas Bubbles. J. Fluids Eng., 98, series 1, no. 1, 49-57.

Ishii, (1975) Thermo-Fluid Dynamic Theory of Two-Phase Flow Pans: Eyrolles

Kobus, H.E. (1968) Analysis of the flow induced by air-bubble systems. Proc. 11th conference on Coastal Eng., London vol II, chpt. 65, 1016-

Kobus, H.E. (1973) Bemessungsgrundlagen und Anwendungen für Luftschleier im Wasserbau. Berlin: E. Schmidt Verlag.

Kotsovinos, N.E. and List, E.J. (1977) Plane turbulent buoyant jets. Part 1. Integral properties. J. Fluid Mech., 81, 25-44.

Leclair, B.P. and Hamielec, A.E.(1971) Viscous Flow Through Particle Assemblages at Intermediate Reynolds Numbers - A Cell Model for Transport In Bubble Swarms.Con.J.Chem.Eng.,49. 713-720.

* L'Ecuyer. Heat Transfer to a Gas Bubbling Through Liquid.

Lewis, D.A. and Davidson, J.F. (1982) Bubble Splitting in Shear Flow. Trans. Inst. Chem. Eng., 60, 283-291.

Miksis, M.J., Vanden-Broeck, J.M. and Keller, J.B. (1981) Axisymmetric bubble or drop in a uniform flow. J. Fluid Mech., 108, 89-100.

Miksis, M.J., Vanden-Broeck, J.M. and Keller, J.B. (1982) Rising bubbles. J. Fluid. Mech., 123, 31-41.

Milgram, J.H. (1983) Mean flow in round bubble plumes. J. Fluid Mech., 133, 345-376.

Milgram, J.H. and Burgess, J.J. (1984) Measurements of the surface flow above round bubble plumes Appl. Ocean Research, 6, 40-44.

Milgram, J.H. and Van Houten, R.J. (1982) Plumes from subsea well blowouts. Proc. 3rd Intl. Conf. Boss. vol. I, 659-684.

Private communication . Crawley, F . Britoil, Glasgow

Moore, D.W. (1959) The rise of a gas bubble in a viscous liquid. J. Fluid Mech., 6, 113-130.

Morton, B.R. (1959) Forced Plumes, J. Fluid Mech., 5, 151-163.

Morton, B.R., Taylor, G.I. and Turner, J.S. (1956) Turbulent gravitational convection from maintained and instantaneous sources. Proc. Roy. Soc. London. A., 234, 1-23.

Mundheim, Ø., Torhaug, M., Melgaker, P., Ose, T., Westergaard, R.H., Sjøen, K., Karel, K., Vesterhaug, O., Olshausen, K. and Wold, M. (1981) Offshore Blowout Control [Rep. No. STF 88 A81004] Otter Group, Trondheim.

Parlange, J-Y. (1969) Spherical cap bubbles with laminar wakes J. Fluid Mech., 37, 257-263.

Perry, R.H. and Green, D. (1984) Perry's Chemical Engineers' Handbook, Sixth Edition. USA: McGraw-Hill.

Ricou, F.P. and Spalding, D.B. (1961) Measurements of entrainment by axisymmetrical turbulent jets. J. Fluid Mech., 11, 21-32.

Rosenberg, B. (1950) The Drag and Shape of Air Bubbles moving in Liquid. The David W. Taylor Model Basin, Rep. No. 727.

Seidell, A. (1941) Solubilities of Organic Compounds, 3rd edition. New York: Van Nostrand.

Sevik, M. and Park, S.H. (1973) The Splitting of Drops and Bubbles by Turbulent Fluid Flow. J. Fluids Eng., 95, 53-60.

Sjøen, K. (1983) Modelling of Bubble Plumes from Subsea Blowouts. Ph.D. thesis. Norwegian Institute of Technology.

Smith, J.M. (1982) Undersea Cryogenic Gas Escapes. Short study, Technische Hogeschool Delft, Laboratorium Voor Fysische Technologie.

Smith, J.M. (1984) Private communication

Soo, S.L. (1976) On one-dimensional motion of a single component in Two Phases. Int. J. Multiphase Flow, 3 79-82

Stephen, H. and Stephen, T. (1963),(ed) Solubilities of Inorganic and Organic Compounds, vol I. : Pergamon Press.

Taylor, G.I. (1945) Dynamics of a mass of hot air rising in air. USAEC Rep No. MDDC-919 LADC -276, Los Alamos Scientific Laboratory, Los Alamos.

Tekeli, S. and Maxwell, W.H.C. (1978) Behaviour of Air Bubble Screens. Rep. No.UILU-Eng- 78-2019. Dept. Civil Eng., Univ. Illinois.

Topham, D.R. (1975) Hydrodynamics of an oilwell blowout. Beaufort Sea Technical Rep. No. 33, Inst. Ocean Sciences, Sidney, B.C.

Topham, D.R. (1978) Observations of the formation of hydrocarbon gas hydrates at depth in seawater. I.O.S. note 4, Inst. Ocean Sciences, Sidney, B.C.

Topham, D.R. (1984a) The formation of gas hydrates on bubbles of hydrocarbon gases rising in seawater. Chem. Eng. Sci., 39, 821-828.

Topham, D.R. (1984b) The modelling of hydrocarbon bubble plumes to include gas hydrate formation. Chem. Eng. Science, 39, 1613 - 1622.

Tsang, G (1984) Modelling criteria for bubble plumes - a theoretical approach. Can. J. Civ. Eng., 11, 293-298.

Turner, J.S. (1969) Buoyant plumes and thermals. Ann. Rev. Fluid Mech. 1, 29-44.

Van Wylen, G.J. and Sonntag, R.E. (1978) Fundamentals of Classical Thermodynamics, S.I. version, 2nd edition, revised printing. U.S.A.: John Wiley & Sons, Inc.

Vanden-Broeck, J-M and Keller, J.B.(1980) Deformation of a bubble or drop in a uniform flow. J. Fluid Mech., 101, 673 - 686.

Wegener, P.P., Sundell, R.E. and Parlange, J-Y. (1971) Spherical Cap Bubbles Rising in Liquids. Zeitschrift Für Flugwissenschaften, 19, 347-352.

Wegener, P.P.and Parlange, J-Y. (1973) Spherical-Cap Bubbles. Ann. Rev. Fluid Mech., 5, 79-100.

Wilkinson, D.L. (1979) Two-Dimensional Bubble Plumes. Proc. ASCE. J. Hydraulics Div., 105, 139-154.

Witherspoon, P.A. and Bonoli, L. (1969) Correlation of Diffusion Coefficients for Paraffin, Aromatic, and Cycloparaffin Hydrocarbons in Water. I & E.C. Fundamentals, 8, 589-591.

Yamamoto, S., Alcauskas, J.B. and Crozier, T.E. (1976) Solubility of Methane in Distilled Water and Seawater. J. Chem. & Eng. Data, 21, 78-80.